

OSLO METROPOLITAN UNIVERSITY
STORBYUNIVERSITETET

Master's Degree in
Structural Engineering and Building Technology
Department of Civil Engineering and Energy Technology

MASTER THESIS

<p>THESIS TITLE</p> <p>Hygrothermal performance of thermally upgraded log walls of an in-use cultural heritage building from the 17th century based on current and future climate scenario</p>	<p>DATE</p> <p>09.06.2021</p>
	<p>NUMBER OF PAGES</p> <p>110 + 32</p>
<p>AUTHOR(S)</p> <p>Sindre Didrichsen Kris Anders Flaskerud</p>	<p>SUPERVISOR(S)</p> <p>Dimitrios Kraniotis</p>

<p>IN COLLABORATION WITH</p> <p>Vestfold og Telemark fylkeskommune (Vestfold and Telemark County)</p>	<p>CONTACT PERSON</p> <p>Jørgen Solstad</p>
-------------------------------------------------------------------------------------------------------	---------------------------------------------

<p>SUMMARY</p> <p>Norway is a country with a tremendous number of historic buildings and maintaining these is important for several different reasons. However, climate change leads to a warmer and more humid environment which in turns leads to an increased risk of biological, chemical, and mechanical decay. This master thesis has been centred around evaluating the hygrothermal performance of the log walls of the in-use cultural heritage building of Bentegården, located in Tønsberg. This building is the oldest of its kind in the city and has over the years been thermally upgraded through several different occasions. This has resulted in a building containing a large variety of solutions. A 3D scanning has been performed to create a digital model of the building. Supplied by historical documentation, local knowledge and infrared thermography, this has created a basis for determining the hidden elements within the building envelope. Numerical simulations have been conducted for the different wall assemblies with current and future climate data primarily based on observed data from weather stations and a “business as usual” climate scenario. The results indicated little to no risk of mould growth in the logs subjected to the current climate. However, there are evidently a greater risk of mould growth in the future according to the hygrothermal simulations, especially where the timber is not protected by exterior insulation.</p>

<p>3 KEYWORDS</p>
<p>Hygrothermal performance</p>
<p>Climate change</p>
<p>Log building</p>

Preface

This master thesis was conducted during the spring of 2021 at the department of civil engineering at Oslo Metropolitan University.

The thesis concerns the current and future condition of a cultural heritage log-house from the 17th century located in Tønsberg, Norway. Evaluations were based on a hygrothermal numerical simulation of the building model generated from available information supplied by a 3D laser scan and thermography.

The project group would like to express our appreciation to our supervisor Dr Dimitrios Kraniotis for guidance and insightful suggestions throughout the work. In addition, we are grateful to PhD candidate Petros Choidis for assistance with fieldwork and climate models. Our digital model was built with the appreciated assistance from department engineer Ernst Erik Hempel and his assistance with the 3D laser scanner and point cloud process.

We also would like to thank the resident at Bentegården, Sissel Øvrid, for the hospitality and Jørgen Solstad from Vestfold and Telemark County who provided valuable information and knowledge.

Oslo Metropolitan University

Department of Civil Engineering

Oslo, 09. June 2021



Sindre Didrichsen



Kris Anders Flakerud

Abstract

Norway is a country with a tremendous number of historic buildings and maintaining these is important for several different reasons. However, climate change leads to a warmer and more humid environment which in turns leads to an increased risk of biological, chemical, and mechanical decay.

This master thesis has been centred around evaluating the hygrothermal performance of the log walls of the in-use cultural heritage building of Bentegården, located in Tønsberg. This building is the oldest of its kind in the city and has over the years been thermally upgraded through several different occasions. This has resulted in a building containing a large variety of solutions.

A 3D scanning has been performed to create a digital model of the building. Supplied by historical documentation, local knowledge and infrared thermography, this has created a basis for determining the hidden elements within the building envelope. Numerical simulations have been conducted for the different wall assemblies with current and future climate data primarily based on observed data from weather stations and a “business as usual” climate scenario.

The results indicated little to no risk of mould growth in the logs subjected to the current climate. However, there are evidently a greater risk of mould growth in the future according to the hygrothermal simulations, especially where the timber is not protected by exterior insulation.

Table of content

Preface	ii
Table of content	vi
List of appendices	ix
List of figures	ix
List of tables	xiii
Abbreviations	xv
1. Introduction	1
1.1 Background.....	1
1.2 State of the art.....	2
1.3 Purpose, research question and limitations.....	4
2 Theory	5
2.1 Cultural heritage management in Norway	5
2.2 Traditional log buildings in Norway	6
2.3 Heat, air and moisture.....	7
2.3.1 Heat transport	7
2.3.2 Thermal bridges.....	8
2.3.3 Moisture	8
2.3.4 Mollier diagram.....	10
2.3.5 Moisture in wooden materials	10
2.3.6 Air infiltration	11
2.4 Building physics in older buildings and retrofitting	12
2.4.1 Post-insulation of exterior walls.....	13
2.4.2 U-values for timber walls	16
2.5 Building Information Modelling	17
2.6 Climate change and scenarios.....	18
2.7 Biological degradation.....	20

3	Method	22
3.1	Experimental site - Bentegården.....	23
3.2	Data collection	26
3.2.1	Available documentation and local knowledge	26
3.2.2	Fieldwork	26
3.3	Infrared thermography	27
3.4	3D laser scanning and Revit modelling	28
3.4.1	Point cloud data collection	29
3.4.2	Point cloud data processing	31
3.4.3	Revit modelling	33
3.5	Hygrothermal numerical simulations	33
3.5.1	WUFI Pro	33
3.5.2	Classification of mould risk and WUFI Bio.....	34
3.5.3	Outdoor climate conditions	37
3.5.4	Indoor climate conditions	38
3.5.5	Defining components and initial conditions.....	42
4	Results	44
4.1	Construction and rehabilitation history of Bentegården.....	44
4.2	Thermography	50
4.2.1	Exterior walls, roof and floor	50
4.2.2	Infiltration and thermal bridges.....	52
4.3	Digital model and identification of assemblies	53
4.4	Climate data	57
4.4.1	Illustration and comparison of climate models	57
4.4.2	Temperature and Relative Humidity from data loggers.....	60
4.5	Results from simulations in WUFI.....	62
4.5.1	Input parameters and assemblies.....	63

4.5.2	Moisture content.....	64
4.5.3	Mould index	72
4.5.4	Comparison of current climate following RCP8.5 and observations.....	82
5	Discussion.....	84
6	Conclusion	87
7	Future research	88
	References	89

List of appendices

APPENDIX A - Input data from WUFI.....	1
APPENDIX B - Moisture content 2010-2020, current climate vs RCP8.5.....	2
APPENDIX C - Mould index 2010-2020, current climate vs RCP8.5.....	7
APPENDIX D – Report from field study, loggers.....	11
APPENDIX E - Report from field study, laser scan.....	15
APPENDIX F - Report from field study, thermography.....	18
APPENDIX G – Report from point data cloud processing.....	22
APPENDIX H – Report from the 3D modelling process.....	27

List of figures

Figure 2.1 Typical structure of a log building. Text from the figure has been removed. Included with permission from SINTEF.....	6
Figure 2.2 Heat transport mechanisms	7
Figure 2.3 Relative humidity of a typical year in Oslo climate	9
Figure 2.4 Molliers diagram (Engineering ToolBox, 2003)	10
Figure 2.5 Distribution of heat loss. The graph is reproduced based on the data from (Svensson et al., 2012).	13
Figure 2.6 - Insulation on interior side of logs, alternative 1. Translated from (SINTEF Byggforsk, 2004). Included with permission from SINTEF.....	14
Figure 2.7 - Insulation on interior side of logs, alternative 2. Translated from (SINTEF Byggforsk, 2004). Included with permission from SINTEF.....	14
Figure 2.8 - Insulation on interior side of logs. Translated from (SINTEF Byggforsk, 2004).Included with permission from SINTEF.....	15
Figure 2.9 Risk of rot-decay in Norway. Translated from The Norwegian Meteorological Institute.....	21
Figure 3.1 Overview of key elements	22
Figure 3.2 Location of Bentegården.....	23
Figure 3.3 Location of Bentegården in Tønsberg	23
Figure 3.4 Bentegården seen from southeast. Photo by Kris A. Flaskerud.....	24
Figure 3.5 Bentegården seen from northeast. Photo by Kris A. Flaskerud.....	24

Figure 3.6 – 1 st floor plan drawing	24
Figure 3.7 - 2nd floor plan drawing	25
Figure 3.8 IR-camera Fluke Ti105. Photo by Kris A. Flaskerud	28
Figure 3.9 - Leica BLK360 #1. Photo by Kris A. Flaskerud	29
Figure 3.10 - Leica BLK360 #2. Photo by Kris A. Flaskerud	29
Figure 3.11 - 1st floor, position of each scan	30
Figure 3.12 - 2nd floor, position of each scan.....	30
Figure 3.13 - Exterior side, position of each scan	30
Figure 3.14 Point cloud bundle of exterior scans	31
Figure 3.15 Point cloud bundle of exterior scans	31
Figure 3.16 Point cloud bundle of interior scans 1st floor	32
Figure 3.17 Point cloud bundle of interior scans 1st floor	32
Figure 3.18 - Point cloud bundle of interior scans 2nd floor	32
Figure 3.19 - Point cloud bundle of interior scans 2nd floor	32
Figure 3.20 - Location of weather stations (2 & 3) and Bentegården (1). Created using a map from norgeskart.no	38
Figure 3.21 Humidity classes, translated from (SINTEF Byggforsk, 1999). Added with permission from SINTEF	39
Figure 3.22 - PeakTech 5180 logger. Photo by Kris A. Flaskerud	40
Figure 3.23 - Extech RHT10 logger. Photo by Kris A. Flaskerud.....	40
Figure 3.24 - 1st floor, location of loggers.....	41
Figure 3.25 - 2nd floor, location of loggers	41
Figure 4.1 – Old picture of Bentegården. Date: unknown. Published with permission from Vestfold and Telemark County	45
Figure 4.2 – Bentegården. Date: 1971. Published with permission from Vestfold and Telemark County.....	45
Figure 4.3 - Interior side of the second floor. Date: 1969. Published with permission from Vestfold and Telemark County	46
Figure 4.4 - Interior side of the south facade seen from the library. Date: 1969. Published with permission from Vestfold and Telemark County	46
Figure 4.5 - Detail from construction drawing with interior insulation.	46
Figure 4.6 - Picture from the inspection in 2007.....	47
Figure 4.7 - During rehabilitation work. Date: 2018. Published with permission from Vestfold and Telemark County	47

Figure 4.8 - Rehabilitation work finished. Date: 2018. Published with permission from Vestfold and Telemark County	47
Figure 4.9 Second floor on the south wall. Published with permission from Vestfold and Telemark County	48
Figure 4.10 Main bedroom. Photo by Kris A. Flaskerud	48
Figure 4.11 Interior side of the roof. Photo by Kris A. Flaskerud	48
Figure 4.12 Second floor window on the east façade. Photo by Kris A. Flaskerud.....	49
Figure 4.13 Location of measurements 1 st floor	50
Figure 4.14 Location of measurements 2 nd floor	50
Figure 4.15 Thermographic image, roof 2 nd floor	51
Figure 4.16 Thermography image floor, TV-room	51
Figure 4.17 Thermography image floor, library.....	51
Figure 4.18 Thermography image floor, living room	51
Figure 4.19 Thermography image window, kitchen	52
Figure 4.20 Thermography image window, TV-room.....	52
Figure 4.21 Thermography image window, bedroom.....	52
Figure 4.22 Thermal bridges captured in the north-west corner of living room.....	52
Figure 4.23 Thermal bridges captured in the south-west corner of the library	52
Figure 4.24 Thermal bridges captured in the south-west corner of the recreational room	52
Figure 4.25 Revit model - 3D view	53
Figure 4.26 Rendered model - 3D view	53
Figure 4.27 Section view of the first floor	53
Figure 4.28 Section view of the second floor.....	53
Figure 4.29 Detail drawing of the south wall.....	54
Figure 4.30 Bentegården from above. This illustration is not oriented towards true north.	55
Figure 4.31 Annual temperature, observed climate data and RCP8.5	57
Figure 4.32 Annual RH, observed climate data and RCP8.5	58
Figure 4.33 Annual precipitation, observed climate data and RCP8.5	58
Figure 4.34 Monthly average temperature, observed data and RCP8.5.....	59
Figure 4.35 Monthly average precipitation, observed data and RCP8.5.....	59
Figure 4.36 Data from loggers inside, temperature.....	60
Figure 4.37 Data from loggers inside, relative humidity	60
Figure 4.38 Data from loggers outside, temperature.....	61
Figure 4.39 Data from loggers outside, relative humidity	61

Figure 4.40 - Assembly 1 - moisture content	65
Figure 4.41 Wall assembly 2 - moisture content.....	66
Figure 4.42 Wall assembly 3 - moisture content.....	67
Figure 4.43 Wall assembly 4 - moisture content.....	67
Figure 4.44 Wall assembly 5 - moisture content.....	68
Figure 4.45 Wall assembly 6 - moisture content.....	69
Figure 4.46 Wall assembly 7 - moisture content.....	69
Figure 4.47 Wall assembly 9 - moisture content.....	70
Figure 4.48 Wall assembly 10 - moisture content.....	71
Figure 4.49 Wall assembly 11 - moisture content.....	71
Figure 4.50 Wall assembly 1, monitor position	72
Figure 4.51 Mould index, humidity class 1, assembly 1	72
Figure 4.52 Mould index, humidity class 3, assembly 1	72
Figure 4.53 Wall assembly 2, monitor position	73
Figure 4.54 Mould index, humidity class 1, assembly 2.....	73
Figure 4.55 Mould index, humidity class 3, assembly 2.....	73
Figure 4.56 Wall assembly 3, monitor position	74
Figure 4.57 Mould index, humidity class 1, assembly 3.....	74
Figure 4.58 Mould index, humidity class 3, assembly 3.....	74
Figure 4.59 Wall assembly 4, monitor position	74
Figure 4.60 Mould index, humidity class 1, assembly 4.....	75
Figure 4.61 Mould index, humidity class 3, assembly 4.....	75
Figure 4.62 Wall assembly 5, monitor position	75
Figure 4.63 Mould index, humidity class 1, assembly 5.....	75
Figure 4.64 Mould index, humidity class 3, assembly 5.....	75
Figure 4.65 Wall assembly 6, monitor position	76
Figure 4.66 Mould index, humidity class 1, assembly 6.....	76
Figure 4.67 Mould index, humidity class 3, assembly 6.....	76
Figure 4.68 Wall assembly 7, monitor position	77
Figure 4.69 Mould index, humidity class 1, assembly 7.....	77
Figure 4.70 Mould index, humidity class 3, assembly 7.....	77
Figure 4.71 Wall assembly 8, monitor position	77
Figure 4.72 Mould index, humidity class 1, assembly 8.....	78
Figure 4.73 Mould index, humidity class 3, assembly 8.....	78

Figure 4.74 Wall assembly 9, monitor position	78
Figure 4.75 Mould index, humidity class 1, assembly 9.....	78
Figure 4.76 Mould index, humidity class 3, assembly 9.....	78
Figure 4.77 Wall assembly 10, monitor position	79
Figure 4.78 Mould index, humidity class 1, assembly 10.....	79
Figure 4.79 Mould index, humidity class 3, assembly 10.....	79
Figure 4.80 Wall assembly 11, monitor position	80
Figure 4.81 Humidity class 1, assembly 11	80
Figure 4.82 Humidity class 3, assembly 11	80
Figure 4.83 Wall assembly 1, RCP8.5 evaluation - moisture content	82
Figure 4.84 Assembly 1 - Mould index, RCP8.5 evaluation, humidity class 1	83
Figure 4.85 Assembly 1 - Mould index, RCP8.5 evaluation, humidity class 3	83

List of tables

Table 2-1 - U-value timber with insulation. This table combines table 51, 52 & 53 from (SINTEF Byggforsk, 2013). Included with permission from SINTEF.....	16
Table 2-2 - U-value timber (SINTEF Byggforsk, 2013). Included with permission from SINTEF.	17
Table 2-3 Temperature increase for Vestfold according to RCP8.5. Seasonal and annual increase compared to 1971-2000.....	19
Table 2-4 Precipitation for Vestfold according to RCP8.5, Including winter (1), spring (2), summer (3) and autumn (4) and annual increase compared to 1971-2000	20
Table 3-1 Mould index and description of growth rate.....	35
Table 3-2 – Location of loggers	41
Table 3-3 Logger data collection	42
Table 4-1 Location and surface temperature.....	50
Table 4-2 Location and surface temperature.....	50
Table 4-3 1st floor wall assemblies. Table I	55
Table 4-4 1st floor wall assemblies Table II.....	56
Table 4-5 2nd Floor wall assemblies. Table I	56
Table 4-6 2nd Floor wall assemblies. Table II.....	56
Table 4-7 Wall assembly of building extension.....	57

Table 4-8 Data from loggers and calculated moisture excess, February 13 th 15:00	62
Table 4-9 Data from loggers and calculated moisture excess, February 21 st 01:00.....	62
Table 4-10 Material and database in WUFI	63
Table 4-11 Characteristics of wall assemblies used in the simulations	64
Table 4-12 Summary of the maximum mould index	81

Abbreviations

AR5	<i>Assessment Report 5</i>
BIM	<i>Building Information Modelling</i>
CAD	<i>Computer Aided Design</i>
ESD	<i>Empirical statistical downscaling</i>
GCM	<i>General circulation models</i>
RCP	<i>Representative Concentration Pathways</i>
IPCC	<i>Intergovernmental Panel on Climate Change</i>

1. Introduction

1.1 Background

Norway is a country with a tremendous number of historic buildings and maintaining these is important for several different reasons. Cultural heritage provides us knowledge about our ancestors and serves an undoubtable importance in characterizing the identity of a place. Besides this, maintaining these buildings can serve a purpose considering sustainability and economic value.

As the climate continuous to rapidly change, buildings that dates centuries back is exposed to an environment which is getting more and more distanced from what they were built to withstand. According to Hanssen-Bauer et al. (2017) a worst-case climate scenario describes a situation with an increase in annual temperature of about 4,5 °C, 18 % increase in annual precipitation and 15-55 cm increase in mean sea level depending on location along the coast. This in turns leads to an increased risk of biological, chemical, and mechanical decay.

An international project called Hyperion got the ambition to create a tool to better understand the effect of climate change on cultural heritage sites and monuments for easier decision making, visualization of future climate scenarios, prioritization of rehabilitation actions and preventive measures, by others (Hyperion, 2020). One of the test sites involved with this project is Tønsberg, which is considered as the oldest city in Norway. Nordbyen is an area in Tønsberg characterized by a lot of old low raised and well-preserved wooden houses. Among these are Bentegården, an inhabited timber building which dates back to the century-end of the 1700s and is considered the oldest in Tønsberg.

Being the oldest house in the oldest city of Norway, Bentegården most certainly got history written within its walls worth exploring. What can we learn from observing such a well-preserved log building and what challenges may Bentegården and other similar building face with an ever-changing climate?

1.2 State of the art

The research involved with cultural heritage preservation can arguably be seen from two different perspectives, both with the intention of reducing the loss of important structures. One perspective is with respect to reducing the biological and physical degradation. A second perspective is with respect to the overall energy efficiency, hence making it suitable for housing and current technical requirements.

In Norway, there are ongoing monitoring programs e.g. Dammann (2020) focusing on the preservation of cultural heritage. This work is based on hypotheses about the relationship between cause and effect and gathers data using systematic verifiable methods (Riksantikvaren, 2020b). It is further described that more scientific research is important to understand what area of cultural heritage monitoring should be focused on and how this process can be improved. Additionally, scientific research is crucial to interpret and explain the data collected. Similar communication is pointed out as missing between the academic and management sector according to Sesana et al. (2019), which bases its research on a semi-structured interview with experts on cultural heritage preservation in Norway, UK, and Italy.

Fatorić and Seekamp (2017) demonstrated through a systematic literature review that research on the effect of climate change on cultural heritage entered the agenda in 2003 with a significantly increasing trend over the past century. Included in this is the development of methods for non-destructive techniques for characterization and diagnosis of cultural heritage (Solla et al., 2020).

One of the most used non-destructive methods for describing the cause and effect of degradation of buildings and other structures is thermography (Barrile et al., 2021). Furthermore, Glavaš et al. (2019) demonstrated that this technology can be applied to help detect non-homogeneous outer shell elements, hidden openings and structural elements by investigating several Baroque buildings in Croatia. For categorizing the deeper layers of the building envelope, however, the study concluded that conventional thermography needs to be coupled with other forms of non-destructive testing.

Another ever-growing non-destructive technique is laser scanning. The Norwegian Institute for Cultural Heritage (NIKU) describes this as an accurate and cost-effective method for the documentation and monitoring of various assemblies of cultural monuments (NIKU, n.d.). Within cultural heritage research, this technology is being used in work related to buildings and ruins e.g. (Gustavsen, 2010, 2011), archaeological localities e.g. (Thuestad et al., 2021),

and archaeological findings and artefacts e.g. (Stein & Gustavsen, 2013). In other words, technology brings great benefits to a wide range of cultural heritage research. Furthermore, specifically for buildings, laser scanning can be used as a part of the BIM approach which serves purposefully in terms of facility management, support in the restoration or rehabilitation processes and further research (Solla et al., 2020).

With sufficient information about individual components, the process of using hygrothermal simulations has been described in different papers to evaluate retrofitting measures e.g. (Coelho et al., 2019) and the effect of climate change e.g. (Rajčić et al., 2018). Something that is repeated throughout several papers is the importance of evaluating a variety of cases. This is mainly because the results are dependent on a large number of variables, including the buildings volume, window to wall area ratio to name a few (Coelho et al., 2019), however, simulations can provide quantitative information about the future rate of decay on groups of cultural heritage with similar characteristics (Sesana et al., 2019).

1.3 Purpose, research question and limitations

The purpose of this master thesis is to complement the work related to the EU project HYPERION by evaluating the impact of climate change on the cultural heritage building, Bentegården located within one of the projects test-sites of Tønsberg. To accommodate this, the following research questions has been investigated:

- How do observed local climate data correspond with climate predictions?
- What is the moisture content of the log walls and how does this develop in a warmer and more humid climate?
- When and where does a potential risk of mould growth occur?

These questions form the basis for the following compound problem to be addressed:

What is the hygrothermal performance of log walls subjected to various retrofitting measures in cultural heritage buildings located in a Nordic climate and how will this be affected by climate change?

Answering this problem has been conducted by gathering all available information about the assemblies, supplied by 3D-laser scanning and thermography followed by hygrothermal numerical simulations using current climate data and future climate predictions. Seen in the perspective of this will there be discussions regarding benefits and limitations with the use of 3D laser scanning and infrared thermography as a method for clarifying the lack of information concerning construction assemblies.

As indicated, this thesis focuses on heritage buildings located in a Nordic climate. However, local climate variations may cause local variations, but the climate data used is limited to the area of Tønsberg. Furthermore, only the exterior walls are investigated through numeric simulations and potential energy savings from retrofitting measures has not been quantified.

2 Theory

2.1 Cultural heritage management in Norway

Ever since 1687, Norway has had a law intended to protect cultural heritage. With its introduction, it applied to private findings of movables but has over the centuries evolved with several protection provisions in other laws, especially in the 19th century. At the end of the 19th century and the beginning of the 20th century, work was done to gather a new and strong law to protect the cultural heritage. In 1905 this resulted in *fortidsminneloven*, which was one of the first laws decided after the dissolution of the union between Norway and Sweden and included protection of all buildings from antiquity and the Middle Ages. *Riksantikvaren*, which for the first time took office in 1912 saw the need for protection of cultural heritage from the 17th, 18th and 19th century, which set the foundation for *bygningsfredningsloven* (law on building protection) in 1920. This, together with a law from 1951 which introduced an obligation to give notification when planning work that could affect cultural heritage has put the foundation for the current cultural heritage act established in 1978. (Holme et al., 2020)

With current legislation, all cultural heritage from before 1537 is automatically listed (kulturminneloven, 1979a). Additionally, the listing of newer buildings and other historic material is assessed based on their uniqueness and variety both as part of our cultural heritage and identity and as part of a comprehensive environmental and resource management (Kulturminneloven, 1979b).

From 1975 to 1995, extensive work was carried out to map all buildings in Norway built before 1900. This resulted in about 515 000 buildings being registered in a register called SEFRAK. Although all these buildings are not listed, the register function as a heads up for the municipalities to evaluate the potential threat to cultural heritage. (Riksantikvaren, 2020c)

Annually, several buildings listed in the SEFRAK-register is lost. Dammann (2020) describes a loss of about 28 % since registering in a selection of 10 municipalities with a combined total of 7458 before any loss. 43 % of the cases are registered as demolished, while 30 % is due to decay and 22 % is registered with unknown cause. Although there has been a significant loss since the introduction of the SEFRAK-register, there is a sinking trend in terms of annual loss and the results point to the connection between use and building preservation. (Dammann, 2020)

2.2 Traditional log buildings in Norway

Through thousands of years, wood has been central in Norwegian building history due to its versatility and availability and the development of construction methods reflects the economic growth and standard of living in the country. (Edwardsen & Ramstad, 2014)

Log buildings is undoubtedly one of the most iconic construction methods used in Norway but has also been central in the rest of Scandinavia, middle- and east-Europe and Asia. Ever since the Middle Ages up until late the 19th century, it was the dominant method utilized in the country. Over the course of this period, unique techniques are evident for different regions as a result of material access, climatic differences and local carpenter traditions. (SINTEF Byggforsk, 2017)

In short, the basic structural principle of log buildings is the horizontal logs which are mounted on top of each other and interlocked at the corners to form the walls of the building. Furthermore, purlins are mounted to form the structural part of the roof. These basic principles are illustrated in Figure 2.1. (SINTEF Byggforsk, 2019b)

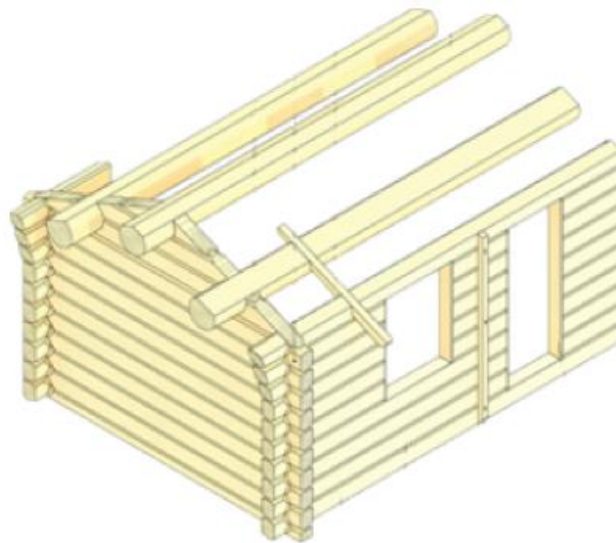


Figure 2.1 Typical structure of a log building. Text from the figure has been removed. Included with permission from SINTEF.

Mainly spruce or pine was utilized in the traditional log buildings, which are common tree species throughout the country (SINTEF Byggforsk, 2019b). Although local availability had significance, pine was usually preferred due to a higher amount of heartwood with resin, which is more resistant to decay (Britannica, 2012). Further development of the building envelopes resistance led to the common practice of panelling, which also reduced the requirement of the logs. (Riksantikvaren, 2012)

Following the practice of panelling the log buildings, surface treatment became common and linseed oil paint was probably first introduced to buildings around Norway after the 17th century. The application was a traditional treatment of panels, doors and windows all over Norway. The preparation of the paint was before the industrialisation executed by an experienced carpenter. During the second world war, there was a shortage of linseed oil lasting until the 1950s. The shortage resulted in the introduction of alkyd paint and acrylic paint, while a large part of the knowledge around painting with linseed oil was forgotten. (Riksantikvaren, 2002)

Today, the old method involving linseed oil paint is recommended when applying the surface treatment on cultural heritage building regardless of whether it previously has been applied with a combination of linseed oil paint and alkyd paint. (Brønne, 2021).

2.3 Heat, air and moisture

2.3.1 Heat transport

Whenever there is a temperature difference in a system, heat transport will occur from the warmer to the colder area by conduction (1), convection (2) or radiation (3) as illustrated in Figure 2.2. In construction materials, these three forms of heat transport are combined to form the total heat transport (Edvardsen & Ramstad, 2014).

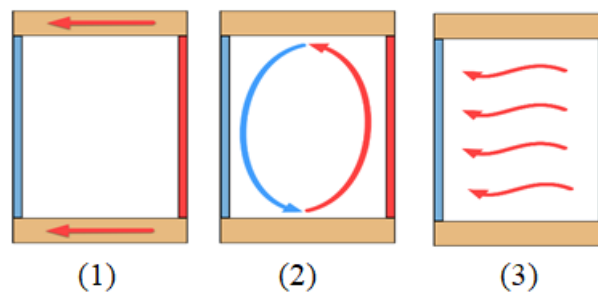


Figure 2.2 Heat transport mechanisms

A fourth type of heat transport is latent heat, which is related to change of state. This is exemplified in Hens (2017) with water that evaporates and absorbs heat, moves to a colder spot, condenses and re-emits the heat of the evaporation.

2.3.2 Thermal bridges

A thermal bridge is a section with substantially greater heat loss than its surroundings and is caused by either geometry or material properties. Furthermore, it is distinguished between linear thermal bridges and point thermal bridges.

Geometric thermal bridges are caused by a difference in the interior and exterior surface area which are caused by an angle or a change of thickness.

Thermal bridges caused by materials is based on the thermal resistance of a material. This occurs where there is a material with a higher thermal conductivity than its connecting materials.

It is practically impossible to completely avoid thermal bridges as the exterior surface area always will be greater than the interior surface area, and it is necessary to use materials with higher thermal conductivity for the load-bearing of the structure. The aim is therefore to reduce the thermal bridges as much as possible to avoid consequences such as increased heat loss and energy demand, reduced surface temperature, condensation and reduced thermal comfort (SINTEF Byggforsk, 2019a).

2.3.3 Moisture

According to Edvardsen and Ramstad (2014), about 60-80 % of all construction damage is related to moisture. Moisture is sourced both inside and outside the building envelope and there are five main mechanisms related to moisture transport (Edvardsen & Ramstad, 2014):

- (1) Torrential rain - specifically rain transported by air leakages in the building envelope.
- (2) Capillary suction – moisture transport caused by capillary action within the pores of materials.
- (3) Liquid flow – leakages, for example through the roof or sanitary installations.
- (4) Moisture convection – water vapour transported by air leakages.
- (5) Water vapour diffusion – water vapour transport caused by a difference in water vapour content in the exterior and interior air.

Increasing temperature also increases the amount of water vapour the air can hold, and when the maximum quantity of water vapour at a given temperature is reached it is defined as saturated. The relative humidity describes the relationship between the absolute moisture content in the air and the moisture content when saturated and is given as a percentage or as a number between 0 and 1.

When the relative humidity reaches 100 %, condensation occurs. Additionally, high relative humidity over a longer period causes a serious threat of mould growth. Although this is also dependent on the substrate (Sedlbauer, 2002), the mould will typically grow if the relative humidity at the surface exceeds 80 % over a period of about four weeks (Hens, 2017).

The water vapour content in outdoor air is affected by geographical location and time of the year. The mean relative humidity outdoors in Norway is usually between 50 and 90 %, but close to 100 % in foggy and rainy weather (Edvardsen & Ramstad, 2014). Figure 2.3 illustrates the relative humidity for each month of a typical year in Oslo with data gathered from (SINTEF Byggforsk, 1999).

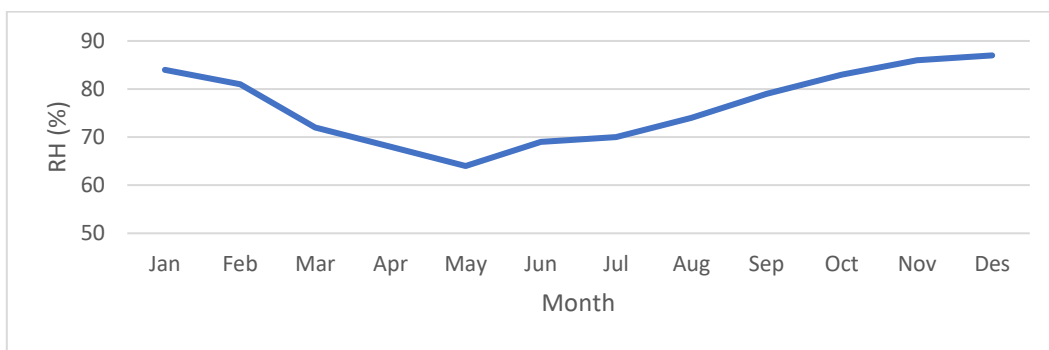


Figure 2.3 Relative humidity of a typical year in Oslo climate

Humidity levels indoors depend on the moisture content in the outer air of which is ventilated into the building and its quantity in addition to interior moisture excess.

$$V_{interior} = V_{exterior} + \Delta V \quad \text{Eq. 1}$$

As the moisture production and temperature varies, the humidity indoors changes a lot throughout the day. Additionally, there is usually a significant difference for the different rooms within the building. The smallest variations throughout the day are typically in the living room while the largest is typically in the bathroom. (Holme, 2010)

2.3.4 Mollier diagram

The mollier diagram, Figure 2.4, is an engineering tool that illustrates the relationship between temperature, relative humidity, water vapour pressure and moisture content in the air graphically.

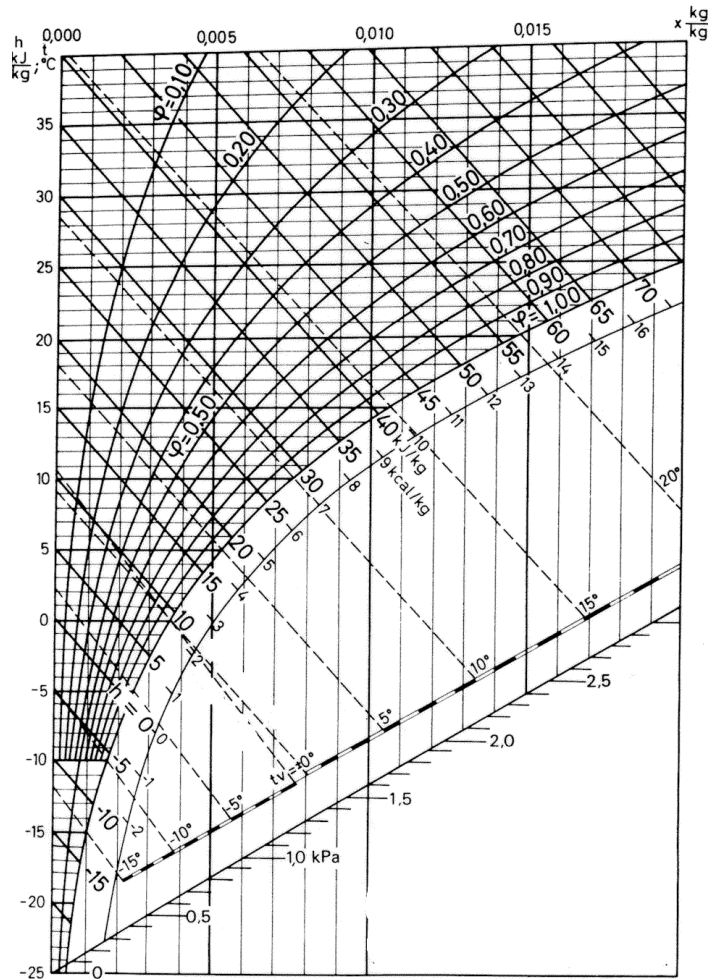


Figure 2.4 Molliers diagram (Engineering ToolBox, 2003)

2.3.5 Moisture in wooden materials

Wooden constructions are especially vulnerable to moisture related problems during all stages of its service life.

There are two forms of water storage within the wood, which are bound water in the cellulose inside the cell walls and free water inside the cells. When the wood begins to dry out, the free water inside the cells is the first to evaporate. When this is completely gone, the evaporation process begins for the water bound within the cell walls. For spruce and pine, the moisture content is around 30 % at this point. Further drying entails shrinkage of the wood (SINTEF Byggforsk, 2015).

Wooden materials can be said to find its equilibrium moisture content when it's in balance with the moisture content in the air surrounding it. If protected from rain, this usually results in a moisture content between 18 % and 20 %. Concerning mould growth, SINTEF Byggforsk operates with a critical value of 20 % for this to begin (SINTEF Byggforsk, 2015).

2.3.6 Air infiltration

Air infiltration can occur in openings in the building envelope with varying form and size and may cause significant physical consequences for the building and the comfort of the occupants. First and foremost, air infiltrations can affect the ventilation system of the building and increase the heating or cooling demand. Additionally, it can be a causing factor for moisture problems, the spread of fire, pollution of the interior air, sound, and radon infiltration. (SINTEF Byggforsk, 2014)

The driving force for the airflow through air leakages is considered as a combination of wind and pressure difference caused by temperature difference in the interior and exterior air. The combination of these two mechanisms usually results in an inside-to-outside pressure difference (Younes et al., 2012). In terms of moisture problems, leakages of moist indoor air can lead to condensation and dampening in cold parts of the construction. This is especially relevant for roof constructions as a result of over pressurisation in the upper part of the building (SINTEF Byggforsk, 2014).

In the Norwegian regulations on technical requirements for construction works (TEK17, 2017), there are minimum requirements for leakage figures at 50 Pa pressure differential. For most buildings, this requirement is specified as 1,5 air exchanges per hour, but for timber constructions a higher figure is acceptable. More specifically, TEK 17 accepts a maximum figure of 6 air exchanges per hour.

2.4 Building physics in older buildings and retrofitting

Traditional buildings were built by hand with materials from the local area, an energy-efficient building method causing a minor impact on the environment. The material properties were utilized to obtain a long service life and the constructions were easy to maintain. These buildings were built with diffusion open materials to secure the drying of the materials and provide certain ventilation (Riksantikvaren, 2020a).

The ventilation is mainly based on the stack effect in older buildings. This is a principle that is based on air movement into or out of buildings caused by air buoyancy, the difference in air density. The buoyancy force can be either negative or positive. Positive thermal buoyancy is caused by warm air with a lower density than cold air resulting in an upward draft and warm air escaping through exhaust ducts and air leakages in the upper part of the house. Valves and air leakages provide fresh air entering the construction, in addition to aeration through windows. Ventilation is also provided from wood-firing during winter which causes a negative pressure letting fresh air into the building and through open windows during summer (Riksantikvaren, 2013).

While old buildings rely on diffusion open materials and natural ventilation, modern buildings rely on energy efficiency through more air- and watertight buildings which require a ventilation system. Implementation of modern solutions from today's new constructions may cause unfortunate consequences if applied to old constructions (Riksantikvaren, 2020a). It is important to understand the consequences prior to any extensive measures regarding sealing and/or insulation. Several conditions are necessary to evaluate e.g. how it's constructed, and which particular measures should be performed to prevent damages, protection against moisture, ventilation and heating. Additionally, there are regulations and potential preferences from the owners which prevent altering the aesthetics of the building. (Riksantikvaren, 2013).

Figure 2.5 illustrates a distribution of heat loss in a typical non-insulated log building in Oslo climate (Svensson et al., 2012). Although these values may vary from case to case, it gives a clear indication of what to expect in this type of building. The absolute largest heat losses are from the windows and the outer walls, while the least is from the thermal bridges. According to Svensson et al. (2012), heat loss from thermal bridges in log buildings is neglectable unless the building is insulated, especially on the interior side.

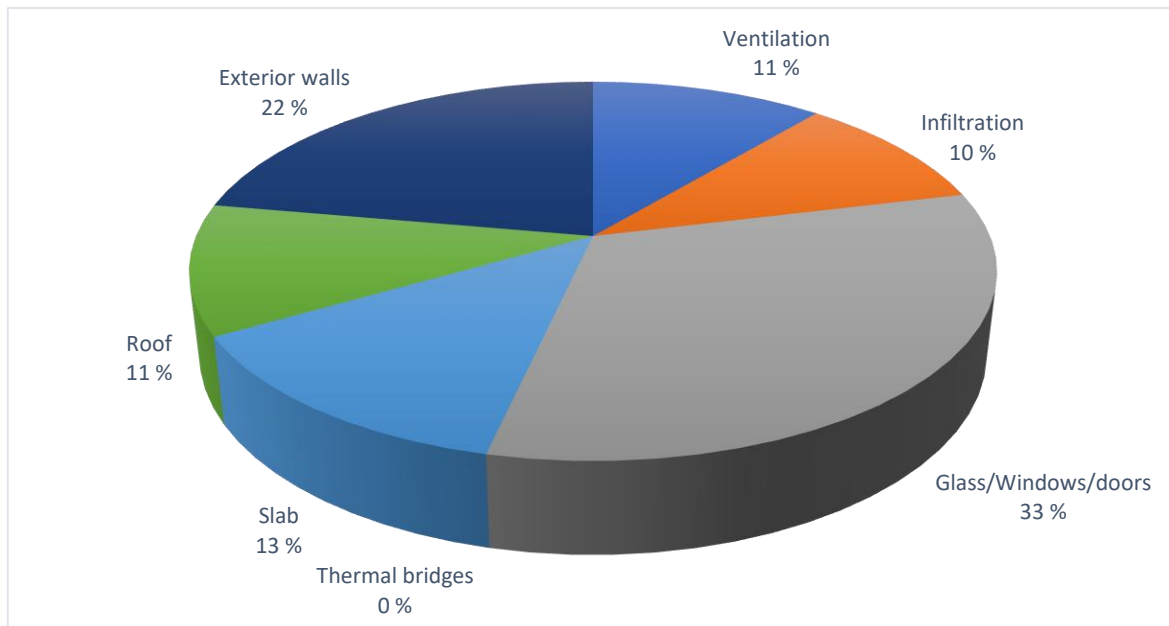


Figure 2.5 Distribution of heat loss. The graph is reproduced based on the data from (Svensson et al., 2012).

In the report, a total of 15 different measures is simulated and reported based on their contribution to the energy savings. This included measures like temperature control, installation of insulation in different parts of the building, sealing of air leakages and replacement or improvement of windows. The result indicated that measures related to the windows had the best energy savings, with values ranging from 21-25 %. Additionally, 300 mm post insulation installed in the roof and floor saw a reducing effect of 20 % but may lead to the need for additional measures to prevent potential damage. Other solutions indicated an efficiency in the range of 6-16 %, with post-insulation of outer walls being the most efficient within this interval. (Svensson et al., 2012)

2.4.1 Post-insulation of exterior walls

As mentioned above, post-insulating the exterior walls is an effective measure to reduce energy consumption, however, it can affect the architectural and cultural heritage values. Additionally, the expenses often overcome the energy savings and therefore most beneficial combined with related work (Riksantikvaren, 2013).

Post-insulation on the exterior side of the outer walls is valuable to obtain good moisture control and a low heat loss. Insulation on the exterior side secures a coherent insulation layer avoiding thermal bridges. Additionally, the moisture control is better preserved due to the original structure kept warmer and dryer (SINTEF Byggforsk, 2004).

A disadvantage of exterior post-insulation is the impact on exterior building elements and proportions. Depending on the thickness of the insulation, the thickness of the wall is extended which cause e.g. decreased roof overhang, changed transition between foundation and wall, and moving windows further out should be considered (Riksantikvaren, 2013).

SINTEF Byggforsk (2004) describes two different methods regarding log house with exterior insulation. The first method, Figure 2.6, is described by installing a wind barrier to the logs to make it airtight, followed by a layer of mineral wool and another layer of wind barrier. After the new layer of wind barrier, a ventilation layer and the outer cladding is installed.

The second method, Figure 2.7, is regarding walls with an existing interior vapour barrier and interior cladding. The mineral wool layer can be installed directly to the logs provided that the outer wind barrier is mounted with tight seals and transitions to the existing wall.

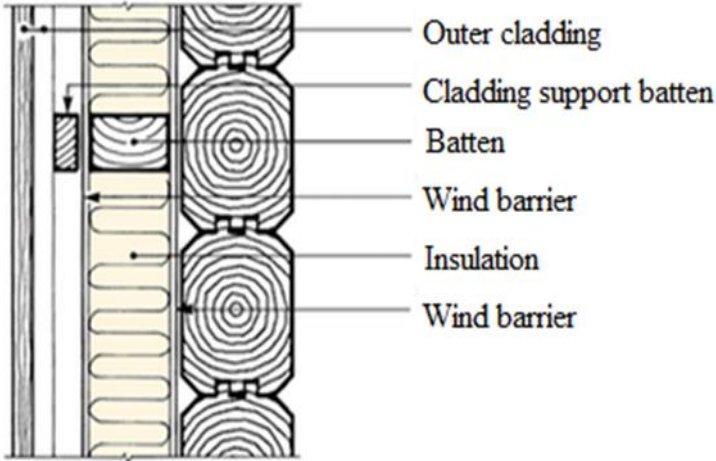


Figure 2.6 - Insulation on interior side of logs, alternative 1. Translated from (SINTEF Byggforsk, 2004). Included with permission from SINTEF.

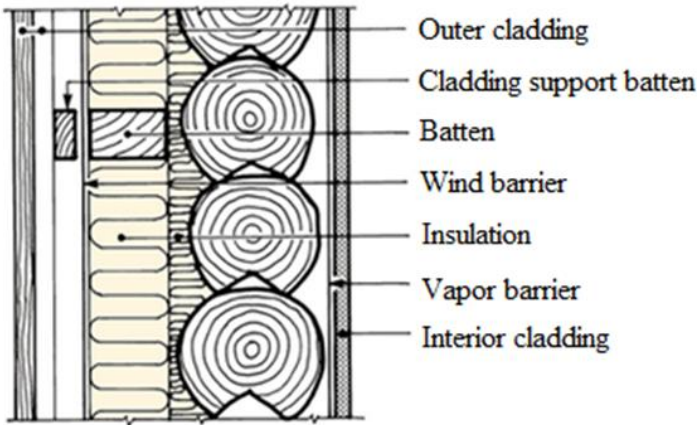


Figure 2.7 - Insulation on interior side of logs, alternative 2. Translated from (SINTEF Byggforsk, 2004). Included with permission from SINTEF.

Post-insulation on the interior side gives the possibility to only insulate a specific wall, but as mentioned, the thermal bridges from section walls and floors are unavoidable. Another disadvantage is a loss of indoor area and that all installations on the wall need to be adjusted. Usually, post-insulation on the interior side is only considered if the exterior should be preserved or the condition is good (SINTEF Byggforsk, 2004).

Riksantikvaren (2013) describes an increased risk of wood rot inside the structure, due to less drying and increased level of moisture. Local climate and a condition assessment should be conducted before measures involving interior post-insulation. Installation may also cause damage or destruction of ceiling, panels, list, tapestry, floor and wall panels. Less daylight can also be a factor, due to deeper window sills (Riksantikvaren, 2013).

SINTEF Byggforsk (2004) describes a method regarding the installation of interior insulation in log buildings as illustrated in Figure 2.8. It is recommended to install a wind barrier against the logs if the wall isn't airtight, which they usually aren't. The inside of the insulation is then covered with a sealed vapour barrier before the interior cladding.

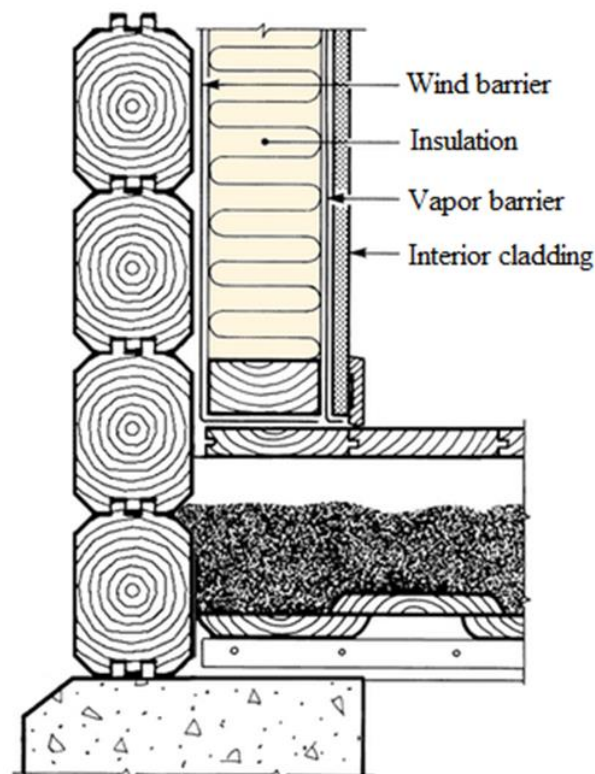


Figure 2.8 - Insulation on interior side of logs. Translated from (SINTEF Byggforsk, 2004). Included with permission from SINTEF.

2.4.2 U-values for timber walls

This section is included to illustrate what the literature provides regarding the U-value of typical timber walls. The values in Table 2-1 is created based on data tabulated in (SINTEF Byggforsk, 2013). The wall of which the calculations are performed is based on the following:

- The insulation is mounted between studs with a thickness of 48 mm.
- The connection surface between the logs is 50 % of the thickness of the logs.
- In the case of external insulation, the externally ventilated cladding is assumed, and sufficiently large ventilation and drainage gap behind the cladding to ensure good ventilation and drainage.
- Where the wall is insulated on the interior side, 12.5 mm of cladding and vapour barrier are assumed.

The L'' -value (m/m^2), which describes the length of the wood per square meter wall is taken as $3,5 m/m^2$. This is described as a typical value for housing with a room height of 2,4m.

Furthermore, the table below includes values for both interior and exterior insulation for three different thermal conductivity values.

Table 2-1 - U-value timber with insulation. This table combines table 51, 52 & 53 from (SINTEF Byggforsk, 2013). Included with permission from SINTEF.

Timber (mm)	Insulation (mm)	U-value (W/m ² K)					
		λ_d 0,033 W/mK		λ_d 0,035 W/mK		λ_d 0,037 W/mK	
		Exterior	Interior	Exterior	Interior	Exterior	Interior
150	50	0,41	0,40	0,42	0,41	0,42	0,42
	100	0,28	0,28	0,29	0,29	0,30	0,29
	150	0,22	0,22	0,22	0,22	0,23	0,23
	200	0,177	0,176	0,182	0,180	0,187	0,186
	250	0,150	0,149	0,154	0,154	0,159	0,158
200	50	0,36	0,35	0,37	0,36	0,37	0,37
	100	0,26	0,26	0,26	0,26	0,27	0,27
	150	0,20	0,20	0,22	0,21	0,21	0,21
	200	0,167	0,166	0,173	0,170	0,177	0,175
	250	0,143	0,142	0,147	0,146	0,151	0,150
250	50	0,32	0,32	0,33	0,32	0,33	0,33
	100	0,24	0,24	0,24	0,24	0,25	0,25
	150	0,190	0,188	0,194	0,193	0,20	0,197
	200	0,158	0,157	0,162	0,161	0,166	0,165
	250	0,137	0,135	0,140	0,139	0,144	0,143

Besides providing information about typical u-values, the values illustrate that there is no significant difference in the U-value of the assembly based on the position of the insulation layer. Table 2-2 shows the typical U-value for a non-insulated timber wall. (SINTEF Byggforsk, 2013).

Table 2-2 - U-value timber (SINTEF Byggforsk, 2013). Included with permission from SINTEF.

Timber (mm)	U-value (W/m²K)
50	2,0
100	1,2
150	0,84
200	0,65
250	0,54

2.5 Building Information Modelling

Building information modelling (BIM) can be described as the process involved with a digital presentation of a building. The history of 3D modelling began in the 1970s following the early years of computer aided design (CAD) and has in many ways grown into an essential part of the modern age of the architecture, engineering, and construction industry (Volk et al., 2014). The benefits that BIM brings enhances processes related to the entire life cycle of a building, including project planning and implementation, facility management, rehabilitation work and demolition. All of this is based on a geometrically true model with a visual display of all relevant or desired information.

Traditionally, BIM has primarily been used for brand new structures but gradually researchers have developed techniques for generating as-built BIMs (Laefer & Truong-Hong, 2017). This includes utilization of image and laser scanning data which if captured using today's technology can be sub-millimetre accurate. The captured data can then be used to create a practically identical digital model to the one present in the real world.

2.6 Climate change and scenarios

Higher temperature, more frequent and intense precipitation and rise in sea level greatly threaten cultural heritage. Climate change, however, is depending on a large number of variables and it is difficult to predict with certainty what to expect in the second half of the 21st century. To accommodate this issue, climate models are continuously evolving to investigate the response of various forcing levels. This development is driven by more of the complex processes which define future climate included in the calculations, supplied by more advanced supercomputers. (Flato et al., 2014)

Climate models are produced at different scales, where general circulation models (GCM) show the earth's climate system on a global scale. Included in GCMs are many climate aspects of which are simulated over a three-dimensional grid around the earth (IPCC, 2014). As GCMs operates at such large scales it provides data with a relatively coarse resolution. Capturing local-scale effects is, therefore, dependent on scale projections which are done using techniques referred to as downscaling (Vaittinada Ayar et al., 2016). Two different methods are being used for this, which are empirical statistical downscaling (ESD) and regional climate models (RCM). While RCMs is created like GCMs, mainly separated by a denser grid, ESD is based on a statistical relationship between global and local variables and is largely used to supplement RCMs.

Euro-cordex, is the European branch of a coordinated regional climate downscaling experiment, funded by The World Climate Research Programme (EURO-CORDEX, n.d). This is one of 14 different cordex-domains which produces RCMs for its respective region with a dense grid size. Euro-cordex simulations produce its climate models with a grid size of about 12 km based on GCMs provided in the latest assessment report from IPCC. Furthermore, this is what is used in "Climate in Norway 2100", which is the basis for climate assessment in Norway (Hanssen-Bauer et al., 2017).

Representative concentration pathways (RCP) describe possible development in emissions and area utilization and is the last generation of scenarios which is developed in conjunction with the latest assessment report from IPCC, AR5. Hanssen-Bauer et al. (2017) describes a business as usual scenario (RCP8.5) with a rise in temperatures of 4,5 °C, increased precipitation of 18 % and an increase in mean sea level, depending on location along the coast, of 15-55 cm. These values vary within Norway and by seasons. Besides the scenario of RCP8.5, there are other scenarios reflecting a milder climate change, like RCP2.6, RCP4.5

and RCP6 (van Vuuren et al., 2011). The numbers represent the scenarios radiative forcing level at the year 2100 relative to before the industrial revolution (the year 1750). This is a value given in W/m^2 and describes the difference between the incoming energy from the sun and the energy emitted from the earth. (IPCC, 2014)

Unlike the three milder scenarios, RCP8.5 does not have any climate mitigation target, but is also characterized by rapid increase in population, modest improvements in technology and relatively low economic growth per capita (Riahi et al., 2011). This scenario, however, should be considered as it is stated in a report issued by the Norwegian government that high alternatives from national climate projections should be considered when consequences of climate change are assessed (Meld. St. 33 (2012–2013)).

Norsk Klimaservicesenter offers local climate profiles for the individual counties, largely based on (Hanssen-Bauer et al., 2017). Table 2-3 illustrates temperature increase for Vestfold county compared with the climate normal from the period 1971-2000 based on RCP8.5 for 2031-2060 and 2071-2100. (Norsk Klimaservicesenter, 2021)

Table 2-3 Temperature increase for Vestfold according to RCP8.5. Seasonal and annual increase compared to 1971-2000

Season	2031-2060		2071-2100	
	Low	High	Low	High
Winter	1,8	2,9	3,8	5,2
Spring	1,6	2,7	3,1	5,1
Summer	1,1	2,3	2,5	4,3
Autumn	1,1	2,5	3,1	4,7
Year	1,6	2,6	3,3	4,6

Looking at the median value, the annual expected temperature is expected to increase by about 4,0 °C, which is somewhat lower than the country as a whole. Furthermore, the greatest temperature increase occurs during the winter, while the lowest occurs during the summer. (Norsk Klimaservicesenter, 2021)

For precipitation, the median increase in annual precipitation following RCP8.5 is about 10 % in the 2071-2100 period for Vestfold County. Furthermore, both the intensity and frequency are expected to increase. These three elements are illustrated in Table 2-4 as seasonal and yearly data for their respective period following the low and high result of RCP8.5 (Norsk

Klimaservicesenter, 2021). There is a lot of uncertainty associated with future precipitation as there are large gaps in the results. Nevertheless, the greatest increase is during the first half of the year and the lowest during the second half, with some values illustrating a potential reduction. The numbers represent a percentage change compared to the period 1971-2000.

Table 2-4 Precipitation for Vestfold according to RCP8.5, Including winter (1), spring (2), summer (3) and autumn (4) and annual increase compared to 1971-2000

Precipitation		2031-2060					2071-2100				
		(1)	(2)	(3)	(4)	year	(1)	(2)	(3)	(4)	year
Sum	Low	1	1	-9	-8	5	17	8	-20	-14	6
	High	29	25	21	14	13	38	43	21	17	23
Intensity	Low	4	7	-4	-1	5	18	8	0	4	11
	High	20	23	29	14	13	43	43	45	27	29
Frequency	Low	26	26	-9	-8	22	103	26	1	22	47
	High	126	99	127	69	64	250	228	182	153	148

2.7 Biological degradation

Climate change may accelerate the degradation process of all assemblies of buildings, but especially vulnerable are those consisting of wood and other biological material. In these assemblies of materials, there is a natural degradation caused by bacteria, fungi and insects, which are greatly dependent on temperature and humidity (Kaslegard, 2010). Therefore, this process is affected by the change in these conditions. The extent to which climate change is affecting buildings with biological material can be illustrated with numbers from (Almås et al., 2011). According to this article, the number of buildings in Norway located in areas with a high potential risk of rot-decay can be 2,4 million in 2100. This number is approximately 3,9 times greater than what was the case of 2011.

Figure 2.9 illustrates the risk of rot-decay across Norway with the figure to the left from 1971 to 2000 and figure to the right from 2071 to 2100.

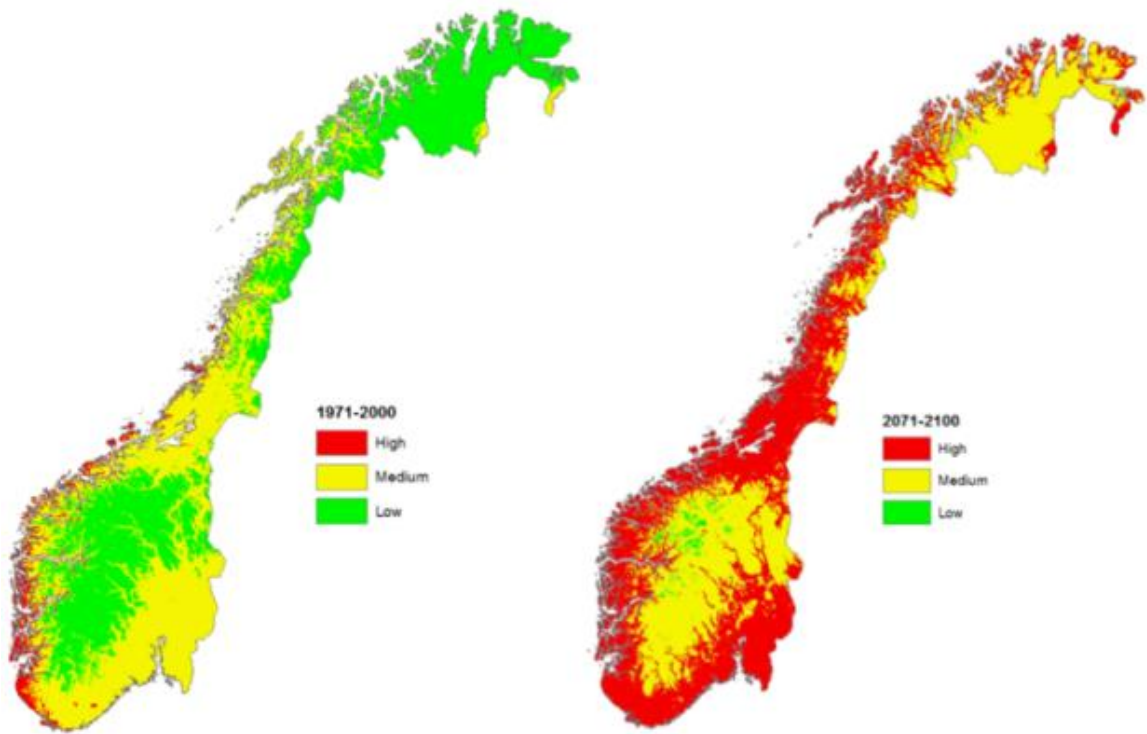


Figure 2.9 Risk of rot-decay in Norway. Translated from The Norwegian Meteorological Institute

3 Method

Answering the research question of this master thesis has been done using quantitative research including primary and secondary data to ultimately evaluate the hygrothermal performance of Bentegården with current and future climate. A 3D scanning has been performed to create a digital model of the building. Supplied by historical documentation, local knowledge and infrared thermography, this has created a basis for determining the hidden elements within the building envelope. Numerical simulations have been conducted for the different wall assemblies with current and future climate data primarily based on observed data from weather stations and scenario RC8.5. Figure 3.1 displays an overview of key elements included.

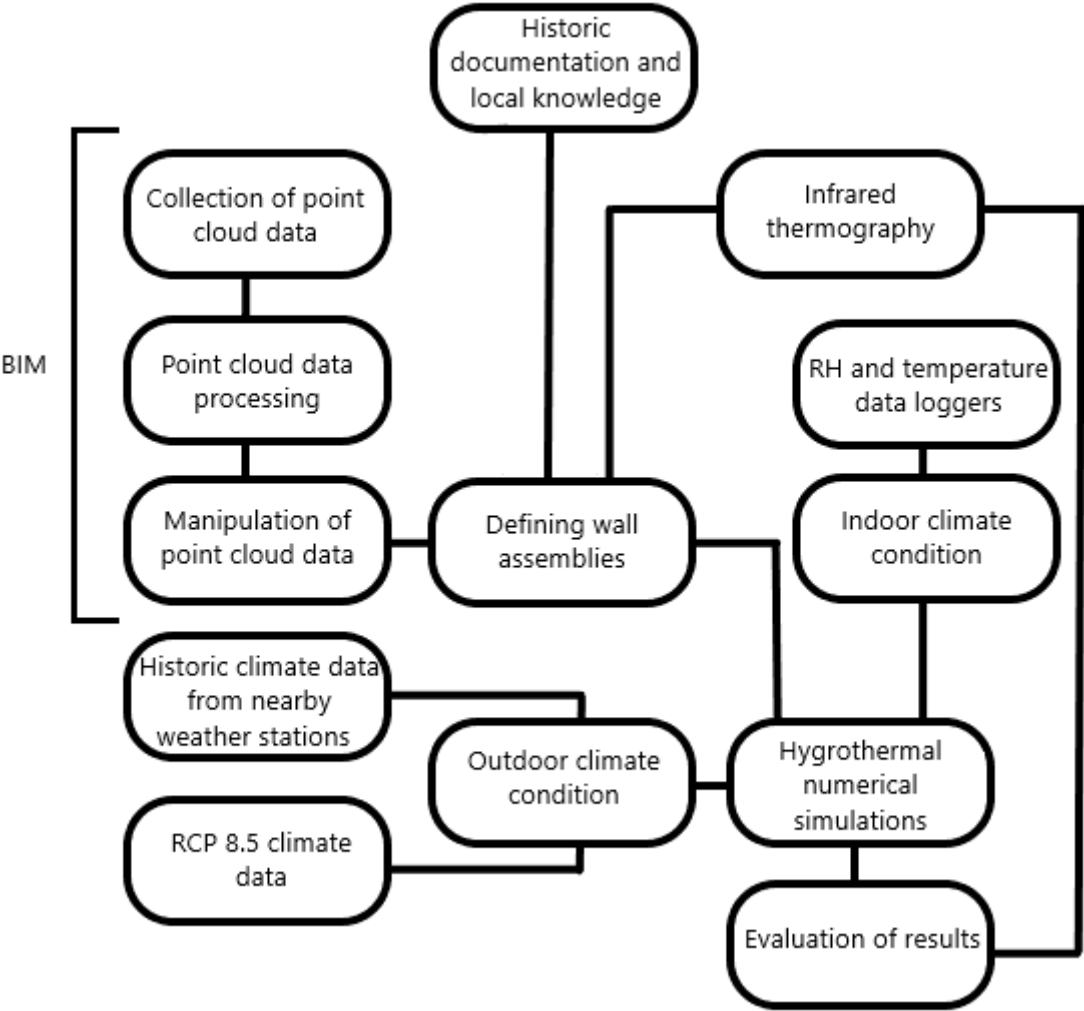


Figure 3.1 Overview of key elements

3.1 Experimental site - Bentegården

The experimental test site of Bentegården is located in Tønsberg municipality which is a part of Vestfold- and Telemark County in the south-eastern part of Norway, Figure 3.2. Tønsberg can be described as a medium-sized municipality by Norwegian standard with a population of about 57 000 (SSB, 2021), and is for a reference located about a 100 km drive south from the capital of Oslo. The location of Bentegården in Tønsberg is illustrated in Figure 3.3.



Figure 3.2 Location of Bentegården

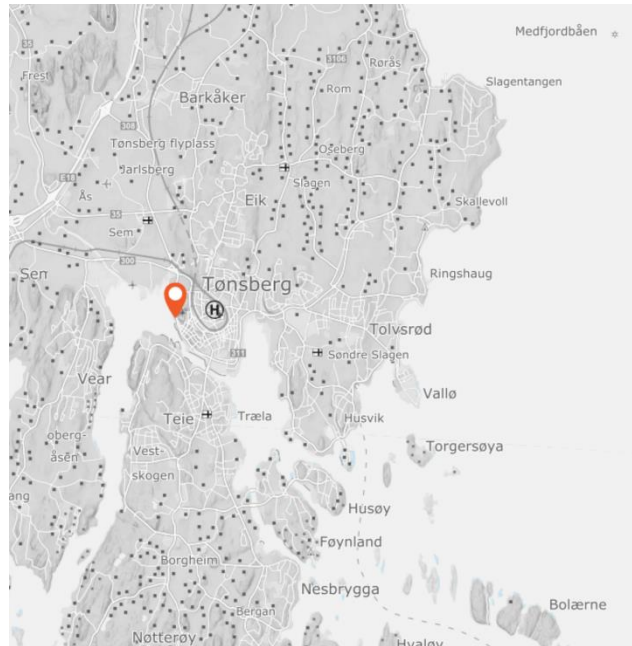


Figure 3.3 Location of Bentegården in Tønsberg

Tønsberg is considered the oldest city in Norway and consists of several cultural heritage buildings located in several districts. The area in which Bentegården is located is called Nordbyen, characterized by low raised wooden houses with sheds and boathouses along the coastline to the southwest. Located to the northeast of Nordbyen is Slottsfjell, a well-known landmark containing ruins from the Middle Ages.

Bentegården, Figure 3.4, is considered the oldest house in Tønsberg with a history that stretches back to the end of the 17th century and was built as a typical home consisting of a farmhouse and a shed. The building is named after Bent Knutsen who bought it in 1881 and is one of two buildings in Nordbyen being protected. The building is 2 storeys high with a basement accessed from the outside going under the living room and library. Furthermore, it can be seen as consisting of an original section and an extension.



Figure 3.4 Bentegården seen from southeast. Photo by Kris A. Flaskerud



Figure 3.5 Bentegården seen from northeast. Photo by Kris A. Flaskerud

The entrance to the building is located in the extension observed in Figure 3.5, leading into a small entrance hall. The plan drawing of the 1st floor is presented in Figure 3.6. The first floor of the extension includes a storage room and kitchen. The original section of this floor further consists of a living room, library, TV-room and the former entrance, now used as a storage room.



Figure 3.6 – 1st floor plan drawing

The original section of the second floor, Figure 3.7, consists of a recreational room and two bedrooms. A bathroom, WC and a cold storage room make up the area for the extension.

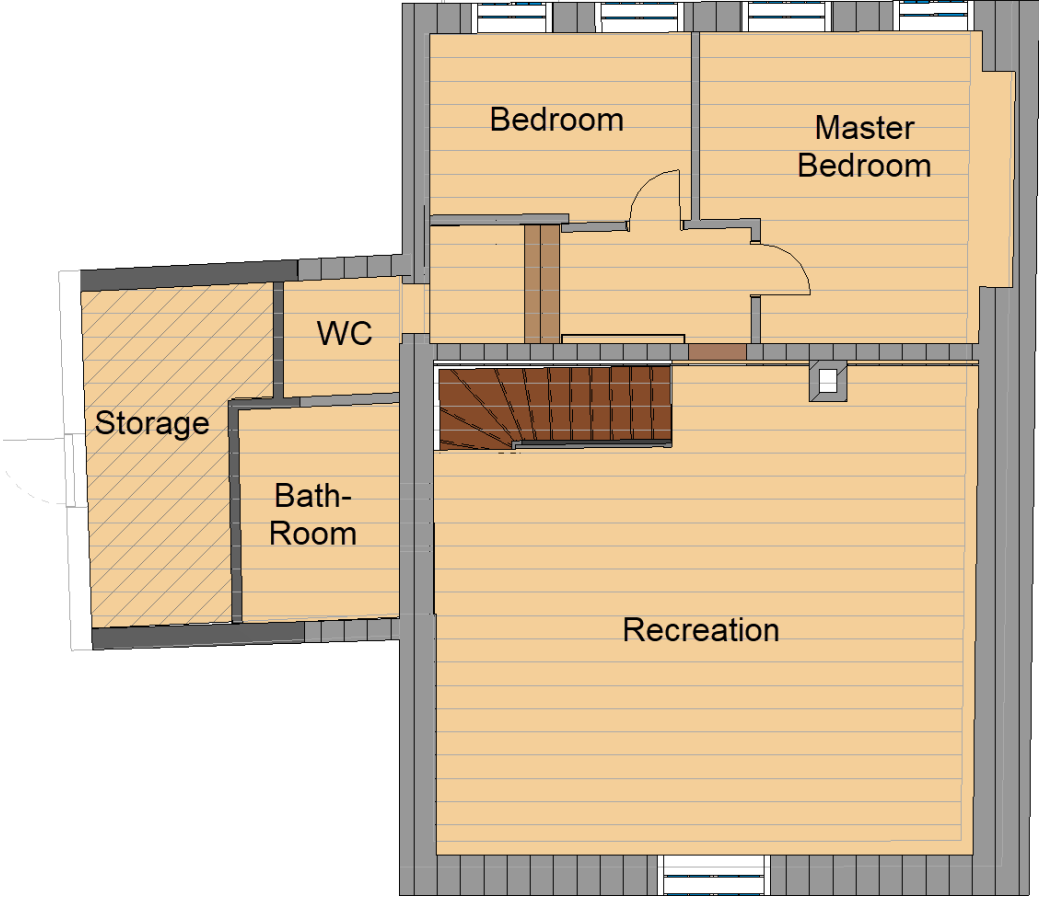


Figure 3.7 - 2nd floor plan drawing

3.2 Data collection

3.2.1 Available documentation and local knowledge

During a preliminary study, an effort was made to collect as much information as possible about Bentegården from archives available online in databases like *Askeladden* and documentation from previously performed work. This work has continued, including observations on historic images previously overlooked or not considered relevant and information gathered from people familiar with the building. The latter is not gathered using a form of structured interviews, but as conversations either through scheduled meetings, by mail, phone calls or during the fieldwork. The contributors through these conversations are Jørgen Solstad and Sissel Øvrid. Solstad is responsible for construction matters that may affect listed buildings and facilities in Vestfold and Telemark County and Øvrid is one of the current residents of Bentegården.

3.2.2 Fieldwork

In cases where there is a lack of documentation regarding information about the characteristics of a building and its condition, non-destructive testing may serve purposefully to clarify this gap. This is especially true for historic buildings as documentation of measures far back in time were less common or is difficult to access.

There are several different methods characterized as non-destructive which through a hybrid workflow can uncover a large variety of information about the building envelope (Masri & Rakha, 2020). This includes methods such as for example infrared thermography and laser scanning which compose the non-destructive methods utilized in this thesis.

The planning of these activities was highly influenced by the uncertainties related to covid-19. During the project planning for the preliminary project and the master thesis, a rough schedule was made for the activities related to the fieldwork. This consisted of two or three visits to Bentegården and was intended to be executed during the autumn of 2020. This plan included a first visit with the intention of performing an airtightness test and thermography, potentially including a 3D laser scan of the building. If all this could not be done on the same day, the 3D laser scan was thought to be performed on the second visit. These two visits were intended to be done in October because the data was supposed to be used in the preliminary project. During the next month of November, a third visit was intended to mount the data loggers, as the data gathered from these were not intended to be used until the work with the master

thesis. Due to some uncertainties, including more restriction because of the Coronavirus, all of these activities had to be postponed until the spring of 2021.

On February 5th, 2021 the first visit to Bentegården was made. During this visit, the entire building got scanned using a 3D laser scanner and infrared thermography capturing were done. Additionally, data loggers were mounted.

3.3 Infrared thermography

The method of infrared thermography intends to visualise the distribution of temperature on the surface of the photographed area. This technique utilizes the radiation which is emitted from all surfaces with a temperature above absolute zero. In the occurrence of thermal contrasts in the captured images, this can potentially provide information about the material composition, interference of different components or defects (Mercuri et al., 2015).

Furthermore, infrared thermography is being described as extensively used due to technical advancement and relatively cheap equipment.

When working with infrared thermography in non-destructive testing, it is distinguished between two different approaches which are passive and active (François et al., 2021). The former represents an approach where the infrared thermography is capturing the situation based on natural heat sources. This requires an exterior and interior temperature difference of about 10 °C to form a measurable heat flux (Glavaš et al., 2019).

Active thermography corresponds to the use of artificial heat sources, like lamps, hot or cold temperature air guns or other devices that cause vibration on the surface. This method is often referred to as computer-aided thermography, as the camera can be connected to a computer and has the sensitivity of the measurements multiplied by a hundred. This method may provide information about deeper levels of an assembly, but the measuring time increases substantially (Glavaš et al., 2019).

In this study, the infrared thermography has been performed with the purpose of supplementing the work of revealing information about elements within the building envelope and locating thermal bridges and infiltrations. This got executed using the technique of passive thermography. On the day this work got carried out, the exterior temperature was read to be about -4,5 °C, which constituted optimal conditions. A report of the process is included in APPENDIX F.

The infrared thermography was performed using an IR-camera called Fluke Ti105. This device got a 3,5-inch LCD screen with a resolution of 160x120 and is able to capture infrared images with a thermal sensitivity of 80 mK within a temperature range of -20 to +250 °C. Figure 3.8 shows the device in question being operated during the fieldwork at Bentegården.



Figure 3.8 IR-camera Fluke Ti105. Photo by Kris A. Flaskerud

A total of 86 IR images was captured during the fieldwork and has been evaluated concerning surface temperature and locating air infiltrations and thermal bridges and their extent.

3.4 3D laser scanning and Revit modelling

The technique of 3D laser scanning utilizes a laser beam to measure the distance between a device and a solid surface, creating a digital point. As the device rotates, this produces a large number of digital points, ultimately forming a point cloud in an X-Y-Z coordinate system. Based on the technical parameters of the device, a point cloud can be created with varying quality, including for example the distance between each individual point.

Seen in the context of this thesis an important step towards understanding how Bentegården is built comes from getting a good as possible overview of the geometry of the building. With an accurate digital model of Bentegården, it enables the possibility of reading the thickness of the building components, area and volume. Additionally, it simplifies the job of making updated floor plans with correct dimensions and room division.

The entire modelling process can be divided into three main steps, which includes point cloud data collection, point cloud data processing and manipulation of the point cloud data, later referred to as Revit modelling.

3.4.1 Point cloud data collection

3D point clouds were collected using a Leica BLK360 Imaging Laser Scanner, which is a portable tool that can be placed on adjustable legs. This scanner is capable of generating point clouds at a point measurement rate up to 360 000 points per second with a ranging accuracy of 4 mm at 10 m distance and 8 mm at 20 m distance. According to the producer it weighs 1 kg, got a height of 165 mm, a diameter of 100 mm and is equipped with a camera system capable of capturing images at a 360° horizontal and 300° vertical field of view. Figure 3.9 and Figure 3.10 illustrates the scanner during the fieldwork.



Figure 3.9 - Leica BLK360 #1. Photo by Kris A. Flaskerud



Figure 3.10 - Leica BLK360 #2. Photo by Kris A. Flaskerud

On-site the scanner was coupled with the operators' phone using a mobile-device app called Cyclone FIELD 360. This gave the opportunity for adjusting the settings prior to the scanning in addition to examine the captured scan and image data. Although the process of point cloud data collection is fully capable of being executed without this app, it is a great tool for ensuring the quality of each individual scan and the connection between them.

As the aim was to make the finalized model of Bentegården as identical as possible to the real building, a great deal of focus was on making sure that all areas were included and that the connection between the individual scans was sufficient. As Cyclone FIELD 360 was used during the work, scans that did not fulfil these criteria could easily be replaced. In some areas, it was necessary to make several scans due to complex geometry. The location of the scanner position for all individual scans is illustrated below. Figure 3.11 presents the different positions at 1st floor, Figure 3.12 the positions at 2nd floor, while Figure 3.13 presents the positions of each scan of the exterior. The process is documented in APPENDIX E.

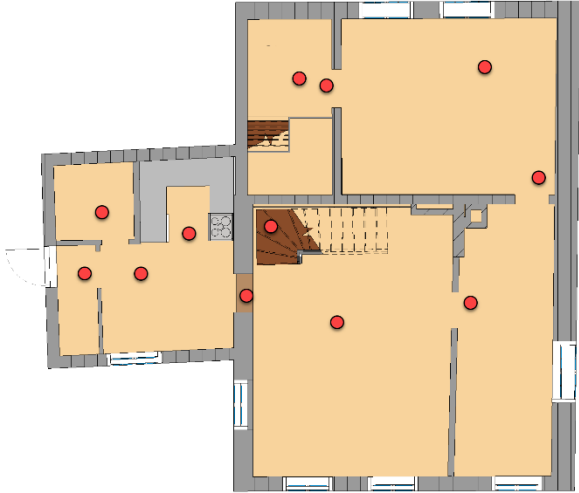


Figure 3.11 - 1st floor, position of each scan

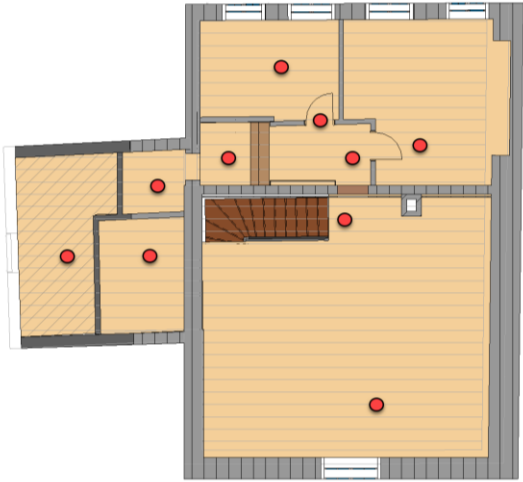


Figure 3.12 - 2nd floor, position of each scan

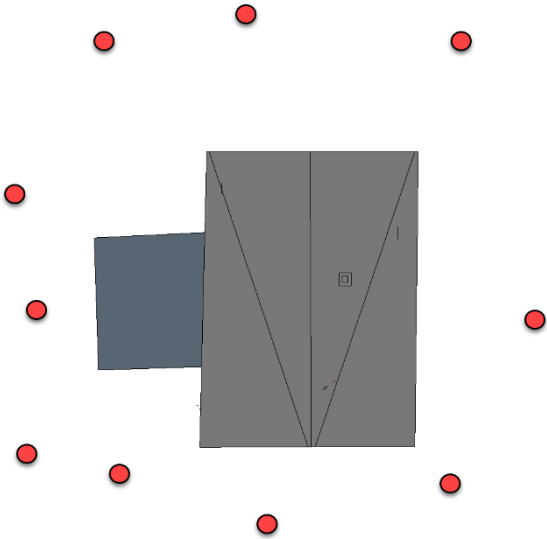


Figure 3.13 - Exterior side, position of each scan

3.4.2 Point cloud data processing

Following the procedure of collecting the point cloud data it is required to process them. This includes finalization of the connection between each individual scans and removal of excess points to create a bundle of point clouds which are easier to work with during the next part of the process and requires less computing power.

The program used for this work is Leica Cyclone REGISTER 360. As this program is created by the same company of which delivers the scanner and the program used during the data collection, it creates an intuitive transition between the process of collecting and operating the data. The work included in this part of the process has been aided by Ernst Erik Hempel from OsloMet who has expertise with digitalization through the use of three-dimensional models of buildings.

The individual scans got connected to form three sets of point cloud bundles, including the exterior section, first floor and second floor. Figure 3.14 and Figure 3.15 illustrates the bundle from the exterior side of Bentegården. The red points indicate the positions of each scan, while the green line indicates the connection between each scan. The figures on the left side also display the exterior walls registered by the laser, while the figures on the right-side display objects registered by the camera. Figure 3.16 and Figure 3.17 represents the cloud bundle of the interior side of the 1st floor. Figure 3.18 and Figure 3.19 represents the cloud bundle of interior side of the 2nd floor.

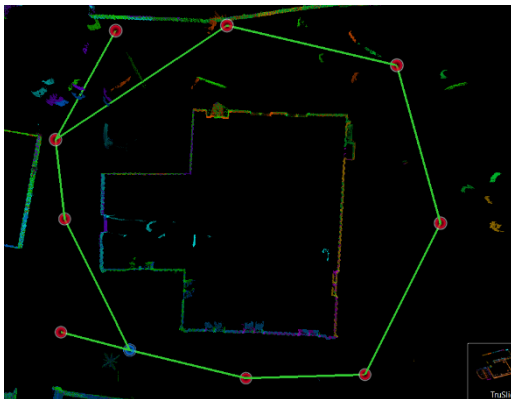


Figure 3.14 Point cloud bundle of exterior scans

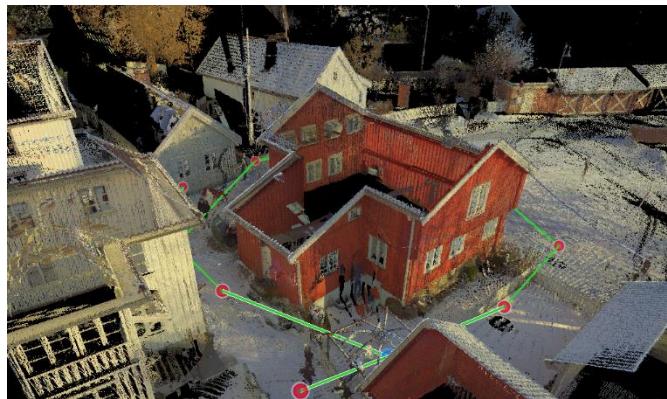


Figure 3.15 Point cloud bundle of exterior scans



Figure 3.16 Point cloud bundle of interior scans 1st floor

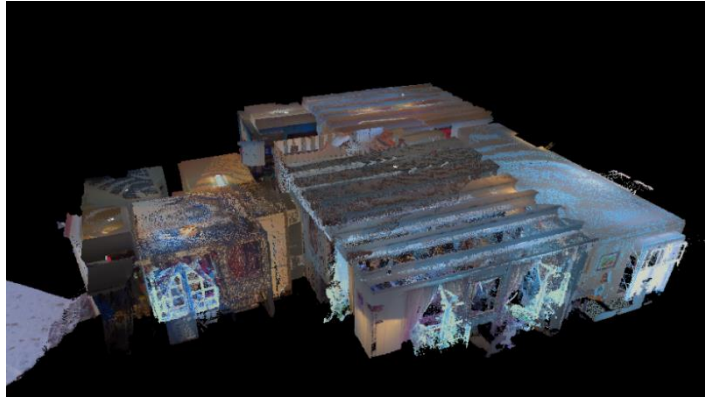


Figure 3.17 Point cloud bundle of interior scans 1st floor

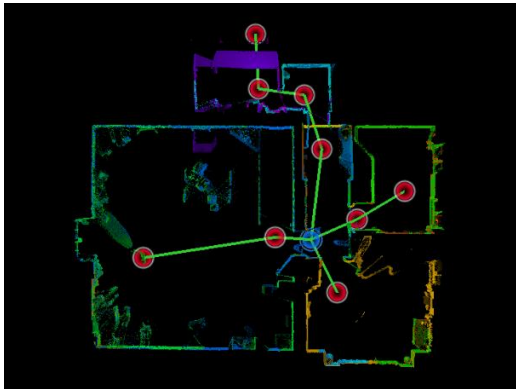


Figure 3.18 - Point cloud bundle of interior scans 2nd floor



Figure 3.19 - Point cloud bundle of interior scans 2nd floor

The next step involved connecting the three individual bundles. Connecting the first and second floor went without any major difficulties, as there were sufficient common points on and around the stairs connecting the two floors. Connecting the interior part to the exterior part, however, did not provide an acceptable result using the method of connecting common points. As the main entrance was the area with the only connection between interior and exterior, a small rotational offset caused a significant difference at the opposite end of the building. In hindsight, some scans should have been taken with open windows to better the connection. Because of this issue, these two bundles had to be fitted manually, which was done within the modelling program, Revit. The point cloud data processing is documented in APPENDIX G.

3.4.3 Revit modelling

In the process of modelling the finalized point cloud model function as a 3D-sketch of which the 3D model can be modelled after. This is executed using Revit, which is a BIM software delivered by Autodesk. The procedure of creating the Revit model is documented in APPENDIX H.

3.5 Hygrothermal numerical simulations

Computer-based hygrothermal simulations serve the purpose of providing valuable information regarding how the building envelope responds to the interior and exterior environment (Glass et al., 2013). Concerning this thesis, it is the most essential tool for answering the research questions and the input for the simulations is based on every other method utilized.

3.5.1 WUFI Pro

The specific program used for the simulations in this thesis is WUFI Pro. WUFI Pro is used to determine the hygrothermal performance of a building component based on real climate conditions, including built-in moisture, driving rain, solar radiation, long-wave radiation, capillary transport, and summer temperature based on one-dimensional calculations.

WUFI is a family of software developed by the German company Fraunhofer IBP. The initials stand for *Wärme- Und Feuchtetransport Instationär*, which can be translated to non-steady heat and moisture transport. The development and marketing of the WUFI Software family began in 1995 and consist today of various software with different compatibility within building component simulation and whole building simulation.

The non-steady heat and moisture transport in WUFI are based on the coupled differential equations showed in Equation 2 and Equation 3, where Equation 2 is the heat transport and Equation 3 is the moisture transport. The two equations include storage terms on the left part and transport terms on the right part. Included in the heat storage of the equation are the dry materials heat capacity and the heat capacity of the moisture in the material. The moisture storage is based on the derivative of the moisture storage function. As illustrated in Equation 2, the heat transport is the sum of the moisture-dependent thermal conductivity and the vapour enthalpy flow. The moisture transport illustrated in Equation 3 is based on the sum of the liquid transport and vapour diffusion.

$$\frac{\partial H}{\partial \vartheta} \frac{\partial \vartheta}{\partial t} = \frac{\partial}{\partial x} \left(\lambda \frac{\partial \vartheta}{\partial x} \right) + h_v \frac{\partial}{\partial x} \left(\frac{\delta}{\mu} \frac{\partial p}{\partial x} \right) \quad \text{Eq. 2}$$

$$p_w \frac{\partial u}{\partial \varphi} \frac{\partial \varphi}{\partial t} = \frac{\partial}{\partial x} \left(p_w D_w \frac{\partial u}{\partial \varphi} \frac{\partial \varphi}{\partial x} \right) + \frac{\partial}{\partial x} \left(\frac{\delta}{\mu} \frac{\partial p}{\partial x} \right) \quad \text{Eq. 3}$$

D_w	<i>Liquid transfer coefficient</i>	(m^2/s)
H	<i>Enthalpy of moist building material</i>	(J/m^3)
h_v	<i>Evaporation enthalpy of water</i>	(J/kg)
p	<i>Water vapour partial pressure</i>	(Pa)
u	<i>Moisture content</i>	(m^3/m^3)
δ	<i>Water vapour diffusion coefficient in air</i>	$(kg/msPa)$
ϑ	<i>Temperature</i>	$(^\circ C)$
λ	<i>Heat conductivity of moist material</i>	(W/mK)
μ	<i>Vapour diffusion resistance factor of dry material</i>	$(-)$
p_w	<i>Density of water</i>	(kg/m^3)
φ	<i>Relative humidity</i>	$(\%)$

3.5.2 Classification of mould risk and WUFI Bio

The development of mould growth is a complex process with its boundary conditions depending on temperature, moisture and substrate over a certain period of time (Sedlbauer, 2002). Furthermore, mould growth on exterior surfaces can be affected by other factors like, UV-radiation, washing by rain, standing water and frost which can accelerate or mitigate mould growth (Viitanen et al., 2015a).

A well-established mathematical model for mould growth is the *VTT Model*, developed at the Technical Research Centre of Finland (Viitanen et al., 2015a). The initial model was created by A. Hukka and H. A. Viitanen based on perilously performed experiments evolving material consisting of small samples of pine and sapwood (Hukka & Viitanen, 1999). Further development of the model included a larger verity of material classifications according to their mould growth sensitivity (Ojanen et al., 2011).

The mould growth index developed in the VTT model is based on a visual description, ranging from 0 to 6. The description of growth rate is not only based on what is observable with the naked eye, but also with the help of a microscope as the growth coverage can be substantial also in this area (Ojanen et al., 2011). Table 3-1 shows the different mould index values and their respective description of growth rate.

Table 3-1 Mould index and description of growth rate

Index	Description of growth rate
0	No growth
1	Small amount of mould on surface (microscope), initial stages of local growth
2	Several local mould growth colonies on surface (microscope)
3	Visual findings of mould on surface, < 10 % coverage, or < 50 % coverage of mould (microscope)
4	Visual findings of mould on surface, 10 - 50 % coverage, or >50 % coverage of mould (microscope)
5	Plenty of growth on surface, > 50 % coverage (visual)
6	Heavy and tight growth, coverage about 100 %

Equation 4 represents the original VTT model for defining the mould growth intensity, where both W and SQ are values based solely on the type of wooden materials and their surface quality (Ojanen et al., 2011).

$$\frac{dM}{dt} = \frac{1}{7 \cdot \exp(-0.68 \ln T - 13.9 \ln RH + 0.14W - 0.33SQ + 66.02)} k_1 k_2 \quad \text{Eq. 4}$$

With the further development of the model, the values of k_1 and k_2 intend to represent coefficient for growth intended to scale the model to include other materials than pine and sapwood. More specifically, k_1 is an intensity coefficient based on the growth level, while k_2 represents a moderation of the growth intensity as the mould index, M reaches maximum.

Based on experimental research, four different sensitivity classes (very sensitive, sensitive, medium resistant and resistant) were developed and parameters for the different sensitivity classes form the basis for input in numerical simulations using the VTT model. (Ojanen et al., 2011)

Another well-established model for predicting mould growth is a model developed by Fraunhofer Institute for Building Physics (Sedlbauer, 2001). The procedure of this biohygrothermal model allows for the assessment of mould growth exposed to transient boundary conditions. Similar to the VTT-model, the IBP-model categorises the substrate into four groups, referred to as substrate group 0, I, II and III. Unlike the empirical VTT-model the IBP-model is theoretical and while the former includes a climate-specific maximum value, the IBP-model allows for a continuation of mould growth considering the conditions are suitable (Viitanen et al., 2015b).

In Viitanen et al. (2015a), VTT and IBP have been collaborating to create a transfer function between their respective models. This allows for the results from the IBP-model to be interpreted in the mould index categorization system of the VTT-model. Additionally, an intuitive traffic light system has been developed to help visualise the risk of which the simulated conditions indicate in terms of mould growth in the specific components.

The traffic light indicator includes the colours green, yellow and red. Green represents an acceptable risk of mould growth which is inevitable in any type of building, while red represents a serious risk to indoor air quality. In the case of yellow traffic light, there is some uncertainty related to the risk of mould growth. In this case, it is up to the user to evaluate whether it is acceptable for the specific project. (Viitanen et al., 2015a)

Included in the WUFI family are add-ons of which can be used together with the main software to gather additional information within the area of interest. One such add-on is WUFI Bio, which can be used to evaluate the mould growth based on the description above. The traffic light system of which indicate acceptable limits of mould growth can be influenced by defining occupant exposition class. There three different classes:

- (1) Indoor surface or positions in contact to indoor air
- (2) Surfaces inside constructions without direct contact to indoor air
- (3) No impact on occupants expected

Growth occurring on locations resulting in less harmful effects on human health increases the acceptable limits within three traffic light categories. The following mold-index, M applies:

- | | | |
|-----------------------|------------------------|---------------|
| (1) Green: $M \leq 1$ | Yellow: $1 < M \leq 2$ | Red: $M > 2$ |
| (2) Green: $M \leq 2$ | Yellow: $2 < M \leq 3$ | Red: $M > 3$ |
| (3) Green: $M \leq 3$ | Yellow: $M > 3$ | Red: no limit |

3.5.3 Outdoor climate conditions

Defining the outdoor climate in WUFI can be done either by using climate files for certain locations supplied with the program or by selecting a user-defined file. In this thesis climate data has been gathered from various weather stations in the area surrounding Bentegården and supplied with completed climate files from another Hyperion-related project produced by Ph. D candidate Petros Choidis.

A total of three different sets of climate data have been used to form the basis for evaluating the following scenarios:

- 1) The current climate based on real data from 2010-2021.
- 2) The current climate according to RCP8.5.
- 3) Climate predictions according to RCP8.5.

The RCP8.5 climate models are created with the hydrostatic version of REMO2015 driven by a global model MPI-ESM-LR with data acquired from EURO CORDEX. A total of three periods has been created based on this method, referred to as historic (1960-1970), current (2010-2020) and future (2060-2070). Only the latter two will be used in this thesis.

Included in the work related to this thesis, climate data is gathered to include observed data from the period 2010-2021. This has been done by gathering relevant hourly data directly using Seklima, provided by *Klimaservicesenter*. The exception is radiation, which are values calculated using solrad.xls (version 1.2), which is a solar position and radiation calculator developed by the Washington State Department of Ecology and is based on models from Bird and Hulstrom (1981), Bras (1990) and Ryan and Stolzenbach (1972). This resulted in a one-year hourly series of data, including direct-, diffuse- and global radiation, which got utilized for the entire period.

With the exception of radiation, all climate parameters are collected from the weather station Melsom, located approximately 6,5 km from Bentegården. More specifically, this includes temperature, relative humidity, precipitation, wind direction and wind speed. For most of the climate parameters, a varying number of hours were missing for various reasons. For some years this only counted for a few or no hours, but for others up to tens of hours, which out of the 8760 hours in a common year arguably is neglectable. Nevertheless, this had to be located and data had to be inserted.

481800 observed sets of observed climate data supplemented by the calculated solar radiation was then used as input in a macro-enabled spreadsheet in excel which can convert the data into a file suitable for WUFI.

Figure 3.20 illustrates the location of Bentegården (1) and the two weather stations utilized to gather data for this thesis. In addition to Melsom (3), climate data from Tønsberg gjestebrygge (2) has been used to validate the data gathered from data loggers mounted at the experimental site. This is described in detail in the next subchapter.

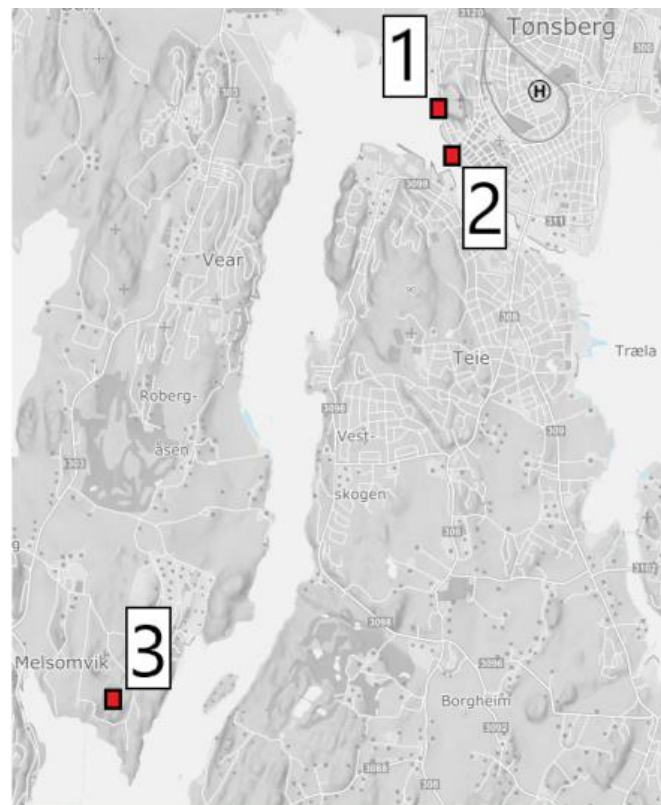


Figure 3.20 - Location of weather stations (2 & 3) and Bentegården (1). Created using a map from norgeskart.no

3.5.4 Indoor climate conditions

There are three different models within WUFI Pro that can be used to define the interior climate. One model uses a sine-shaped curve over a one-year period, while the other two are based on the standards EN 13788 and EN 15026. The two unique standards serve as simplified calculation methods for the complex nature of moisture transfer. What differs the calculation methods is mainly the algorithm for deriving the indoor climate from the outdoor conditions.

EN 13788 derives the interior humidity based on the outdoor humidity. Furthermore, it classifies the interior moisture excess based on humidity classes, characterized by the expected usage of the building. The standard operated with five different humidity classes:

- (1) *Unoccupied buildings, storage of dry goods.*
- (2) *Offices, dwellings with normal occupancy and ventilation.*
- (3) *Buildings with unknown occupancy.*
- (4) *Sports halls, kitchens, canteens.*
- (5) *Special buildings, e.g., laundry, brewery, swimming pool.*

For all humidity classes, the moisture excess is considered with a constant maximum value, ΔV_{max} when the outdoor temperature is at 0 C° or lower. When the outdoor temperature increases ΔV reduces linearly until it reaches 20 C°. At this point, no moisture excess is included in the calculations. This reduction in ΔV is based on an assumption that occupants tend to use more natural ventilation with increasing temperatures e.g., opening windows. All of this is illustrated graphically in Figure 3.21.

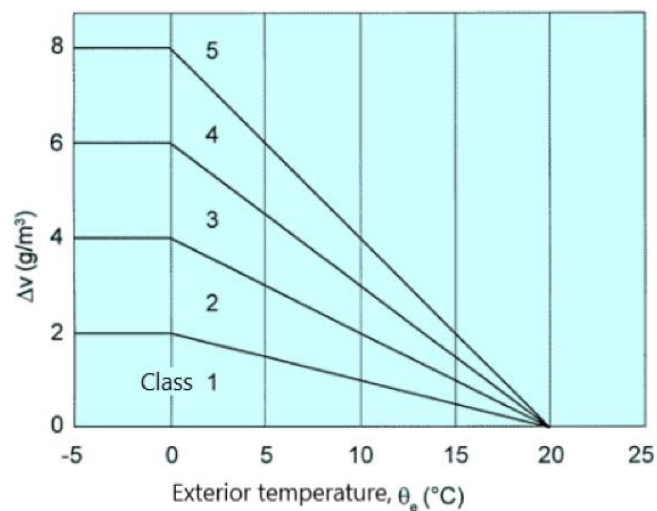


Figure 3.21 Humidity classes, translated from (SINTEF Byggforsk, 1999). Added with permission from SINTEF

Unlike EN 13788 the standard EN 15028 derives the interior moisture level directly based on the outdoor temperature. The equations used in this standard considers a constant a constant indoor temperature of 20 C° when the outdoor temperature is below 10 C°, and a constant indoor temperature of 25 C° with outdoor temperatures above 20 C°. In between these values, there is a linear increase.

A similar distribution is also applied for the relative humidity indoors, although instead of a lower limit of 10 C°, it is set to -10 C°. For normal moisture load, the range of the relative humidity is from 30 to 60 %. When the moisture load is specified as high 10 % is added to these values.

To accurately measure the temperature and relative humidity, data loggers with this capability were mounted at various location at Bentegården. Even though climate data has been gathered both outside and inside, it is strictly used to evaluate the interior conditions. With these climate data, it opens the possibility of calculating the moisture production within the building which in turn can be used to define the humidity class used in the simulations.

Six loggers were installed, whereof four got placed within the building to measure the interior conditions and two got installed outside. The four loggers inside are of the type PeakTech 5180, while the two outside are of the type Extech RHT10. An additional Extech RHT10 logger got placed inside at a later time. The procedure of installing the loggers is documented in APPENDIX D.

PeakTech 5180, Figure 3.22, can store up to 67 000 readings per measurements with a sampling rate that can be specified between 1 second and 12 hours. Its battery is dependent on the settings but is according to the producer capable of gathering data for 3 months with a sampling rate of five seconds.

Extech RHT10, Figure 3.23, got a more limited memory compared with PeakTech 5180 but got longer battery life. More specifically it can store up to 16 000 readings over a period of approximately one year.



Figure 3.22 - PeakTech 5180 logger. Photo by Kris A. Flaskerud



Figure 3.23 - Extech RHT10 logger. Photo by Kris A. Flaskerud

Both loggers operate with similar accuracy with respect to temperature of ± 2 °C for the intervals of -40 to -10 °C and 40 to 70 °C, and ± 1 °C for -10 to 40 °C. For the relative humidity, Extech RHT10 indicates an accuracy of ± 3 % for all values, while PeakTech 5180 differentiate with ± 3 % (40-60 %), ± 3.5 % (20-40 % and 60-80 %) and ± 5 % (0-20 % and 80-100 %).

The position of all six loggers is illustrated in Table 3-2, Figure 3.24 and Figure 3.25. All of the loggers indoors are placed in a position where they are above medium height in their respective rooms, while the loggers outside are completely or partially shaded from direct sunlight. All loggers are specified with a sampling rate of 300 seconds (5 minutes).

Table 3-2 – Location of loggers

Nr.	Room
1	Living room
2	Library
3	TV-room
4	Recreational room
5	West façade
6	North façade

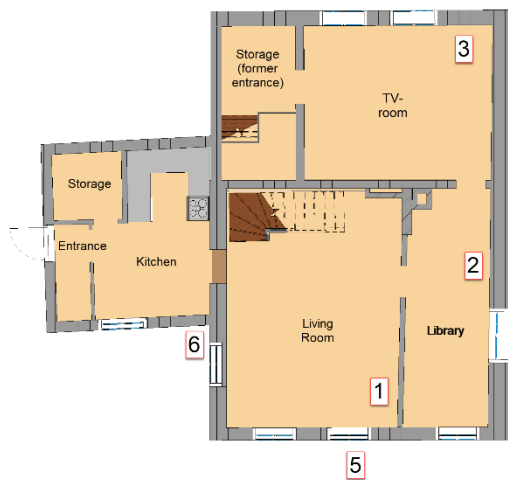


Figure 3.24 - 1st floor, location of loggers



Figure 3.25 - 2nd floor, location of loggers

Information from the data loggers has been gathered on two separate occasions. A first reading was done 19.03.21. During this visit the loggers mounted on the west and north façade (5 & 6) got their data collected and reset due to its limitations in terms of storage. Furthermore, an additional logger got mounted on the second floor, as there were some concerns regarding logger 4.

A second and final reading was completed 19.04.21, where data from all loggers were gathered. Unfortunately, all the PeakTech 5180 loggers had stopped logging at different times. This is not caused by lack of memory, as the number of samples gathered by any of the loggers is far from its capacity of 67 000 readings. It is plausible that they stopped because of power shortage. Regardless of reason, their log time is shorter than what was expected, especially for logger 2 and 4, which got data for about 17 days and 16 days, respectively. The log time of logger 1 and 3 is well above or within the range of a minimum desired log time of around one month. Table 3-3 presents the logger data collection samples, start/end-time and log time.

Table 3-3 Logger data collection

Logger	Samples	Start time	End time	Log time
Living room (1)	23431	05.02.21 09:15:07	26.03.21 04:45:07	48D19H33M
Library (2)	8442	05.02.21 09:15:00	22.02.21 23:18:00	17D14H6M
TV-room (3)	14120	05.02.21 09:15:01	07.03.21 19:12:01	29D10H0M
Recreational room (4)	8038	05.02.21 09:15:00	22.02.21 03:06:00	16D17H54M
	8903	19.03.21 14:32:46	19.04.21 12:22:46	30D21H50M
West façade (5)	21024	05.02.21 12:35:09	19.03.21 14:30:09	72D21H52M
		19.03.21 14:40:01	19.04.21 12.35.01	
North façade (6)	21058	05.02.21 09:35:05	19.03.21 14:25:05	73D2H40M
		19.03.21 14:43:39	19.04.21 12.33.39	

3.5.5 Defining components and initial conditions

Before running any simulations, all components and initial conditions need to be properly defined. For individual components within the assembly, the software provides a material database including materials sourced from different institutes from a variety of countries, including for example Fraunhofer-IBP and the Norwegian University of Science and Technology (NTNU). Additionally, orientation, surface coefficients need to be decided. The latter, as well as the initial conditions of relative humidity and temperature within the assemblies are carefully selected and tested prior to implementation on the actual simulations. This was primarily done to exclude any misleading results caused by input data of which to some extent had to be based on assumptions.

Prior to the presentation of the results gathered from the hygrothermal simulations, the different assemblies and other relevant input data will be illustrated. This is done due to the progressive nature of the work related to the thesis, where this data is highly dependent on results produced and illustrated throughout chapter 4.

4 Results

4.1 Construction and rehabilitation history of Bentegården

Included in this first part of the result is the information gathered from available documentation and local knowledge which forms a basis for systematically describe the important part of the thesis that is the construction and rehabilitation history of Bentegården.

When referring to local knowledge this is namely Solstad, which is responsible for construction matters that may affect listed buildings and facilities in Vestfold and Telemark County and Øvrid which is one of the current residents of Bentegården.

Solstad has good knowledge about historic building traditions and materials. His professional input has clarified uncertainties related to the composition of certain walls and areas with a potential history of rot. According to him, log buildings were commonly built with a square shape, and any extensions, usually built at a later time is not constructed using the same method. This substantiates a claim from Øvrid that the extension was not a part of the original building and does not consist of log walls. Additionally, Solstad mentioned that a common practice around the 70s was to use post-insulation as a reactive measure for areas where it was felt needed to better the comfort. By this is meant that it was common to mount post insulation wall by wall.

Solstad also provided information regarding the surface treatment of the façade and internal walls of Bentegården. The exterior cladding on the south and west façade was treated with pure linseed oil when replaced. The other walls with older cladding consist of a surface of several layers with paint, where most of the layers are supposed to be linseed oil, but some of the layers with elements of alkyd oil-based paint. Paint layers from before 1960 are pure linseed oil, while those between 1960 and 1990 probably consist of alkyd oil-based paint. Furthermore, the interior surface treatment history is not well documented. This surface is probably treated with different types of paint, some also being diffusion thigh.

Being a resident of Bentegården for about a decade, Øvrid was able to share some information about measures performed in recent time, not issued in any known documentations. This includes installation of interior cladding on a previously exposed log wall in the TV-room, which according to her did not include mounting of interior insulation. Furthermore, she described cold drafts from many of the windows, especially in the bedroom where the windows often were frosty during winter. Additionally, she informed about the source of

energy for heating, which included a lot of wood-burning in the living room supplied by radiators elsewhere around the house.

The following timeline illustrates the construction and rehabilitation history of Bentegården based on information gathered during the current work or during the preliminary project.

1) Around year 1690

Bentegården was probably built around year 1690 according to a pledge on the east-façade.

2) Probably somewhere between year 1920 and 1950

- Figure 4.1 is an old photograph revealing that the extension originally was going all the way out to the east façade. Some of this extension is removed for unknown reasons, possibly to make room for a parking spot. According to current residents, this was executed in the 1950s. Figure 4.2 is a photograph from the 70s where the extended part have been rebuilt.



Figure 4.1 – Old picture of Bentegården. Date: unknown. Published with permission from Vestfold and Telemark County



Figure 4.2 – Bentegården. Date: 1971. Published with permission from Vestfold and Telemark County

3) Year 1969

- The first photographs available in the archives is traced back to 1969. The condition of Bentegården seems to be poor observing Figure 4.3 and Figure 4.4.
- On both floors supports are mounted to the roof beams as some of the loadbearing seems to be in a very bad condition.
- The window on the south façade is sealed. Besides this, the rest of the windows seems to be the same as the ones present today.



Figure 4.3 - Interior side of the second floor. Date: 1969. Published with permission from Vestfold and Telemark County



Figure 4.4 - Interior side of the south facade seen from the library. Date: 1969. Published with permission from Vestfold and Telemark County

4) Year 1970 and 1971

- Application for rehabilitation of Bentegården which got approved the same year. It is concluded that the building is not suitable for housing. The work was conducted in 1971 according to the pledge on the wall.
- The rehabilitation work included
 - Opening of the sealed window
 - The drawing illustrates that interior insulation was mounted in some of the walls, evidently on the southern wall. Figure 4.5 shows a clipping of the construction drawing illustrating this.
- The main stair which is present today was installed.

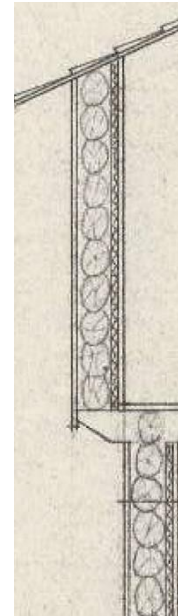


Figure 4.5 - Detail from construction drawing with interior insulation.

5) Year 1984

- A condition report from 1984 informs that the building is in fine condition, and regular maintenance work is recommended.
- Information from the report indicates that a picture showing the extension in its original state was captured in 1920.

6) Year 1989

- According to a project report from TIMBER AS Bentegården was insulated with polar foam on the exterior side which got injected through holes in the cladding.

7) Year 2007

- Minor rehabilitation work on parts of the façade as seen in Figure 4.6 with wooden panels not yet painted.



*Figure 4.6 - Picture from the inspection in 2007.
Published with permission from Vestfold and Telemark County*

8) Year 2017 and 2018

- The cladding on the west façade got replaced or repaired together with installation of exterior insulation in 2017.
- The cladding on the south façade got replaced or repaired together with installation of exterior insulation in 2018. Figure 4.7 is a photograph from the rehabilitation period, while Figure 4.8 presents the rehabilitation work finished.
- The wall's irregularities were not adjusted to keep the buildings originality.



*Figure 4.7 - During rehabilitation work. Date: 2018.
Published with permission from Vestfold and Telemark County*



*Figure 4.8 - Rehabilitation work finished. Date: 2018.
Published with permission from Vestfold and Telemark County*

In addition to what has been mentioned in the above timeline, some measures are evident but not successfully traced to any documentations. Included in this is the removal of timber on the southern wall in the upstairs bedroom. It is not certain whether this is done to remove decayed timber or solely to make more room in the bedroom. Figure 4.9 and Figure 4.10 illustrate this area seen from the exterior and interior side.



Figure 4.9 Second floor on the south wall. Published with permission from Vestfold and Telemark County



Figure 4.10 Main bedroom. Photo by Kris A. Flaskerud.

Another evident subject of renewal not documented in any known sources is the roof, illustrated in Figure 4.11. Although there are some visible cracks in the roof beams it can be characterized as being in relatively good shape based on visual observation.

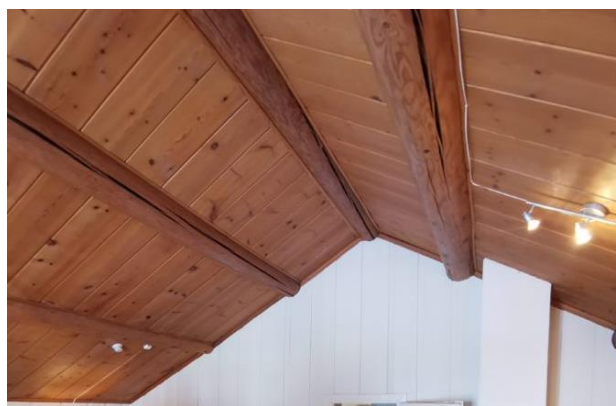


Figure 4.11 Interior side of the roof. Photo by Kris A. Flaskerud

Most true to the original state is the east façade. This can be assumed based on observations but is also described in the TIMBER report and confirmed by Solstad whom informed that it was not desirable to conduct any major measures on this wall as it shows Bentegården in its most original state. This applies to the cladding, the original entrance, and the windows.

Figure 4.12 illustrates one of the windows on the east façade with its leaded window frame.



Figure 4.12 Second floor window on the east façade. Photo by Kris A. Flaskerud

The interior section of the windows however an additional layer of glass installed to improve the insulating properties without significantly altering the architectural features. This is the case for all windows in the building envelope.

4.2 Thermography

As mentioned in chapter 3.3, a large quantity of IR images was captured during the first visit to Bentegården. For practical reasons, not all images will be shown in this chapter, but the ones that have been considered most critical to illustrate the situation for different sections of the building is displayed below.

4.2.1 Exterior walls, roof and floor

Table 4-1 and Table 4-2 shows the surface temperature measured for the walls marked with numbers according to Figure 4.13 and Figure 4.14.

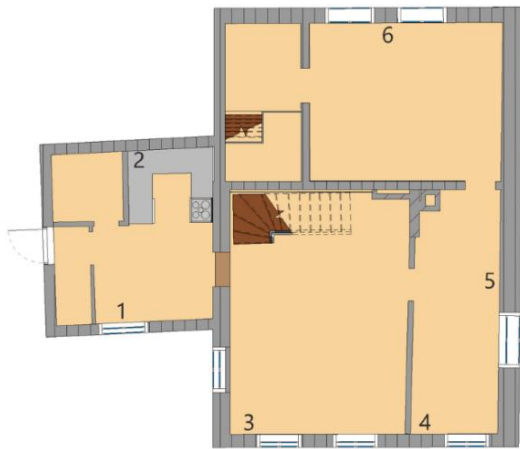


Figure 4.13 Location of measurements 1st floor

Table 4-1 Location and surface temperature

Location	Surface temperature [°C]
1	13,2
2	12,2
3	18,4
4	17,5
5	21,2
6	16,0

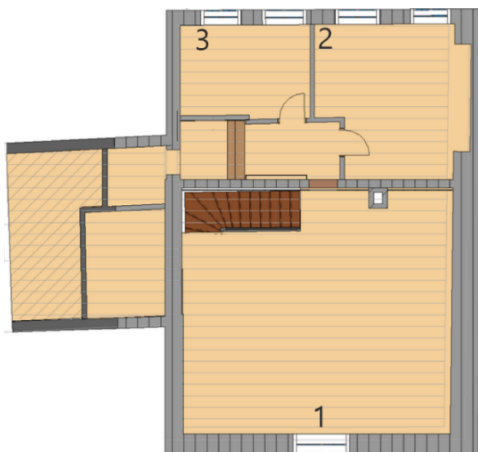


Figure 4.14 Location of measurements 2nd floor

Table 4-2 Location and surface temperature

Location	Surface temperature [°C]
1	18,8
2	15,6
3	14,0

Although naturally being affected by the heating within the living room, there are significantly higher measured surface temperatures on the walls where installation of exterior insulation is known to have been mounted (location 3-5 in Figure 4.13 and location 1 in Figure 4.14). The lowest surface temperatures are found in the extension based on the IR images in the kitchen area, referred to in Figure 4.13 as location 1 and 2.

Other areas of the building envelope, including the roof illustrated in Figure 4.15 and the floor, here exemplified with a selection including IR-images from TV-room, library and living room is shown in Figure 4.16, Figure 4.17 and Figure 4.18.

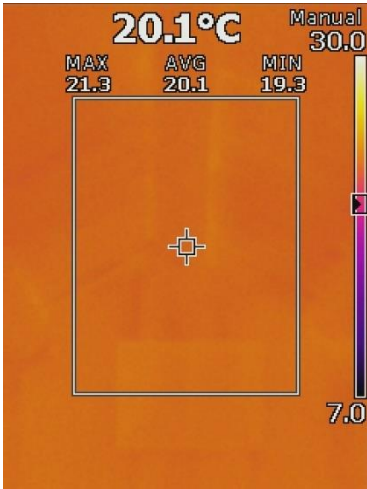


Figure 4.15 Thermographic image, roof 2nd floor

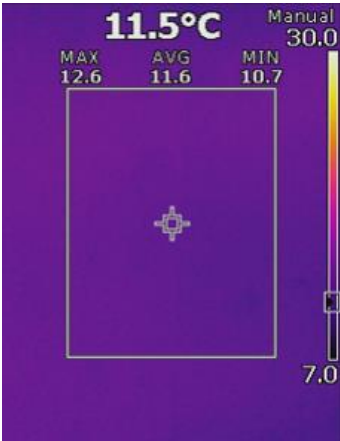


Figure 4.16 Thermography image floor, TV-room

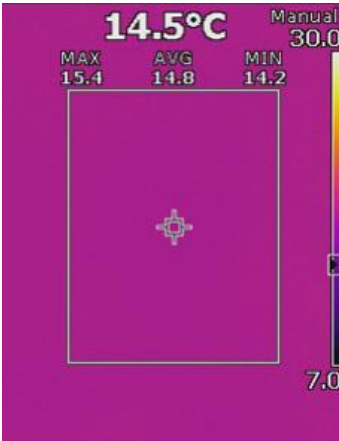


Figure 4.17 Thermography image floor, library

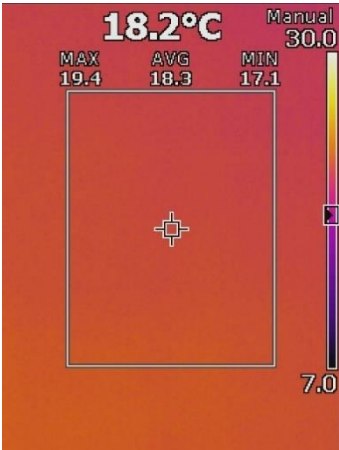


Figure 4.18 Thermography image floor, living room

4.2.2 Infiltration and thermal bridges

Throughout the building, there is significant heat loss caused by thermal bridges and air infiltrations.

Evidently, large heat losses are occurring through the windows, especially in the kitchen and the east façade. This is exemplified in Figure 4.19, Figure 4.20 and Figure 4.21, which are captured in the kitchen, TV-room and bedroom, respectively.

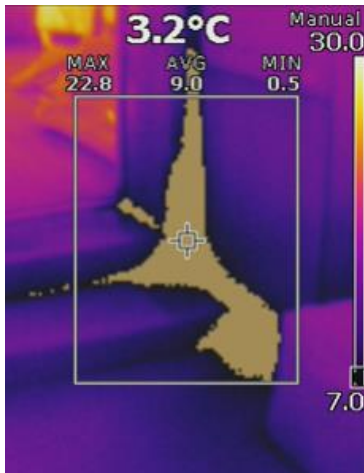


Figure 4.19 Thermography image window, kitchen

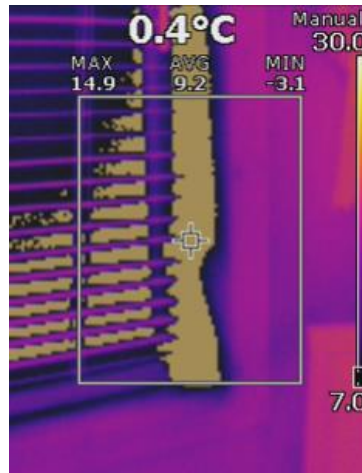


Figure 4.20 Thermography image window, TV-room

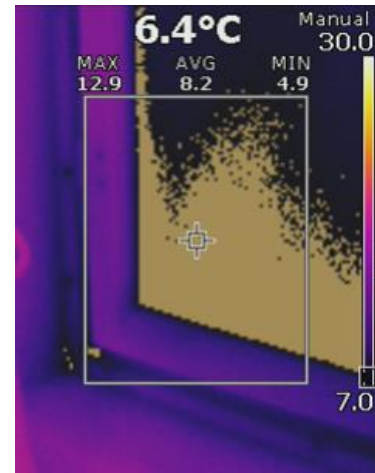


Figure 4.21 Thermography image window, bedroom

The most notable thermal bridges are located in the living room, library and the recreational room. Additionally, there are major occurrences in the rooms within the extension. This is exemplified by the thermal images illustrating the thermal bridges. Figure 4.22, Figure 4.23 and Figure 4.24 present the north-western corner of the living room, the southwestern corner of the library and the south-west corner of the recreational room, respectively.



Figure 4.22 Thermal bridges captured in the north-west corner of living room

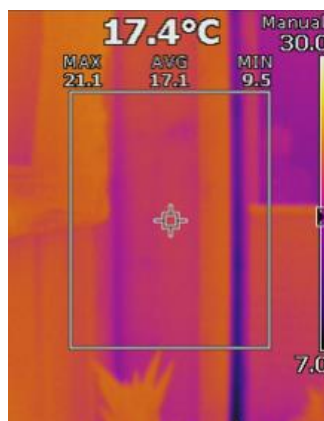


Figure 4.23 Thermal bridges captured in the south-west corner of the library

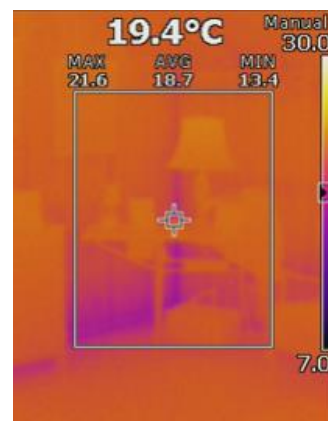


Figure 4.24 Thermal bridges captured in the south-west corner of the recreational room

4.3 Digital model and identification of assemblies

The point cloud data has been utilized according to the description in chapter 3.4, resulting in a Revit model with accurate dimensions. Figure 4.25 shows the building in Revit and Figure 4.26 shows the building after rendering, while Figure 4.27 and Figure 4.28 illustrates the first and second floor.



Figure 4.25 Revit model - 3D view



Figure 4.26 Rendered model - 3D view

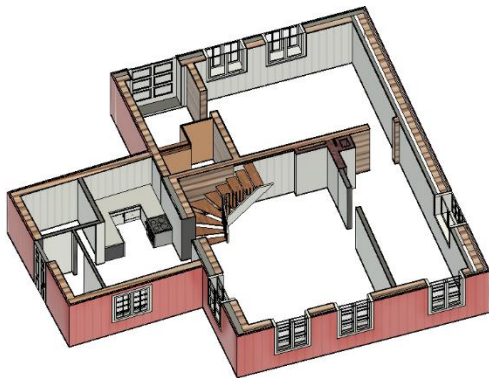


Figure 4.27 Section view of the first floor

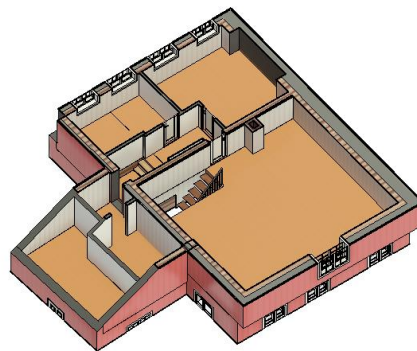


Figure 4.28 Section view of the second floor

As previously mentioned, the information gathered through various documents, drawings, IR images and theory involving historic building traditions serves the purpose of providing information to fill the known volume based on point cloud data with materials. However, some assumptions have been necessary where information has not been possible to obtain.

All walls containing timber is designed with 200 mm diameter logs of pine, based on measurement of the timber in areas where it is exposed. Additionally, the exterior cladding is measured to be 2x20 mm. Where exterior insulation is mounted, evidently on the southern and western façade, this is included as 50 mm glass wool in the model. For walls with interior insulation, a 100 mm layer of glass wool insulation is included with an air layer between this and the timber.

Based on information in chapter 4.1 stating that any extensions, usually built at a later time is not constructed as a log construction has been considered in the design of the walls in this area. Additionally, the result from the thermography suggests that these walls are not insulated.

The thickness from interior panels to exterior claddings varies between the different walls and floors. It is also evident that some walls are sloping both vertically and horizontally. This has not been included in the model. Another neglect is the polar foam described in the TIMBER report, as it is expected to not have any significance today.

Figure 4.29 has been included to show a more detailed drawing, presented with the south wall of the first floor. The wall assembly illustrates the exterior wall from the right side towards the interior side on the left side. The cladding is marked with a red colour, while the air layers have no pattern. The exterior insulation with sewn mats is illustrated with a small cross-grid and the interior insulation have a larger cross-grid. The vertically positioned circles identify the logs and the panel on the left side is the interior surface.

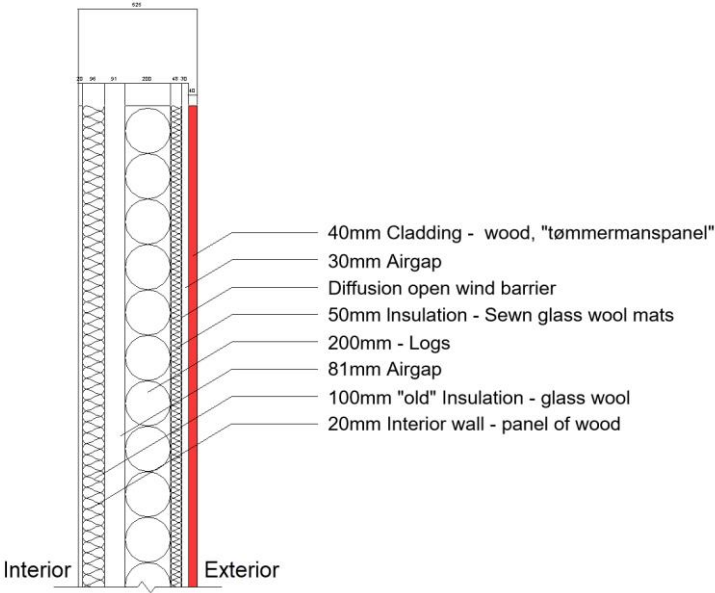


Figure 4.29 Detail drawing of the south wall

Figure 4.30 presents a capture from the digital model of Bentegården seen from above marked with the orientation of the facades. To clarify, this image is only for illustrative purposes, meaning that it is not orientated with true north.



Figure 4.30 Bentegården from above. This illustration is not oriented towards true north.

Table 4-3 and Table 4-4 represents the wall assemblies of the first floor of Bentegården. The second-floor wall assemblies are illustrated in Table 4-5 and Table 4-6. While the extended part of Bentegården is presented with figure Table 4-7. All the assemblies are illustrated with the interior surface to the left and the exterior surface to the right.

Table 4-3 1st floor wall assemblies. Table 1

1 st Floor			
West	North (living room)	North (old entrance)	East
<p>350</p>	<p>450</p>	<p>270</p>	<p>365</p>

Table 4-4 1st floor wall assemblies Table II

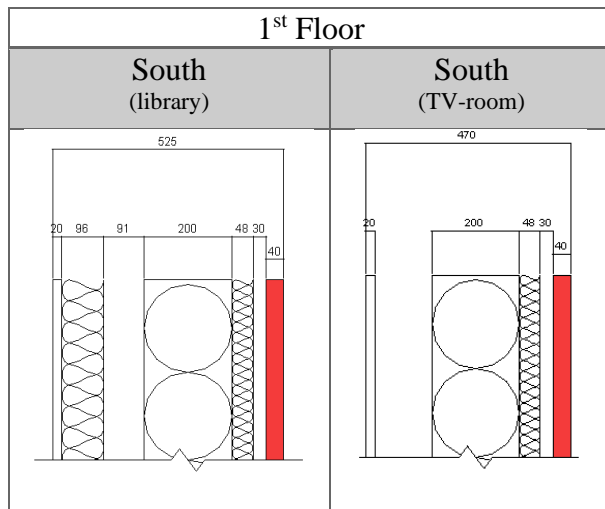


Table 4-5 2nd Floor wall assemblies. Table I

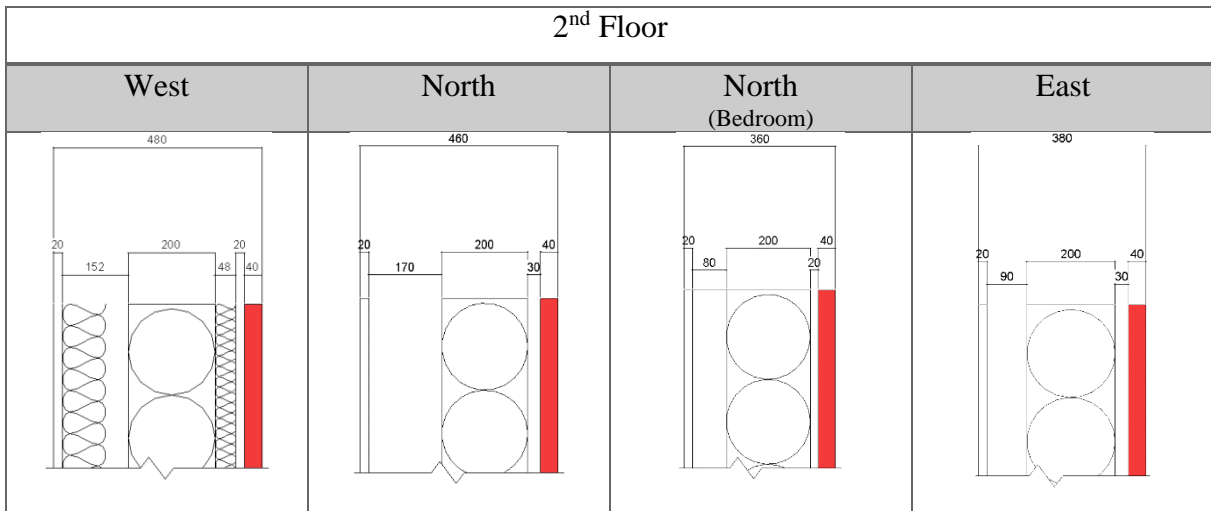


Table 4-6 2nd Floor wall assemblies. Table II

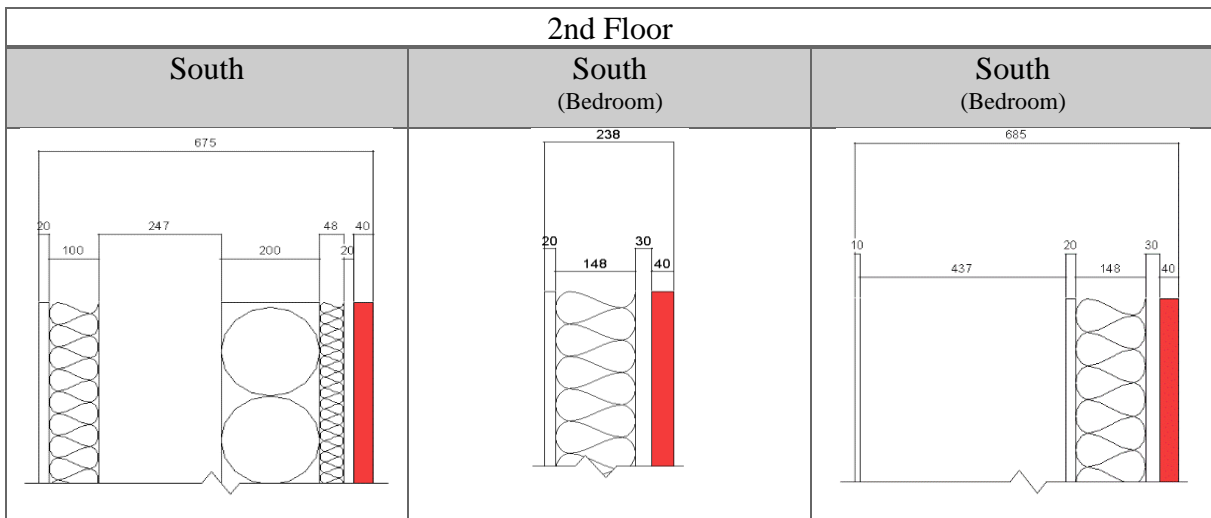
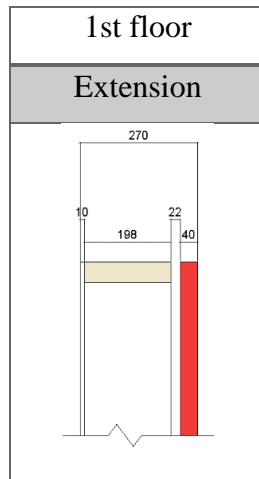


Table 4-7 Wall assembly of building extension



4.4 Climate data

4.4.1 Illustration and comparison of climate models

The following representation illustrates the climate parameters of temperature (Figure 4.31), relative humidity (Figure 4.32) and precipitation (Figure 4.33) for the current and future climate, where blue is the RCP8.5-model and red represent the data gathered from weather stations.

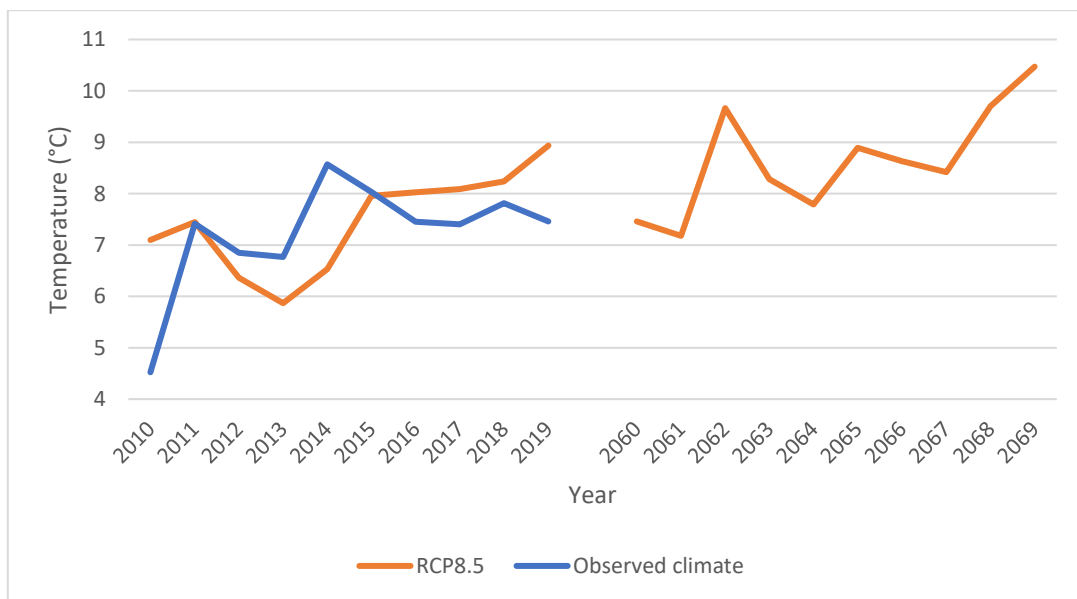


Figure 4.31 Annual temperature, observed climate data and RCP8.5

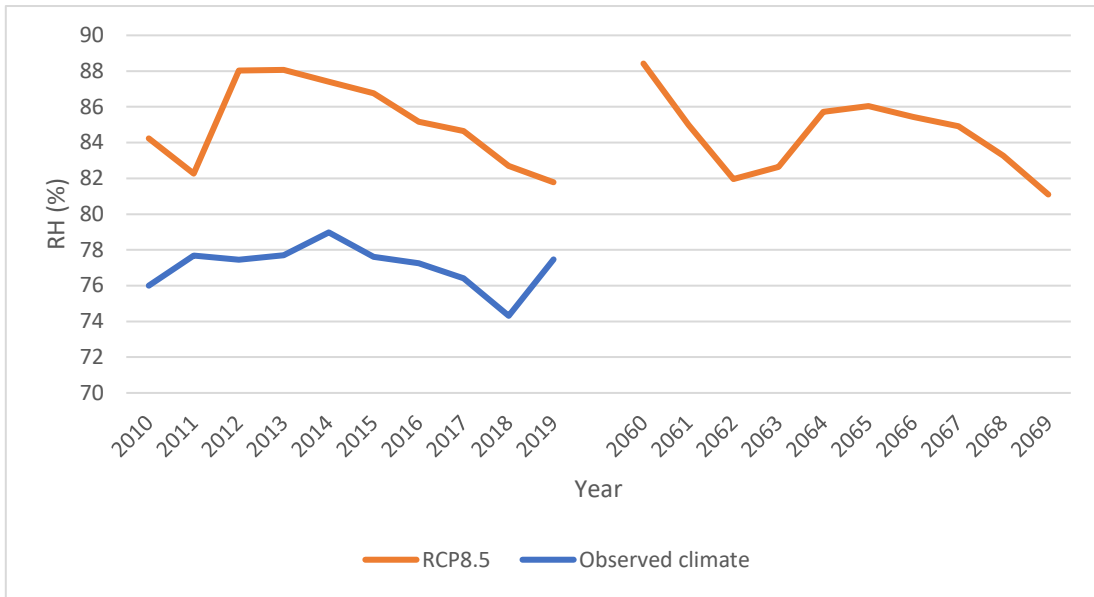


Figure 4.32 Annual RH, observed climate data and RCP8.5

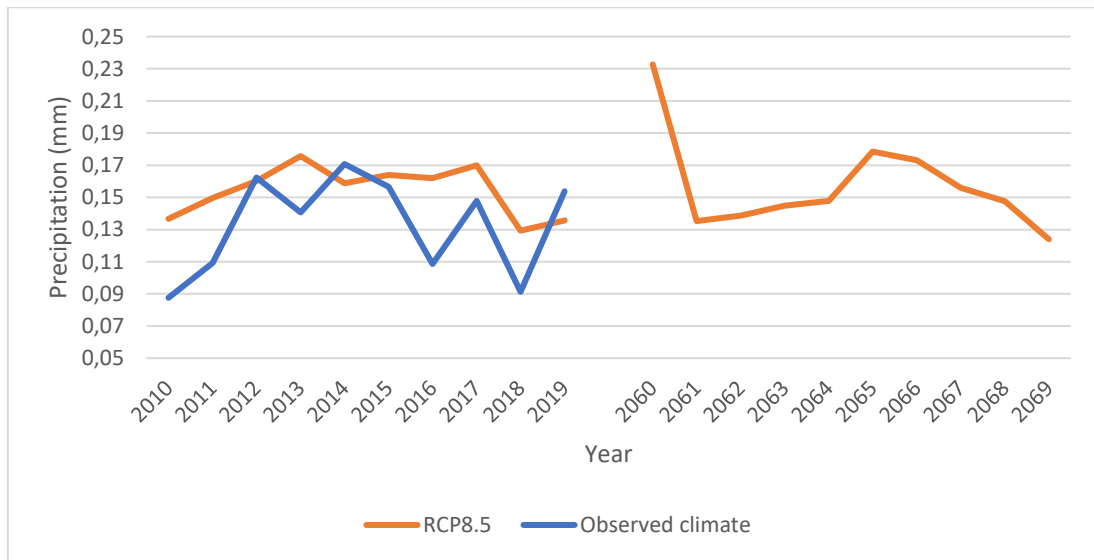


Figure 4.33 Annual precipitation, observed climate data and RCP8.5

Figure 4.34 illustrates the monthly average temperature for the three individual sets of climate data. When comparing the future climate according to RCP8.5 with the two sets of climate data from 2010-2020 the greatest temperature increase is present during the winter and the lowest during the summer.

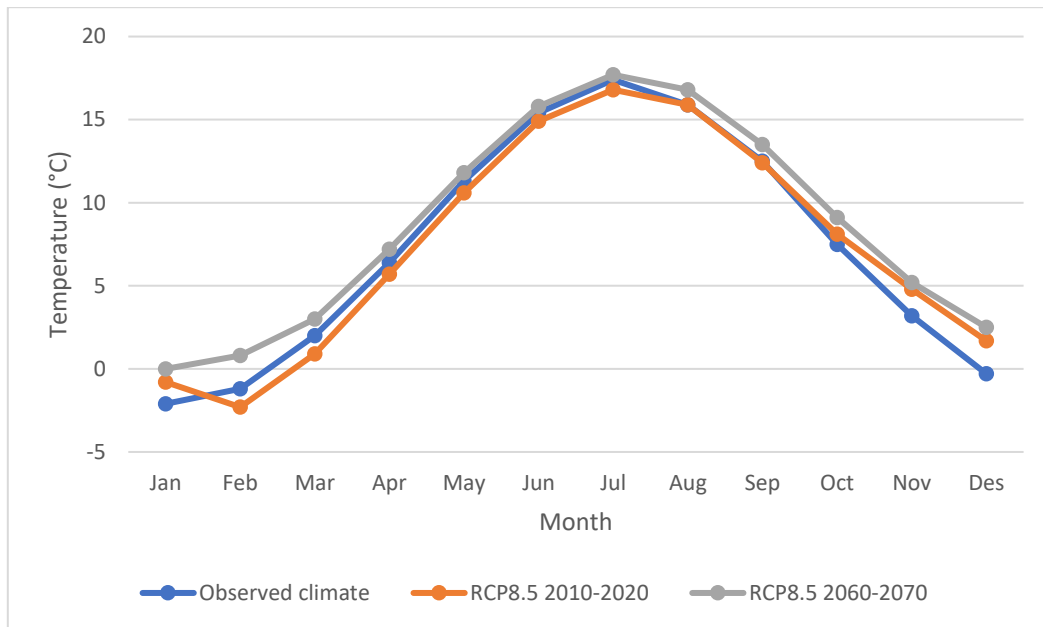


Figure 4.34 Monthly average temperature, observed data and RCP8.5

Figure 4.35 represents the average monthly precipitation for the different climate models. The graphs below suggest a drastic increase during the winter and spring when comparing current and future situation, especially for the measured climate data. The following seasons shows a more even or slightly reduced sum.

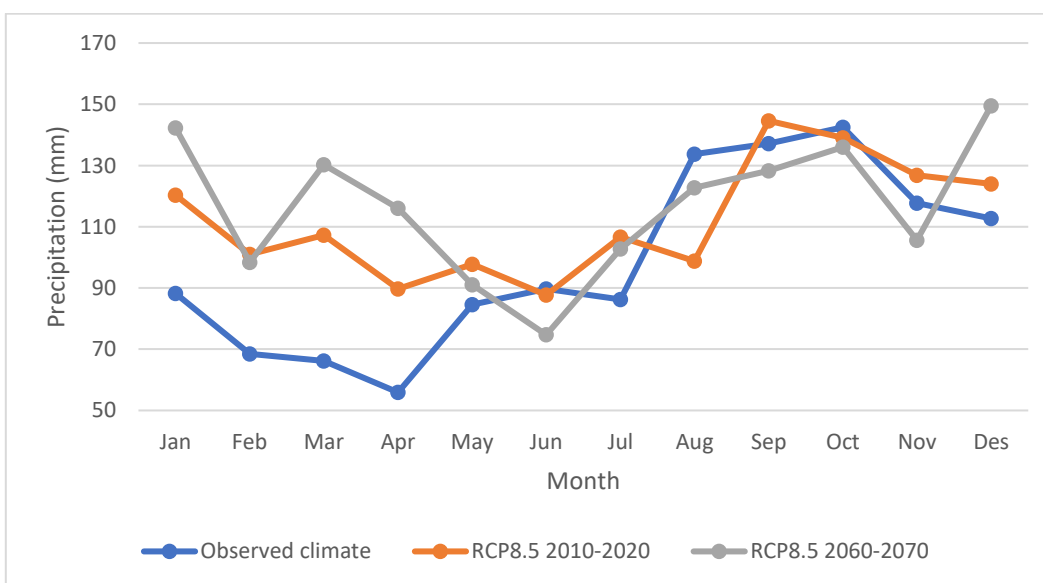


Figure 4.35 Monthly average precipitation, observed data and RCP8.5

4.4.2 Temperature and Relative Humidity from data loggers

The graphical illustration in this chapter shows the data of which has been collected from the interior and exterior loggers mounted at Bentegården. To avoid the extreme values within the first hours of logging, the included values is set from midnight (00:00) on the following day (06.02). Figure 4.36 and Figure 4.37 shows the temperature and relative humidity from the four interior loggers, while Figure 4.38 and Figure 4.39 shows these values for the two exteriorly placed loggers.

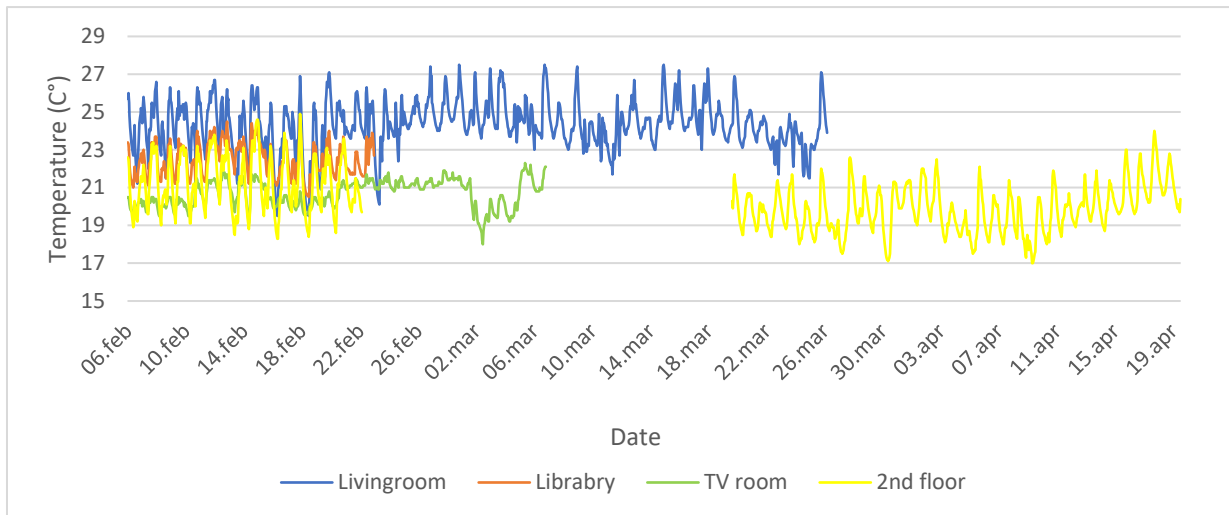


Figure 4.36 Data from loggers inside, temperature

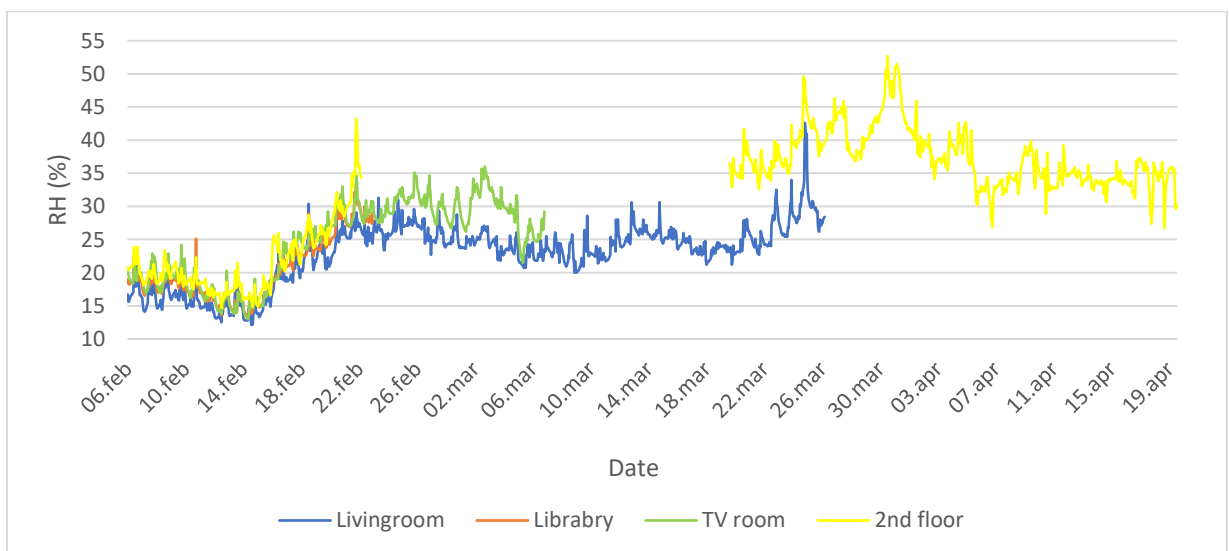


Figure 4.37 Data from loggers inside, relative humidity

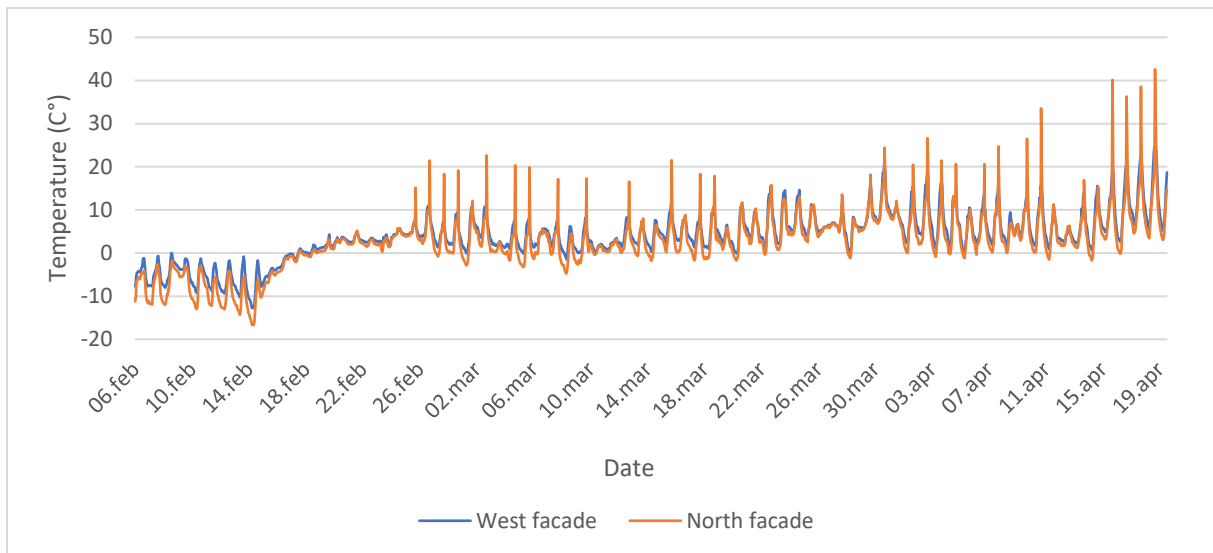


Figure 4.38 Data from loggers outside, temperature

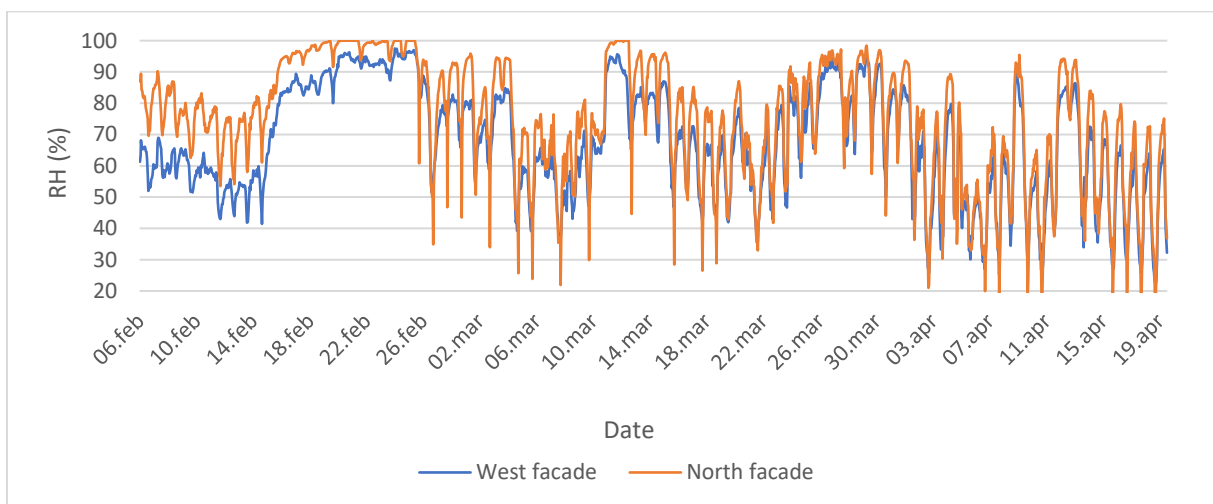


Figure 4.39 Data from loggers outside, relative humidity

For the period of measuring, the indoor temperature can be considered rather high, especially in the living room which is caused by a lot of wood-burning from the residents. What is particularly worth noticing is the low values measured for the interior relative humidity.

The exterior logger mounted on the north façade is clearly affected by direct sunlight, causing very high temperatures for certain periods. The logger on the west façade however, represent the air temperature without any major peaks caused by direct sunlight and has been compared against data from Tønsberg gjestebrygge.

Based on this climate data, the moisture content in the indoor and outdoor air is calculated using the Mollier diagram with its relationship used to find the moisture production within the building. Table 4-8 and Table 4-9 illustrates this for all the different rooms with loggers at two separate hours.

Table 4-8 Data from loggers and calculated moisture excess, February 13th 15:00

Date/time:	February 13 th 2021	15:00			
Location		Temperature [°C]	Relative Humidity [%]	Moisture content [v]	Moisture excess [$\Delta v = v_i - v_o$]
Outside	South wall	-5,6	60,0	1,9 (v_o)	
Inside	Library	23,4	17,1	3,7	1,8
	Living room	23,1	17,9	3,8	1,9
	TV-room	21,3	17,1	3,1	1,2
	Second floor	20,5	19,7	3,4	1,5

Table 4-9 Data from loggers and calculated moisture excess, February 21st 01:00

Date/time:	February 21 st 2021	01:00			
Location		Temperature [°C]	Relative Humidity [%]	Moisture content [v]	Moisture excess [$\Delta v = v_i - v_o$]
Outside	South wall	2,5	94	5,1	
Inside	Library	22,1	27,7	5,5	0,4
	Living room	24,2	25,8	5,6	0,5
	TV-room	20,9	28,9	5,2	0,1
	Second floor	21,8	29,1	5,7	0,6

Based on this data the moisture production is low, with all values within humidity class 1.

4.5 Results from simulations in WUFI

The results from simulations in WUFI is presented with graphs illustrating the potential moisture content of the log layer and graphs of mould index. The latter will serve as the primary indicator for identification for degradation risk. However, as moisture is one of the fundamental boundary conditions for initiating mould growth, this is included as moisture content within the logs. Another reason for looking at the moisture content is to evaluate it against the critical moisture content of 20 % described by SINTEF.

The main part of the hygrothermal simulations was ran with current climate based on the data from weather stations, while the future climate is based on the RCP8.5 model. However, the finale subchapter in this section is about a comparison between the two sets of climates showing the current situation.

Prior to the presenting results, an overview of the input parameters and assemblies is presented.

4.5.1 Input parameters and assemblies

Table 4-10 presents the different layers, materials, and from which database in WUFI they are taken. The cladding consists of a vertical wall cladding where parts of the cladding may be original, while other parts have been replaced as mentioned in chapter 6.1. The layer of logs has been selected as Pine from the database supplied by NTNU. The interior and exterior insulation has been included as mineral wool from the Fraunhofer-IBP database.

Furthermore, a wind barrier was installed when the cladding was replaced on south and west façade. This has been included in these locations and is selected from the Fraunhofer-IBP database.

The exterior and interior sD-value was selected based on the information regarding surface treatment in chapter 4.1. A sD-value of 0,5 was specified for the exterior cladding treated with linseed oil. The interior surface has been treated with different types of paint and therefore a higher sD-value of 1,0 was selected.

Table 4-10 Material and database in WUFI

Layer	Material	Database
Cladding	Pine [Density 510kg/m ³]	NTNU Norwegian
Logs		University of Science and Technology
Interior insulation	Mineral wool [0,040 W/mK]	Fraunhofer-IBP
Exterior insulation	Mineral wool [0,034 W/mK]	
Wind barrier	Polyethylene [sD = 0,1m]	

Table 4-11 presents an overview of the different wall assemblies which is implemented in the different WUFI simulations. The remaining input data from WUFI is illustrated in APPENDIX A.

Table 4-11 Characteristics of wall assemblies used in the simulations

Wall assembly	Floor	Direction	Wind barrier	Exterior insulation	Logs	Air layer	Interior insulation	U-value
1	1	South	x	x	x	81 mm	x	0,141
2	1	South	x	x	x	151 mm	-	0,190
3	1	West	x	x	x	10 mm	-	0,304
4	1	North	-	-	x	160 mm	-	0,253
5	1	North	-	-	x	-	-	0,609
6	1	East	-	-	x	75 mm	-	0,363
7	2	South	x	x	x	247 mm	x	0,106
8	2	South	x	x	-	-	-	0,209
9	2	West	x	x	x	52 mm	x	0,149
10	2	North	-	-	x	170 mm	-	0,244
11	2	East	-	-	x	90 mm	-	0,337

All simulations were performed with two different humidity classes, class 1 and 3. The current situation at Bentegården with two occupants indicates humidity class 1 as stated in chapter 4.4.2. However, the current situation might change in the future which may contribute to a higher moisture production. In addition, according to the standard, a regular house with few residents is typically associated with humidity class 3.

4.5.2 Moisture content

The moisture content of the logs is represented in the bar charts below. Blue bars indicate the years 2010 to 2020, while orange bars indicate the years 2060-2070. The logs were separated into three layers of exterior, middle and interior side to achieve a better insight into each part of the log. The black dotted line indicates a 20 % moisture content of the logs.

The moisture content of the logs is presented for all wall assemblies except for assembly 8 which does not include a layer of logs

Assembly 1 – South wall, living room

Figure 4.40 presents the moisture content of wall assembly 1. Wall assembly 1 in current climate using humidity class 1 have a moisture content below 20 %. The median illustrates a typical moisture content of about 16-17 % with a downward trend towards the interior side. While investigating the same climate with humidity class 3 an upward trend is observed with a median of around 18-19 %.

The future climate with humidity class 1 illustrates a higher amount of moisture with all max values above 20 % moisture content and a median of 19-20 %. Humidity class 3 increase the median moisture content up to 21-22 %.

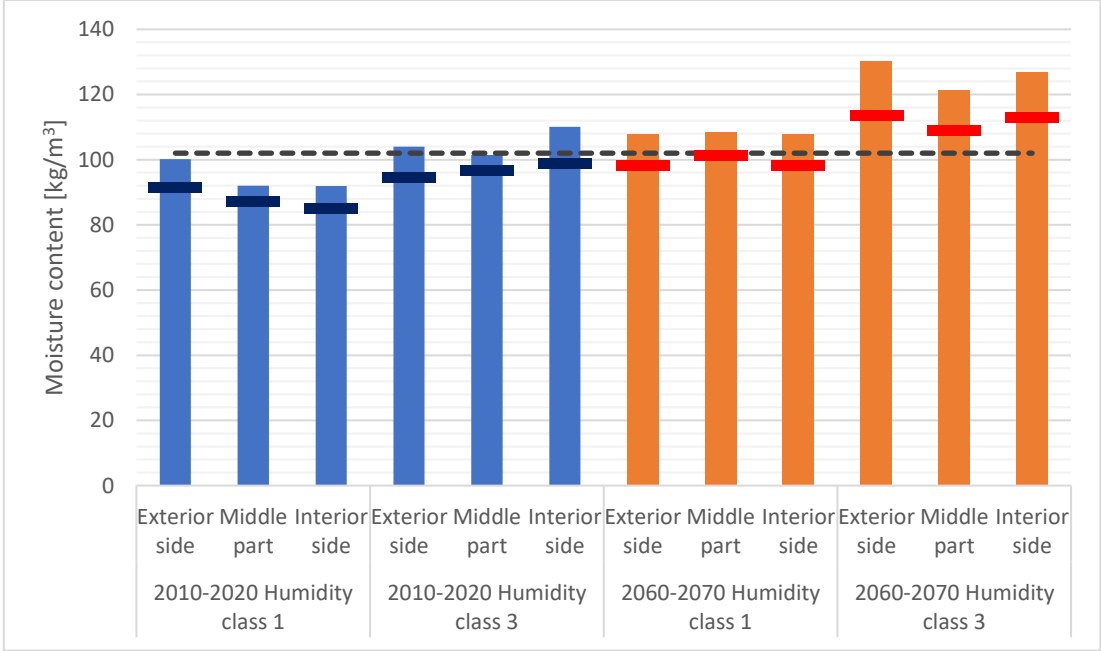


Figure 4.40 - Assembly 1 - moisture content

Assembly 2 – South wall, TV-room

Figure 4.41 presents the moisture content of wall assembly 2. Wall assembly 2 with current climate and humidity class 1 have a maximum moisture content below 20%. The median illustrates a typical moisture content of 16-17 %, while humidity class 3 have a median of around 18-19 %.

Future climate and humidity class 1 shows higher values than observed climate and humidity class 1. The median moisture content of the exterior side is slightly above the critical limit with a median of 21 %. The middle and interior side, however, is lower. Furthermore, humidity class 3 have some higher values with a median between 21-22 % for all layers.

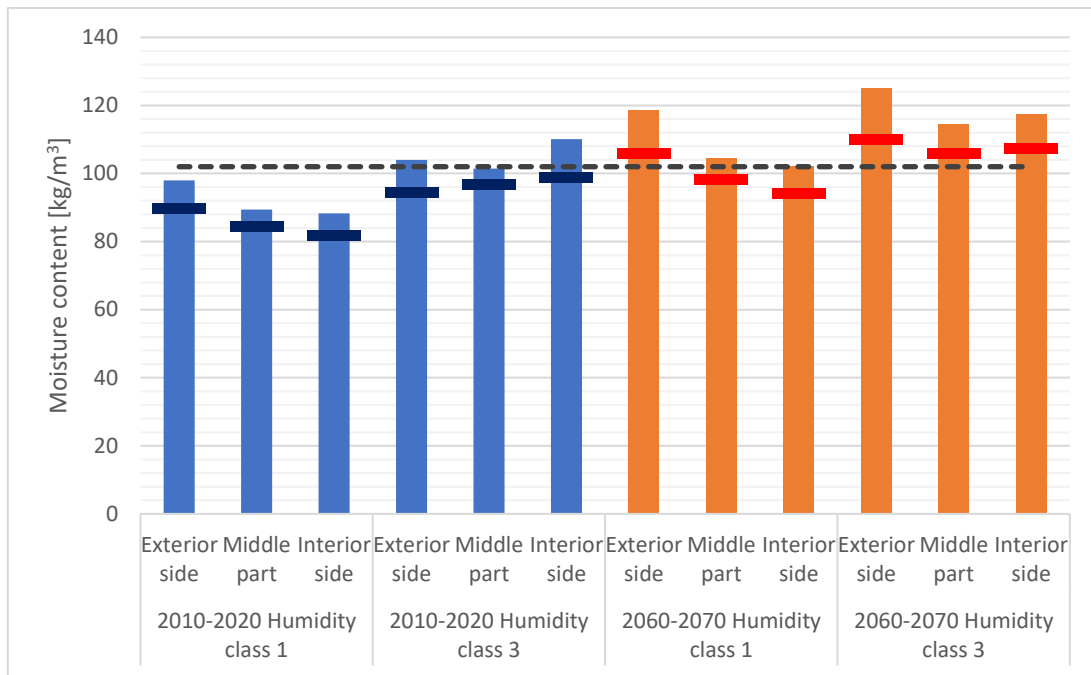


Figure 4.41 Wall assembly 2 - moisture content

Assembly 3 – West wall, living room

Figure 4.42 presents the moisture content of wall assembly 3. Wall assembly 3 with observed climate, simulated with both humidity class 1 and 3 have a moisture content well below 20 %. The median illustrates a typical moisture content of 14-15 %, while humidity class 3 have a median of around 16 %.

Future climate and humidity class 1 and 3 shows higher values than current climate. Humidity class 1 have a median moisture content of 16-18 % and humidity class 3 of 19 %.

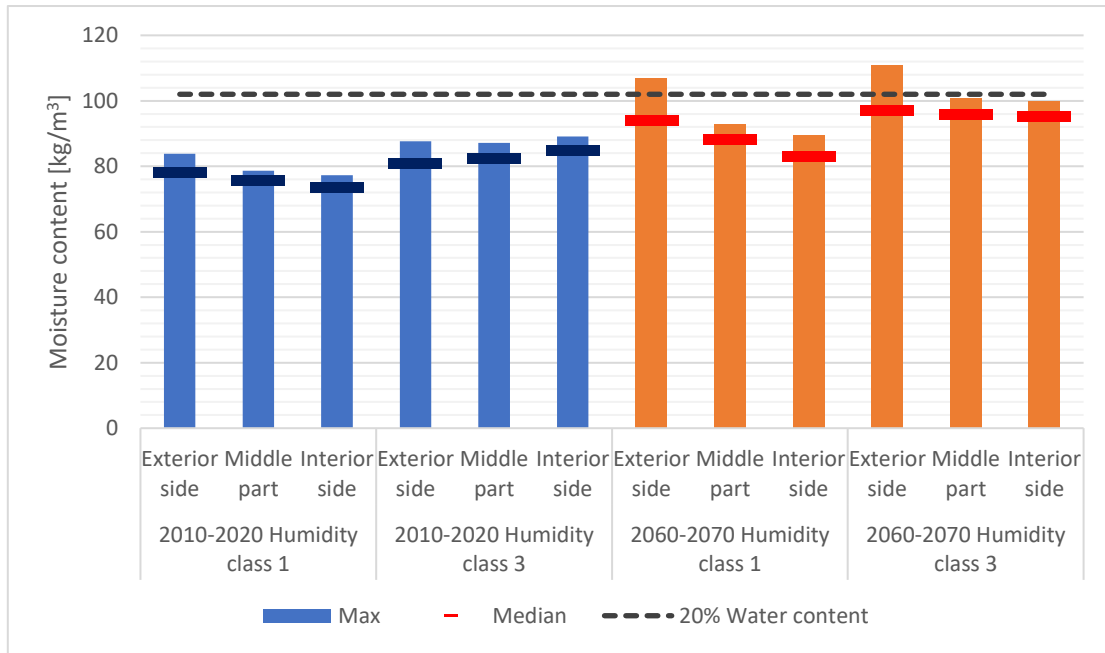


Figure 4.42 Wall assembly 3 - moisture content

Assembly 4 – North wall, living room

Figure 4.43 presents the moisture content of wall assembly 4. Wall assembly 4 with current climate and humidity class 1 got a median ranging from 19-20 %, while humidity class 3 results slightly above the critical value with a median of 21-22 %.

The future climate is above the critical value both with humidity class 1 and 3. Humidity class 1 have a median of 24 % on the exterior side and 20-21 % in the middle and interior side. Humidity class 3 have median values up to 24-25 % on the exterior and interior side.

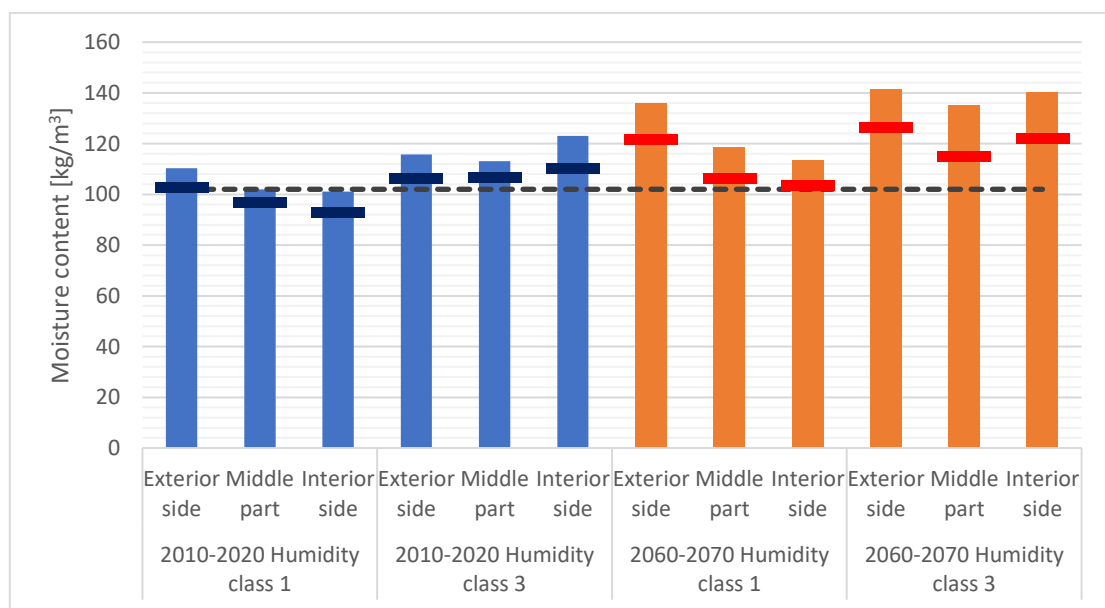


Figure 4.43 Wall assembly 4 - moisture content

Assembly 5 – North wall, old entrance

Figure 4.44 presents the moisture content of wall assembly 5. Wall assembly 5 with current climate and humidity class 1 and 3 have a moisture content below 20 % with a median value between 15 and 19 %.

The moisture content with future climate has higher values, where humidity class 1 have a median value on the exterior side of 21 %, while the middle part and the interior side is lower. The moisture content with humidity class 3 has a median value of 23 % on the exterior side, 20% in the middle part and slightly below 20 % on the interior side.

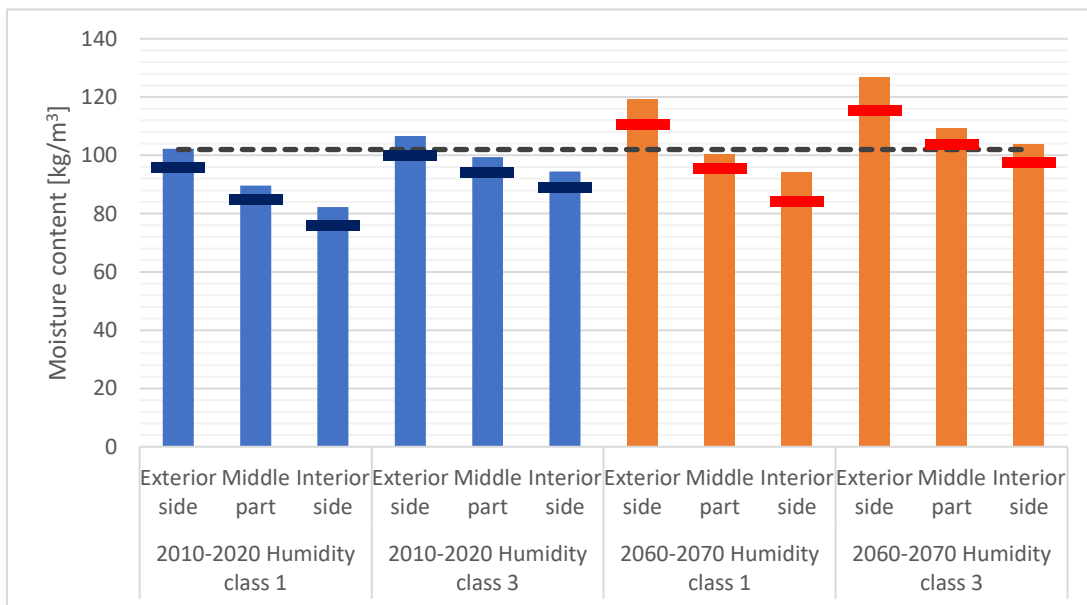


Figure 4.44 Wall assembly 5 - moisture content

Assembly 6 – East wall, TV-room

Figure 4.45 presents the moisture content of wall assembly 6. Wall assembly 6 with current climate have a median value of moisture content below the critical value. Humidity class 1 have a median value of 16-18 % while humidity class 3 is around 19 %.

The future climate and humidity class 1 has a median value of 22 % on the exterior side and 18-19 % on the middle part and interior side. Humidity class 3 have all values higher than the critical value and varies from 21-23 % with the highest value on the exterior side.

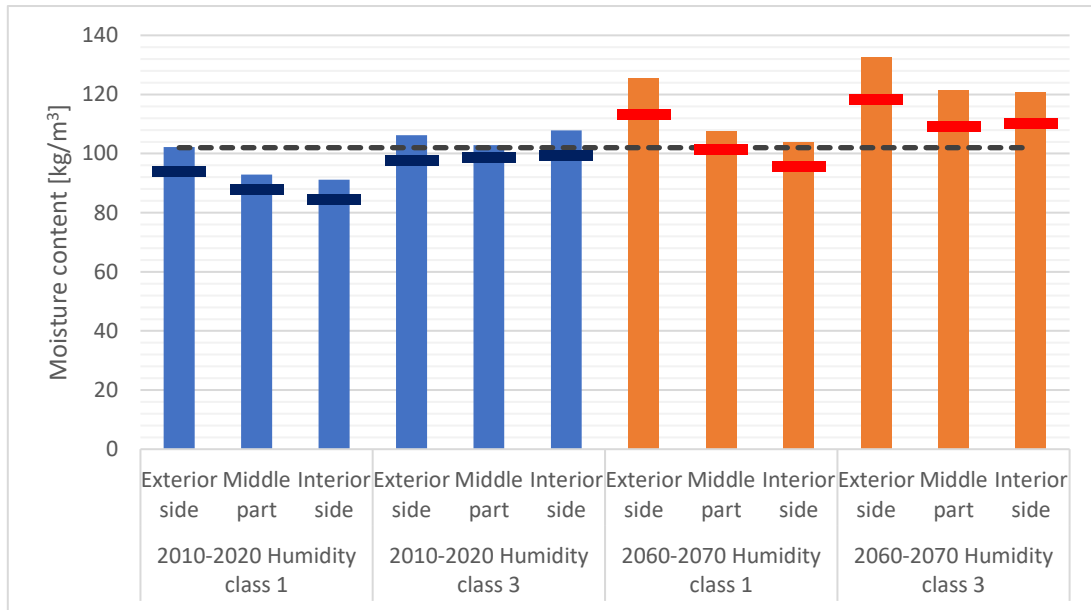


Figure 4.45 Wall assembly 6 - moisture content

Assembly 7 – South wall, recreational room

Figure 4.46 presents the moisture content of wall assembly 7. The moisture content in the wall assembly 7 with current climate, humidity class 1 has a median value of 17-18 %, while humidity class 3 have a median value of 19-20 %.

The moisture content with future climate has a median value of 20-22 % with the highest value on the exterior side of the logs. Humidity class 3 is fairly higher with a median value of 21-23 % and the highest values on the exterior and interior side of the logs.

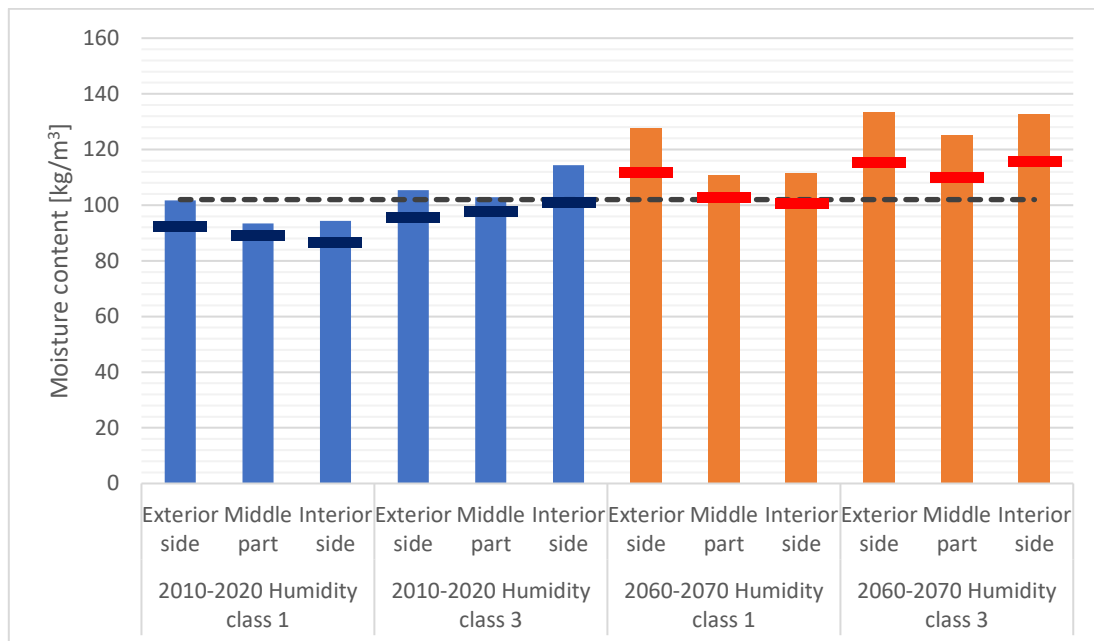


Figure 4.46 Wall assembly 7 - moisture content

Assembly 9 – West wall, recreational room

Figure 4.47 presents the moisture content of wall assembly 9. The moisture content of wall assembly 9 with current climate, humidity class 1 and 3 is below the critical value of 20 %. Humidity class 1 have a median value of 16 % while humidity class 3 have a value of 18-19 %.

The moisture content with future climate, humidity class 1 has a median value of 21 % on the exterior side and 19-20 % in the middle part and on the interior side of the logs. Humidity class 3 have a median value of 22 % on the exterior and interior side of the logs, where the middle part has a value of 21 %.

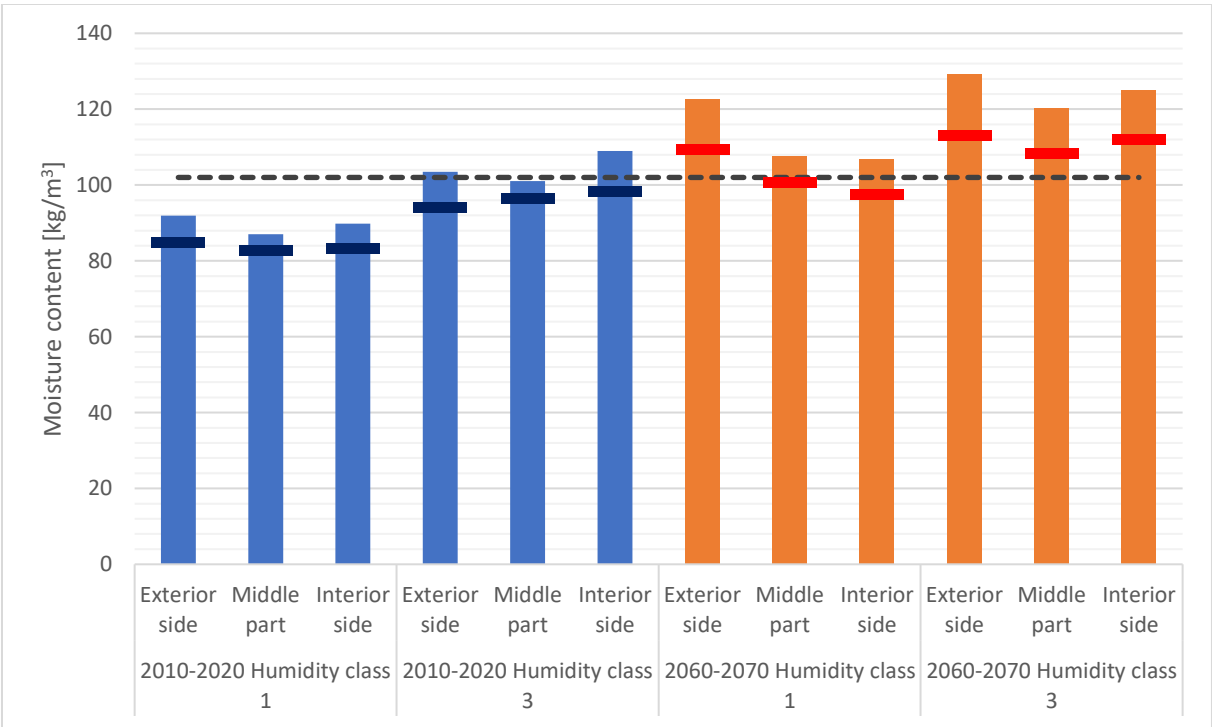


Figure 4.47 Wall assembly 9 - moisture content

Assembly 10 North wall, recreational room

Figure 4.48 presents the moisture content of wall assembly 10. The current climate with humidity class 1 has a moisture content of up to 20 % on the exterior side, while the middle part and the interior side is slightly below.

The future climate with humidity class 1 has a moisture content up to a median value of 24 %, while the exterior side and the interior side is fairly lower. Humidity class 3 have a moisture content up to a median value of 25 %, where also the exterior side and interior side is a little lower.

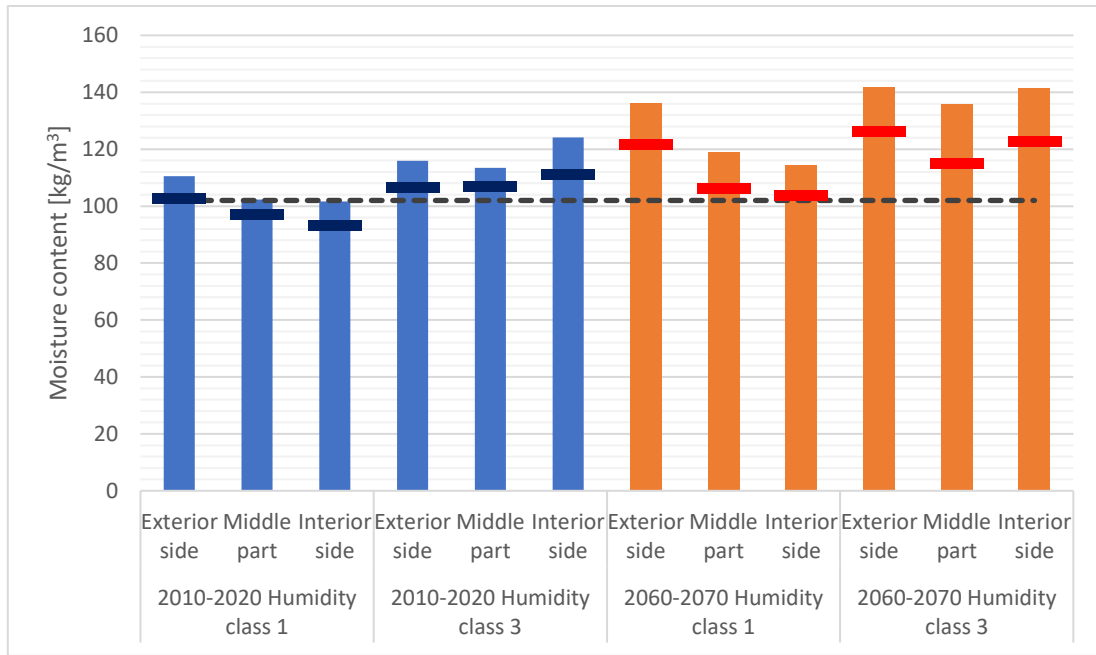


Figure 4.48 Wall assembly 10 - moisture content

Assembly 11 – East wall, bedroom

Figure 4.49 presents the moisture content of wall assembly 11. The current climate gives a moisture content below 20 % for both humidity class 1 and 3.

The future climate has a median value of up to 22 % in the middle layer of humidity class 1, while the middle layer of humidity class 3 is around 23 %.

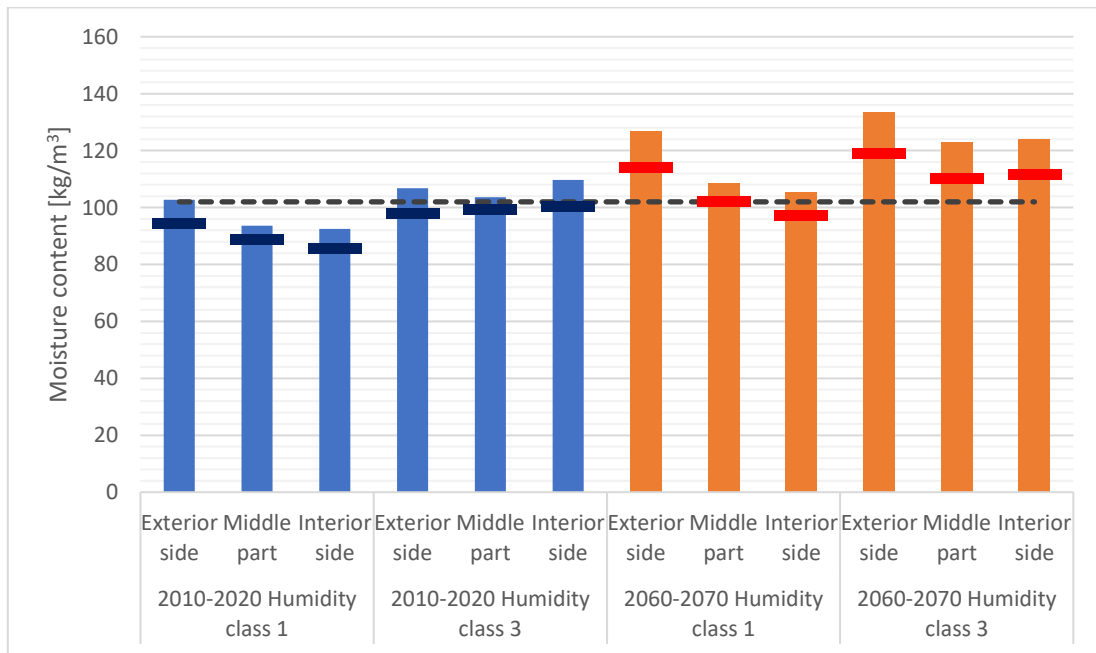


Figure 4.49 Wall assembly 11 - moisture content

4.5.3 Mould index

This section will present the mould indexes for each of the simulated wall assemblies. For every wall assembly, a figure is included to illustrate the wall assemblies with numbers above each layer and a letter representing each of the positions analysed. The bar charts below present the mould index within each layer of the different wall assemblies. Blue bars indicate with climate based on current climate data, while orange bars indicate the years future climate based on RCP 8,5. The horizontal bars represent the median of each layer with a colour related to the specific series.

Assembly 1 – South wall, living room

Figure 4.50 presents wall assembly 1 and its respective monitor positions. Figure 4.51 is the graph with humidity class 1, while Figure 4.52 is humidity class 3.

There is a minor difference between humidity class 1 and 3, where humidity class 3 have slightly higher values. The difference from year 2010 to 2020 and 2060 to 2070 is significant with critical values within several layers. The exterior side of the log structure is at yellow colour according to the traffic light indicator with future climate.

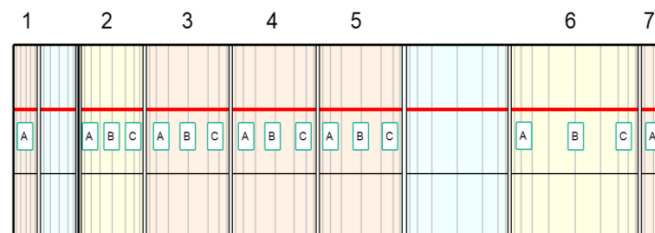


Figure 4.50 Wall assembly 1, monitor position

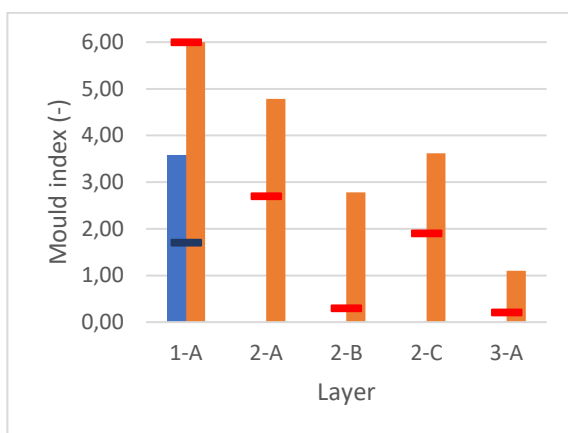


Figure 4.51 Mould index, humidity class 1, assembly 1

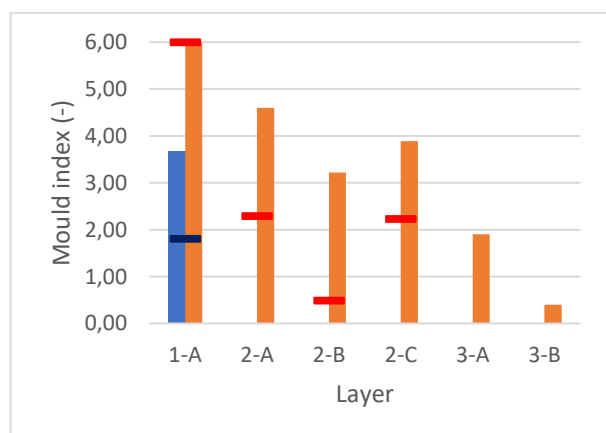


Figure 4.52 Mould index, humidity class 3, assembly 1

Assembly 2 – South wall, TV-room

Figure 4.53 presents wall assembly 2 and its respective monitor positions. Figure 4.54 is the graph with humidity class 1, while Figure 4.55 is humidity class 3.

The first period from 2010 to 2020 for both humidity class 1 and 3 do not indicate any problems expect for the cladding. Future climate presents higher values and red traffic light indicator. The layer of logs is within the green indication.

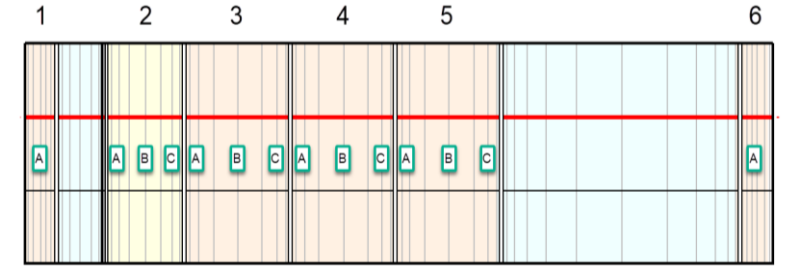


Figure 4.53 Wall assembly 2, monitor position

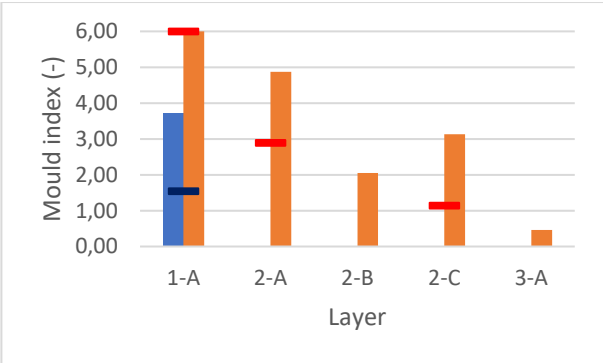


Figure 4.54 Mould index, humidity class 1, assembly 2

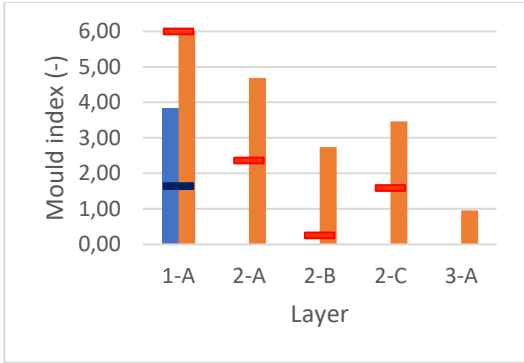


Figure 4.55 Mould index, humidity class 3, assembly 2

Assembly 3 – West wall, living room

Figure 4.56 presents wall assembly 3 and its respective monitor positions. Figure 4.57 is the graph with humidity class 1, while Figure 4.58 is humidity class 3.

The traffic light indicator indicates no trouble within wall assembly 3 from 2010 to 2020, while values are higher with future climate. The exterior side of the insulation and cladding is within red indication, but not any other layer. Humidity class 3 shows fairly higher values than humidity class 1.

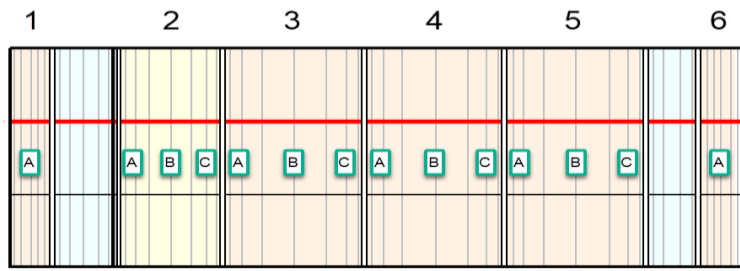


Figure 4.56 Wall assembly 3, monitor position

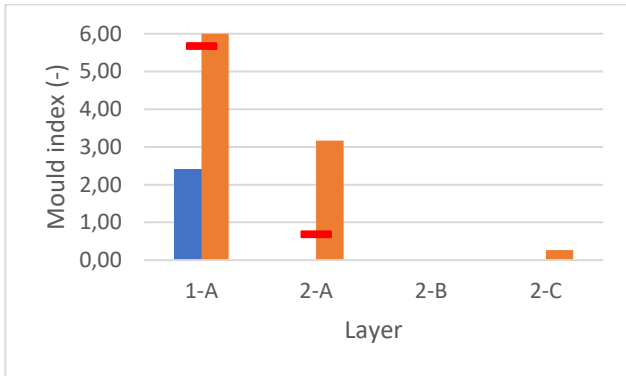


Figure 4.57 Mould index, humidity class 1, assembly 3

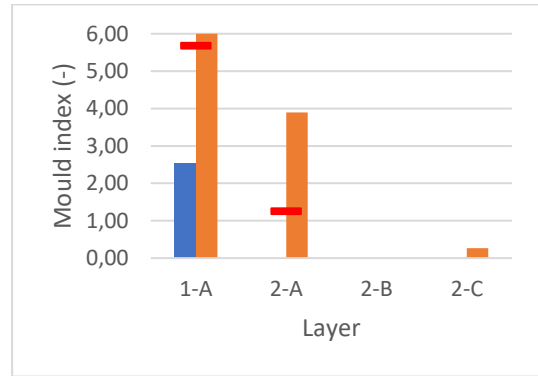


Figure 4.58 Mould index, humidity class 3, assembly 3

Assembly 4 – North wall, living room

Figure 4.59 presents wall assembly 4 and its respective monitor positions. Figure 4.60 is the graph with humidity class 1, while Figure 4.61 is humidity class 3.

With climate from year 2010 to 2020 there is no problems within any layer expect for the cladding. However, year 2060-2070 and humidity class 1 show some trouble in the exterior part of the logs. Within the same year but with humidity class 3, it is at red or close to red traffic light indication in all layers.

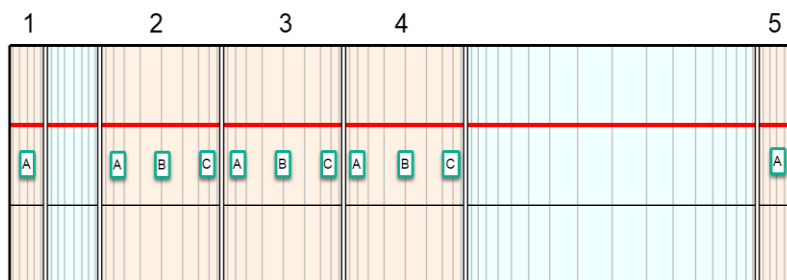


Figure 4.59 Wall assembly 4, monitor position

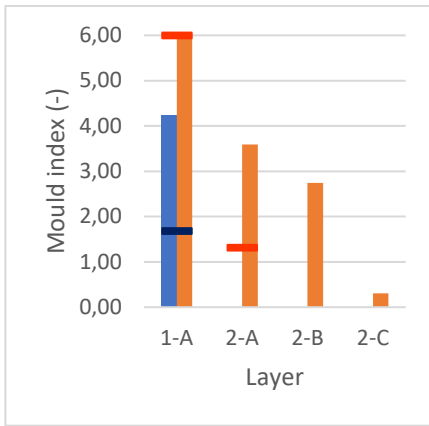


Figure 4.60 Mould index, humidity class 1, assembly 4

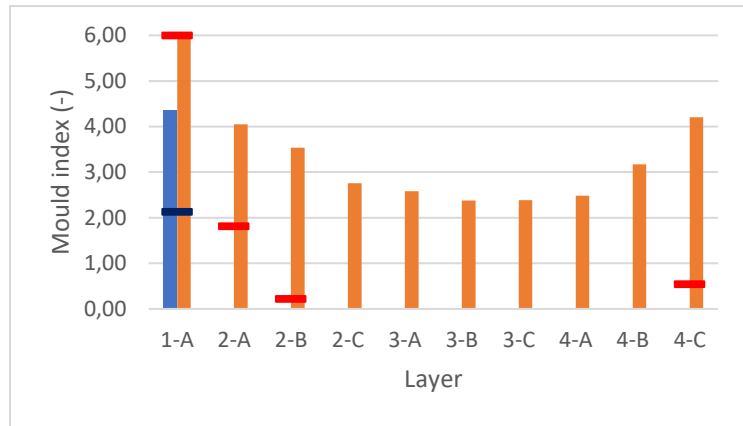


Figure 4.61 Mould index, humidity class 3, assembly 4

Assembly 5 – North wall, old entrance

Figure 4.62 presents wall assembly 5 and its respective monitor positions. Figure 4.63 is the graph with humidity class 1, while Figure 4.64 is humidity class 3.

Wall assembly 5 is within green indication for both current and future climate within all layers except for the cladding.



Figure 4.62 Wall assembly 5, monitor position

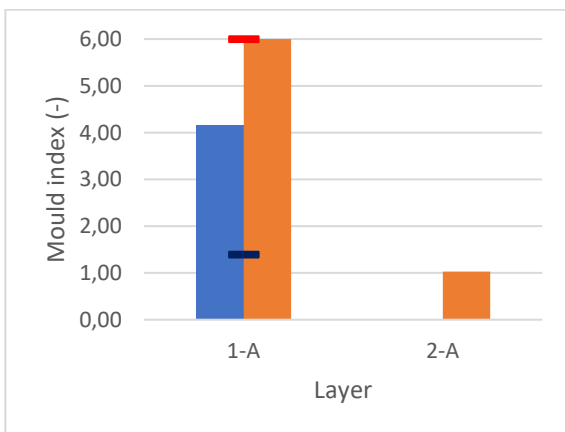


Figure 4.63 Mould index, humidity class 1, assembly 5

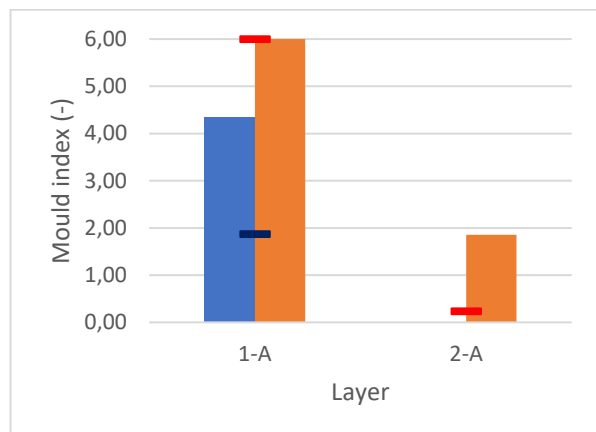


Figure 4.64 Mould index, humidity class 3, assembly 5

Assembly 6 – East wall, TV-room

Figure 4.65 presents wall assembly 1 and its respective monitor positions. Figure 4.66 is the graph with humidity class 1, while Figure 4.67 is humidity class 3.

Wall assembly 6 results are similar to wall assembly 5 with all layers within green indication expect for the cladding.

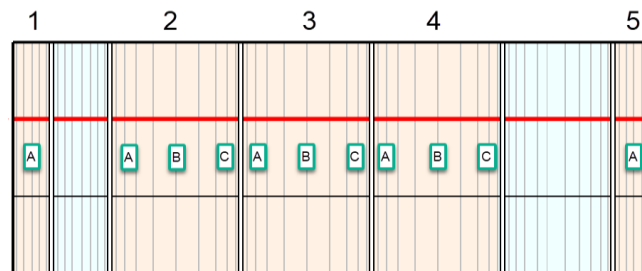


Figure 4.65 Wall assembly 6, monitor position

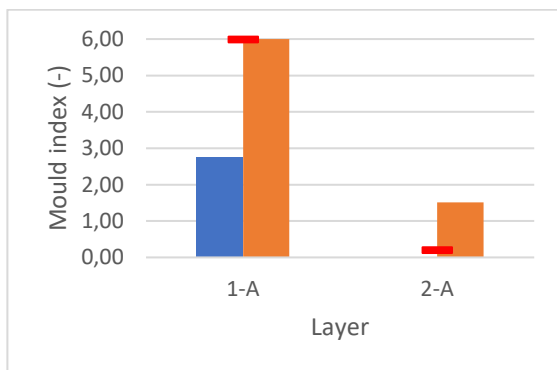


Figure 4.66 Mould index, humidity class 1, assembly 6

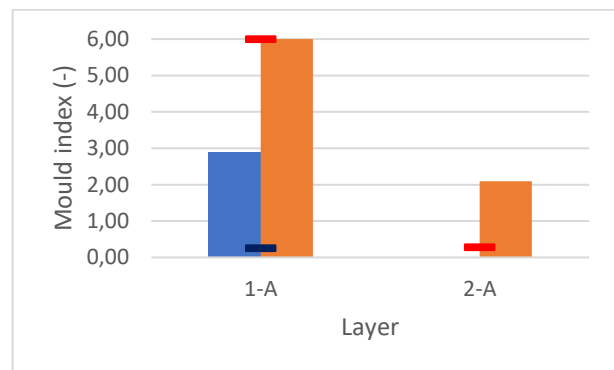


Figure 4.67 Mould index, humidity class 3, assembly 6

Assembly 7 – South wall, recreational room

Figure 4.68 presents wall assembly 7 and its respective monitor positions. Figure 4.69 is the graph with humidity class 1, while Figure 4.70 is humidity class 3.

Assembly 7 show no problems within the layers from year 2010 to 2020 except the cladding while year 2060-2070 illustrates a higher risk. The insulation layer is at red indication and the exterior side of the logs mostly within green indication.

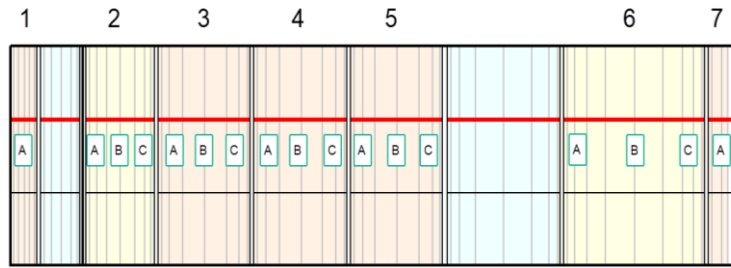


Figure 4.68 Wall assembly 7, monitor position

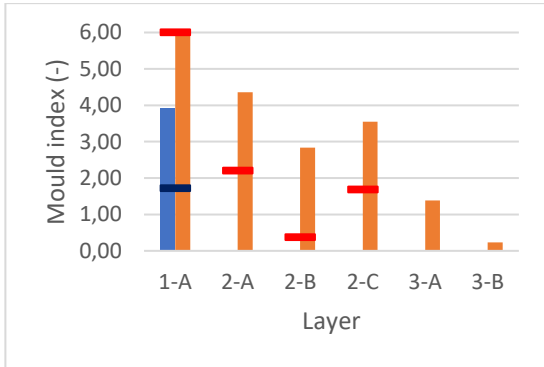


Figure 4.69 Mould index, humidity class 1, assembly 7

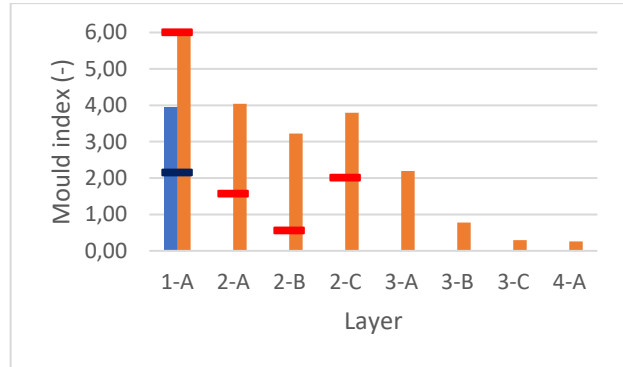


Figure 4.70 Mould index, humidity class 3, assembly 7

Assembly 8 – South wall, bedroom (without logs)

Figure 4.71 presents wall assembly 8 and its respective monitor positions. Figure 4.72 is the graph with humidity class 1, while Figure 4.73 is humidity class 3.

Assembly 8 with current climate and humidity class 1 only indicates problems with the cladding, while humidity class 3 potentially has problems with exterior side of the insulation. Simulations with future climate and humidity class 1 indicates potential problems with the cladding and exterior side of the insulation. Humidity class 3 indicates problems with cladding, exterior part of the insulation and potentially interior side of the insulation.

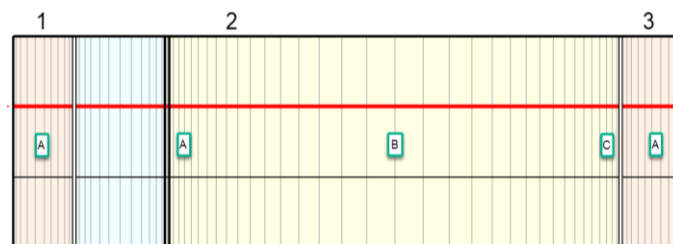


Figure 4.71 Wall assembly 8, monitor position

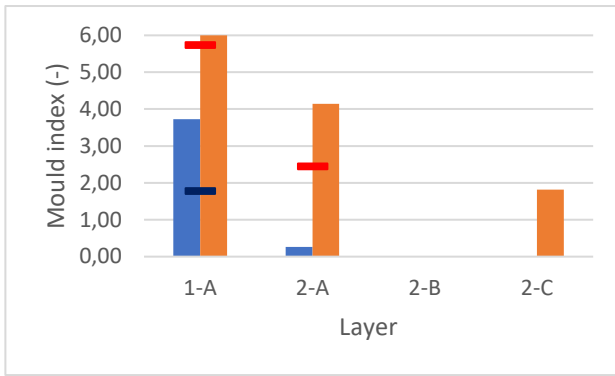


Figure 4.72 Mould index, humidity class 1, assembly 8

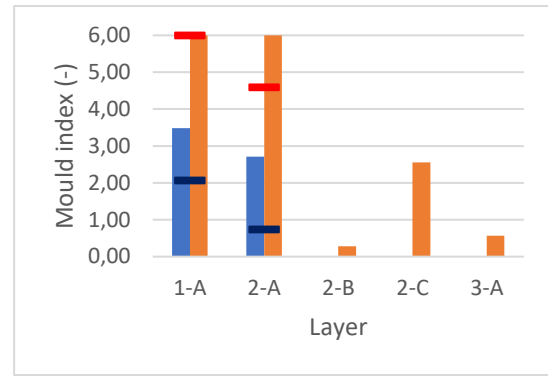


Figure 4.73 Mould index, humidity class 3, assembly 8

Assembly 9 – West wall, recreational room

Figure 4.74 presents wall assembly 9 and its respective monitor positions. Figure 4.75 is the graph with humidity class 1, while Figure 4.76 is humidity class 3. Simulations with climate 2010-2020 humidity class 1 and 3 have no indication of problems with mould. Simulations with climate 2060-2070 humidity class 1 and 3 both indicates problems with the cladding and insulation layer.

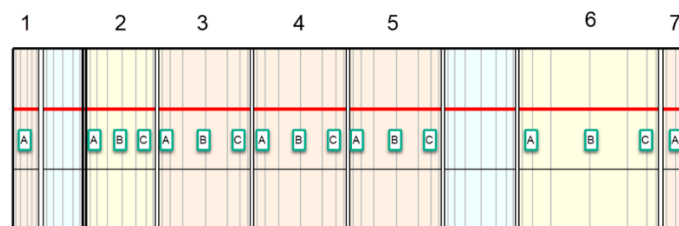


Figure 4.74 Wall assembly 9, monitor position

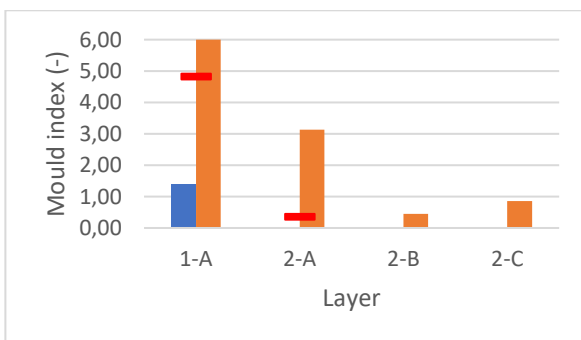


Figure 4.75 Mould index, humidity class 1, assembly 9

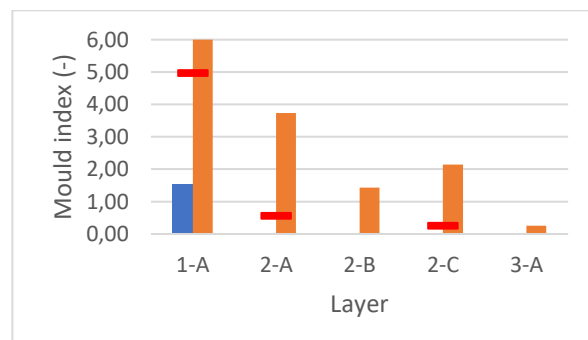


Figure 4.76 Mould index, humidity class 3, assembly 9

Assembly 10 - North wall, recreational room

Figure 4.77 presents wall assembly 9 and its respective monitor positions. Figure 4.78 is the graph with humidity class 1, while Figure 4.79 is humidity class 3.

Simulations with current climate and humidity class 1 and 3 have no indication of problem with mould except for the cladding. While simulations with future climate presents higher values, especially humidity class 3. Humidity class 1 indicates problems with the exterior layer of the logs, while humidity class 3 indicates problems within all layers of the wall.

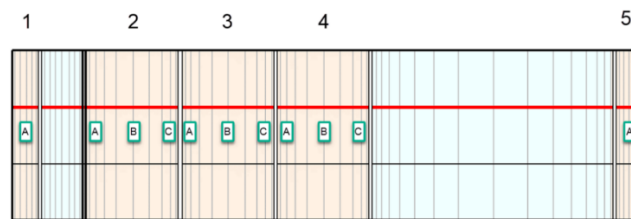


Figure 4.77 Wall assembly 10, monitor position

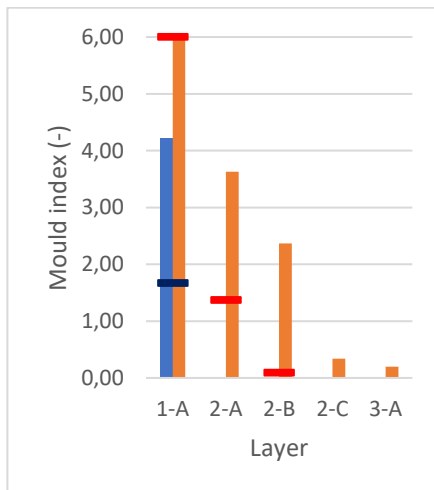


Figure 4.78 Mould index, humidity class 1, assembly 10

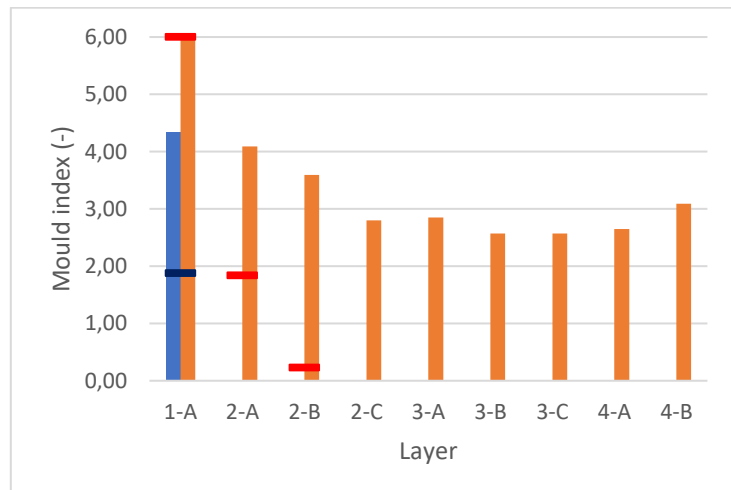


Figure 4.79 Mould index, humidity class 3, assembly 10

Assembly 11 – East wall, bedroom

Figure 4.80 presents wall assembly 9 and its respective monitor positions. Figure 4.81 is the graph with humidity class 1, while Figure 4.82 is humidity class 3.

Simulations with current climate and humidity class 1 and 3 have no indication of problem with mould except for the cladding. Simulations with future climate humidity class 1 and 3 is both within yellow indication at exterior side of the logs and red indication at the cladding.

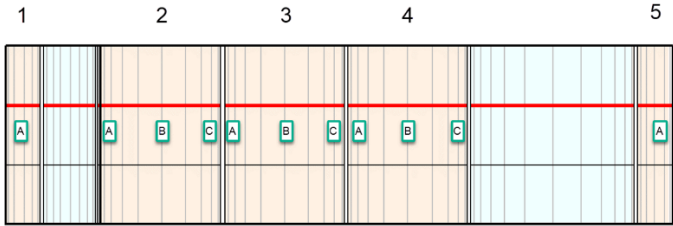


Figure 4.80 Wall assembly 11, monitor position

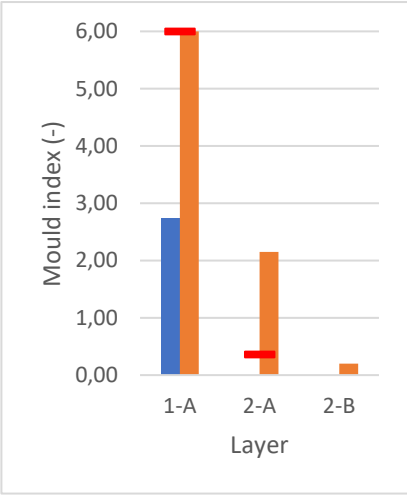


Figure 4.81 Humidity class 1, assembly 11

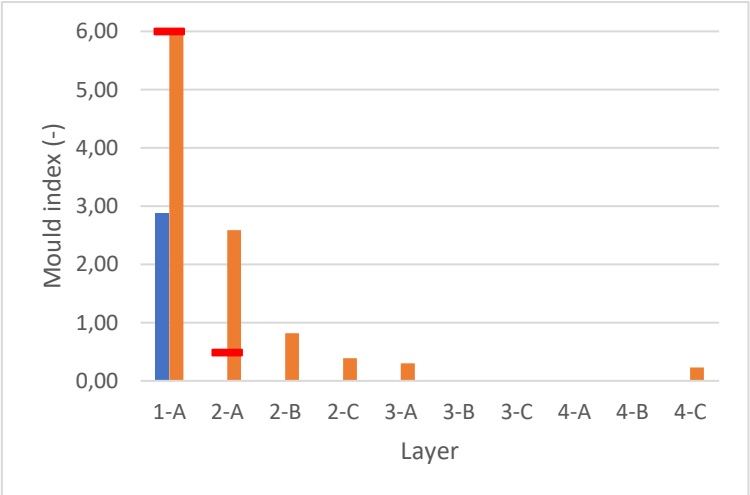


Figure 4.82 Humidity class 3, assembly 11

Summary

Table 4-12 presents a summary of the maximum index values based on current climate and future climate. The colour indication is similar to the mould index, while the diagonal line indicates elements not a part of the structure.

Table 4-12 Summary of the maximum mould index

Asse mbly	Mod	HC	Ex	Insulation			Logs exterior side			Logs middle part			Logs interior side			Insulation			Int	
				A	A	B	C	A	B	C	A	B	C	A	B	C	A	B		C
Asse mbly 1	2010	HC1	■																	
	2060	HC1	■	■	■	■														
	2010	HC3	■																	
	2060	HC3	■	■	■	■														
Asse mbly 2	2010	HC1	■																	
	2060	HC1	■	■	■	■														
	2010	HC3	■																	
	2060	HC3	■	■	■	■														
Asse mbly 3	2010	HC1	■																	
	2060	HC1	■	■																
	2010	HC3	■																	
	2060	HC3	■	■																
Asse mbly 4	2010	HC1	■																	
	2060	HC1	■				■	■												
	2010	HC3	■																	
	2060	HC3	■				■	■	■	■	■	■	■	■	■	■	■	■	■	■
Asse mbly 5	2010	HC1	■																	
	2060	HC1	■																	
	2010	HC3	■																	
	2060	HC3	■																	
Asse mbly 6	2010	HC1	■																	
	2060	HC1	■																	
	2010	HC3	■																	
	2060	HC3	■				■													
Asse mbly 7	2010	HC1	■																	
	2060	HC1	■	■	■	■														
	2010	HC3	■																	
	2060	HC3	■	■	■	■	■	■	■	■	■	■	■	■	■	■	■	■	■	■
Asse mbly 8	2010	HC1	■																	
	2060	HC1	■	■																
	2010	HC3	■																	
	2060	HC3	■	■			■													
Asse mbly 9	2010	HC1																		
	2060	HC1	■	■																
	2010	HC3																		
	2060	HC3	■	■			■													
Asse mbly 10	2010	HC1	■																	
	2060	HC1	■				■	■												
	2010	HC3	■																	
	2060	HC3	■				■	■	■	■	■	■	■	■	■	■	■	■	■	■
Asse mbly 11	2010	HC1	■																	
	2060	HC1	■				■													
	2010	HC3	■																	
	2060	HC3	■				■													

4.5.4 Comparison of current climate following RCP8.5 and observations

A comparison between the current climate from 2010 to 2020 based on observed data with climate 2010 to 2020 based on RCP8.5 was performed as way of evaluating future estimations. This chapter only includes the wall assembly 1 to explain the results while the remaining graphs of wall assembly 2 to 11 is included in APPENDIX B and APPENDIX C.

Figure 4.83 presents the moisture content of wall assembly 1. The blue bars represent the climate from 2010 to 2020 based on current climate, while the green bars indicate the climate from 2010 to 2020 based on RCP8.5. Observing the results with humidity class 1 the median values of exterior side, middle part and interior side increased by 6,5 %, 2,7 % and 2,7 % for RCP8.5, respectively. Furthermore, with humidity class 3 the increase from observed climate versus RCP8.5 for median values on exterior side, middle part and interior side was 4,3 %, 2,6 % and 3,1 %, respectively.

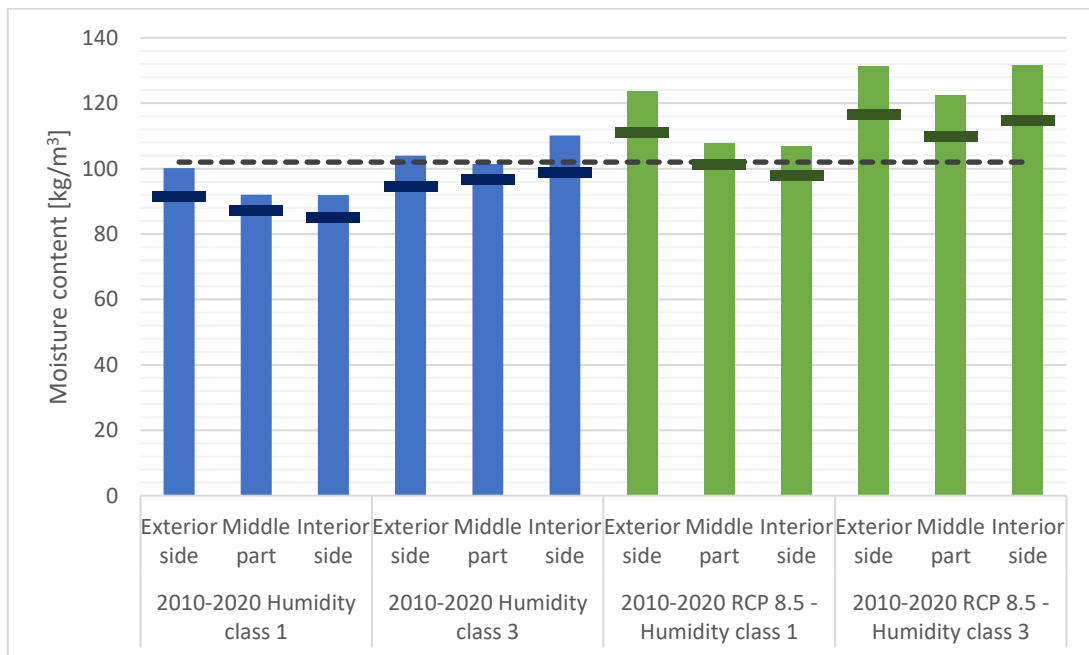


Figure 4.83 Wall assembly 1, RCP8.5 evaluation - moisture content

Figure 4.84 presents the mould index with humidity class 1, while Figure 4.85 presents humidity class 3. The mould index with climate 2010 to 2020 based on current weather indicates no trouble within the construction except for the cladding. Both humidity class 1 and 3 with climate 2010 to 2020 based on RCP8.5 show similar trends and indicates a high risk of mould in the exterior cladding and insulation layer. Humidity class 1 indicates no trouble with the layer of logs, while humidity class 3 are within a yellow indication.

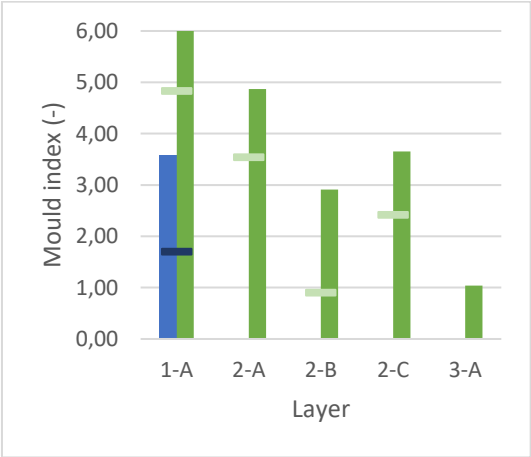


Figure 4.84 Assembly 1 - Mould index, RCP8.5 evaluation, humidity class 1

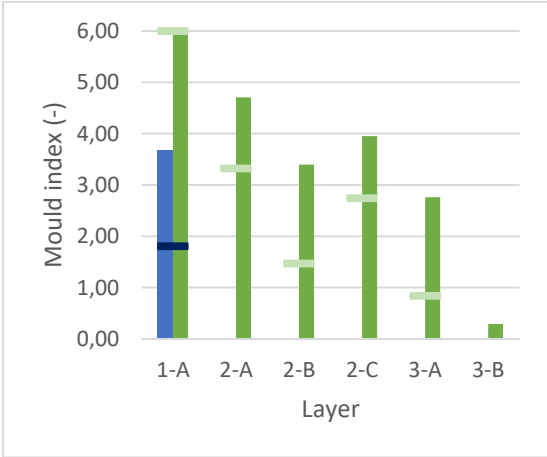


Figure 4.85 Assembly 1 - Mould index, RCP8.5 evaluation, humidity class 3

5 Discussion

Considering all the unique maintenance work performed at different times throughout the history of Bentegården, it has resulted in a building containing a large variety of solutions. This has created a situation where it has been possible to evaluate the hygrothermal performance of walls with different thickness and a combination of retrofitting measures.

The precision of the generated wall assemblies compared to the actual walls at Bentegården can be discussed. The degree of certainty is high for the thickness of the building envelope, however, there are still some uncertainties related to some of the individual elements forming the assemblies. Most of this is related to retrofitting measures performed years back, as defining the thickness and location of this is largely based on photographs and historic drawings. In many ways, infrared thermography has served the purpose of supporting these assumptions. This is justified by higher surface temperature and more thermal bridges in these specific areas. The latter is described in theory as being a common result of interior post-insulation. Besides this, the thermographic images captured concerning the work performed in this thesis may serve purposefully as a basis for evaluating other retrofitting measures. This may include post-insulation of the walls within the extension and replacement of certain windows. However, this needs to be evaluated concerning physical consequences and the building's originality.

Based on the illustration in chapter 4.4.2, the relative humidity in the period of data collection was undoubtedly lower than what is to be expected. Based on the standard EN 13788, the calculated humidity class reflects a situation associated with unoccupied buildings, storage of dry goods. The explanation for this can potentially be found with the help of an air-tightness test and a more thorough examination of moisture buffer performance, nor can it be ruled out that the standard overestimates moisture production in some cases.

Research related to climate and climate change is dependent on having reliable data as input to evaluate trends and consequences. In chapter 4.4.1, the three different sets of climate data got presented by their respective temperature and relative humidity. Specifically, for temperature, there are clear similarities between the observed climate data from weather stations and RCP8.5 climate data for 2010-2020 with an annual average temperature of 7,3 C° and 7,4 C°, respectively. When comparing the temperature in the two sets of current climates with the future RCP8.5 climate, the greatest temperature increase is present during the winter and the lowest during the summer. This corresponds with predictions described in chapter 2.6.

In the case of monthly average temperatures, it is difficult to quantify what can be described as similarities, but one might argue that there are similar trends with an overestimation for the months of January to April and in August. As illustrated with numbers from *Norsk Klimaservicesenter*, the annual precipitation is expected to increase following both low and high values of RCP8.5, but there are uncertainly related to the quantity, especially for the different seasons. The comparison between current and future climate suggested a drastic increase during the winter and spring, especially with respect to the climate data from weather stations. The following seasons showed a more even or slightly reduced sum. All of this corresponds to numbers from *Norsk Klimaservicesenter*.

For the relative humidity, however, there seems to be an overestimation of the moisture content in the air throughout the entire year. The RH from weather stations indicated a yearly average of 77,1 %, while the RCP8.5 data for the same period got an average of 85,1 % and 84,5 % for 2060-2070. Comparing the results with climate 2010 to 2020 based on climate history with the climate based on the RCP8.5 indicates a moisture content of up to 5 % higher with climate based on the RCP8.5. The mould index indicates problems with several wall assemblies, primarily within the insulation. This causes some uncertainty as to how accurate the climate predictions in this thesis are. However, one might argue that a potential overestimation of the future climate and its respective simulated results more clearly excludes areas of potential threats.

The moisture content of the logs is kept below the 20 % critical value between 2010 to 2020 based on observed climate with humidity class 1. A change from humidity class 1 to 3 increased the moisture content within all wall assemblies. While most of the wall assemblies stay around 20% or lower, wall assembly 4 and 10 presents higher values, reaching up to 24 %. Replacing this climate model with the climate from 2060 to 2070 based on RCP8.5 with humidity class 1 returns similar or slightly higher values than 2010 to 2020 with humidity class 3. Furthermore, the moisture content with climate 2060 to 2070 and humidity class 3 presents the overall highest values. Inspecting these results also gives the highest values related to wall assembly 4 and 10 with a moisture content of about 27 % in the logs. According to this, several wall assemblies is at risk regarding mould growth, especially assembly 4 and 10.

Regarding the mould index for the observed 2010-2020 climate, there is no indication of mould growth using either of the humidity classes, except for in the cladding. However, simulations with future climate indicate problems with mould growth within several wall

assemblies. This climate combined with humidity class 1 mostly indicate problems with the cladding and exterior insulation layer, but for wall assembly 4 and 10 there is an indication of problems on the exterior side of the logs, while assembly 11 is kept yellow. By increasing the moisture production according to humidity class 3, there is evidently a risk of mould growth throughout the entire section of the logs for assembly 4 and 10, with the mould index growing increasingly towards the interior and exterior surface. Additionally, assembly 6 and 7 becomes yellow towards the exterior section of the logs.

Wall assembly 4 and 10 are both oriented towards the north, together with wall assembly 5. However, the difference between wall assembly 4 and 10 compared to 5 is a large air layer on the interior side of the logs. This air layer results in a u-value significantly lower in assembly 4 and 10. The u-value of assembly 5 is 0,609 W/m²K, while assembly 4 and 10 is 0,253 W/m²K and 0,244 W/m²K, respectively. The low u-value decreases the heat transport through the wall and due to the orientation, the sun exposure is rather low. This combination might be the reason for higher moisture content and indications of problems with mould within the structure.

The critical value of 20% is surpassed within several layers without the mould index indicating major problems. The highest percentage of moisture content observed in an area not subjected to risk of mould growth according to the mould index were in assembly 2 with future climate and humidity class 3. Here the moisture content of the outer layers of the logs reached 24,5 % without there being any indication of mould growth. In the most problematic assemblies, assembly 4 and 10, the moisture content reached 27 %.

6 Conclusion

This master thesis has been centred around evaluating the hygrothermal performance of the log walls in the in-use cultural heritage building Bentegården, but the results apply to buildings with similar characteristics.

The process has included the use of 3D laser scanning and infrared thermography as a method for clarifying the lack of information concerning construction assemblies. These technologies already well described in theory and previous research and this thesis further emphasizes the value of integrating these technologies in cultural heritage research.

Based on the comparison between the observed climate data and RCP8.5 for 2010-2020, there is evidently an overestimation, especially for the relative humidity. This is resulting in the hygrothermal simulations indicating a situation where visual findings of mould could be expected in the insulation layers. To the authors best knowledge, this is not the case, which corresponds with the simulations using climate data from weather stations and interior climate related to what has been measured on-site. This causes some uncertainty as to how accurate the climate predictions used in this thesis are, although this is fundamental for all climate predictions. Anyhow, it serves purposefully in indicating what sections might be more prone to complications.

For the walls with exterior insulation, the hygrothermal simulations with the future climate based on RCP8.5 and current humidity class indicated no problems with mould growth in the logs, but a high risk of mould growth within the insulation. The only walls presented with a high risk of mould growth in the logs following this scenario were those orientated north without any insulation, but with an interior air layer. By increasing the moisture production according to how the standard categorizes a household with few residents, one of the outer layers of the insulated logs becomes yellow, meaning there is some uncertainty related to the risk of mould growth. Furthermore, the moisture content and mould index illustrate that the critical value of 20 % can be breached without necessarily resulting in problems with mould growth.

It can thus be concluded that there are little to no risk of mould growth in the logs subjected to the current climate, but problems cannot be ruled out following a “business as usual” climate scenario, especially where the timber is not protected by exterior insulation.

7 Future research

Further research will continue on the Hyperion test site of Tønsberg and Bentegården where parts of the work that has been initiated in this thesis may serve purposefully. As mentioned earlier in the thesis, installation of the loggers got postponed due to travel restrictions caused by Covid-19, resulting in a relatively short period of data collection from the temperature and humidity loggers. However, the data loggers will continue collecting data, meaning that any future research will have a better basis for evaluation.

As identified by the IR images, there are evidently potential for improvements related to energy savings at Bentegården. An interesting approach could be to evaluate other retrofitting solutions and their impact on the building's originality, followed by a comparison of the results against similar studies.

The digital model created in relationship with this master thesis can serve as a basis for a whole-building simulation. However, an identification of the remaining assemblies within the building envelope, supported by an air-tightness test to determine the leakage number would be valuable in this case.

References

- Almås, A.-J., Lisø, K. R., Hygen, H. O., Flyen, C., & Thue, J. V. (2011). An approach to impact assessments of buildings in a changing climate [Scientific article]. 227-238. <https://doi.org/https://doi.org/10.1080/09613218.2011.562025>
- Barrile, V., Fotia, A., & Francesca Panzera, M. (2021). No-Destructive Analysis: 3D Modeling by Thermography for Cultural Heritage. In C. Bevilacqua, F. Calabrò, & L. Della Spina, *New Metropolitan Perspectives* Cham.
- Bird, R. E., & Hulstrom, R. L. (1981). A Simplified Clear Sky Model for Direct and Diffuse Insolation on Horizontal Surfaces. <https://www.nrel.gov/docs/legosti/old/761.pdf>
- Bras, R. L. (1990). *Hydrology: an introduction to hydrologic science*. Addison-Wesley.
- [Record #57 is using a reference type undefined in this output style.]
- Brønne, J. (2021). *Slik maler du gamle hus*. Retrieved 25.03 from <https://www.byggogbevar.no/pusse-opp/maling/artikler/male-trehus-og-tradisjonelle-malinger>
- Coelho, G. B. A., Entradas Silva, H., & Henriques, F. M. A. (2019). Development of a three-dimensional hygrothermal model of a historic building in WUFI@Plus vs EnergyPlus. *MATEC Web Conf.*, 282, 02079. <https://doi.org/10.1051/mateconf/201928202079>
- Dammann, Å. (2020). *STATUS FOR VERNEVERDIGE KULTURMINNER I UTVALGTE KOMMUNER - Sammendragsrapport 2000-2019 Bø i Telemark, Flora, Kautokeino, Melhus, Nittedal, Nord-Aurdal, Saltdal, Samnanger, Sandnes og Tromsø*. NIKU. <https://hdl.handle.net/11250/2658600>
- Edvardsen, K. I., & Ramstad, T. Ø. (2014). *Trehus*.
- Engineering ToolBox. (2003). *Mollier Diagram*. Retrieved 16.05 from https://www.engineeringtoolbox.com/psychrometric-chart-mollier-d_27.html
- EURO-CORDEX. (n.d). *EURO-CORDEX - Coordinated Downscaling Experiment - European Domain*.
- Fatorić, S., & Seekamp, E. (2017). *Are cultural heritage and resources threatened by climate change? A systematic literature review*.

- Flato, G., Marotzke, J., Abiodun, B., Braconnot, P., Chou, S. C., Collins, W., Cox, P., Driouech, F., Emori, S., & Eyring, V. (2014). Evaluation of climate models. In *Climate change 2013: the physical science basis. Contribution of Working Group I to the Fifth Assessment Report of the Intergovernmental Panel on Climate Change* (pp. 741-866). Cambridge University Press.
- François, A., Ibos, L., Feuillet, V., & Meulemans, J. (2021, 2021/02/15/). In situ measurement method for the quantification of the thermal transmittance of a non-homogeneous wall or a thermal bridge using an inverse technique and active infrared thermography. *Energy and Buildings*, 233, 110633. <https://doi.org/https://doi.org/10.1016/j.enbuild.2020.110633>
- Glass, S., TenWolde, A., & Zelinka, S. (2013, 10/01). Hygrothermal Simulation: A Tool for Building Envelope Design Analysis. *Wood Design Focus*, 23, 18-25.
- Glavaš, H., Hadzima-Nyarko, M., Haničar Buljan, I., & Barić, T. (2019). Locating Hidden Elements in Walls of Cultural Heritage Buildings by Using Infrared Thermography. *Buildings*, 9(2), 32. <https://www.mdpi.com/2075-5309/9/2/32>
- Gustavsen, L. (2010). *Laserskanning av ruinene på Slottsfjellet, Tønsberg, Vestfold*. N. i. f. kulturminneforskning.
- Gustavsen, L. (2011). *Laserskanning av Oktogonen i Nidaros Domkirke* (NIKU Oppdragsrapport;226/2011, Issue. N. i. f. kulturminneforskning. <http://hdl.handle.net/11250/2505275>
- Hanssen-Bauer, I., Førland, E. J., Haddeland, I., Hisdal, H., Mayer, S., Nesje, A., Nilsen, J. E. Ø., Sandven, S., Sandø, A. B., Sortberg, A., & Ådlandsvik, B. (2017). Climate in Norway 2100 - a knowledge base for climate adaptation. <https://www.miljodirektoratet.no/globalassets/publikasjoner/M741/M741.pdf>
- Hens, H. (2017). Building physics heat, air and moisture: fundamentals and engineering methods with examples and exercises.
- Holme, J. (2010). *Mould growth in buildings* [Doctoral thesis, NTNU].
- Holme, J., Stang, K., Guribye, R., Fjeli, S., & Finne, M. (2020). Kulturminnevern - kulturminneloven med kommentarer. <https://www.riksantikvaren.no/revidert-utgave-av-kulturminnevern-kulturminneloven-med-kommentarer/>
- Hukka, A., & Viitanen, H. A. (1999, 1999/12/01). A mathematical model of mould growth on wooden material. *Wood Science and Technology*, 33(6), 475-485. <https://doi.org/10.1007/s002260050131>

- Hyperion. (2020). *HYPERION's Vision*. <https://www.hyperion-project.eu/hyperions-vision/>
- Kaslegard, A. S. (2010). Klimaendringer og kulturarv i Norden. <https://norden.diva-portal.org/smash/get/diva2:701587/FULLTEXT01.pdf>
- Lov om kulturminner, (1979a). <https://lovdata.no/dokument/NL/lov/1978-06-09-50>
- Lov om kulturminner, (1979b). <https://lovdata.no/dokument/NL/lov/1978-06-09-50>
- Laefer, D. F., & Truong-Hong, L. (2017, 2017/02/01/). Toward automatic generation of 3D steel structures for building information modelling. *Automation in Construction*, 74, 66-77. <https://doi.org/https://doi.org/10.1016/j.autcon.2016.11.011>
- Masri, Y. E., & Rakha, T. (2020). A scoping review of non-destructive testing (NDT) techniques in building performance diagnostic inspections. <https://doi.org/https://doi.org/10.1016/j.conbuildmat.2020.120542>
- [Record #33 is using a reference type undefined in this output style.]
- Mercuri, F., Cicero, C., Orazi, N., Paoloni, S., Marinelli, M., & Zammit, U. (2015, 2015/06/01). Infrared Thermography Applied to the Study of Cultural Heritage. *International Journal of Thermophysics*, 36(5), 1189-1194. <https://doi.org/10.1007/s10765-014-1645-x>
- NIKU. (n.d.). *Laserskanning*. <https://www.niku.no/laserskanning/>
- Norsk Klimaservicesenter. (2021). *Klimaprofil Vestfold*. <https://klimaservicesenter.no/kss/klimaprofiler/vestfold>
- Ojanen, T., Peuhkuri, R., Viitanen, H., Lähdesmäki, K., Vinha, J., & Salminen, K. (2011). Classification of material sensitivity—new approach for mould growth modeling. 9th Nordic symposium on building physics,
- Rajčić, V., Skender, A., & Damjanović, D. (2018). An innovative methodology of assessing the climate change impact on cultural heritage. *International Journal of Architectural Heritage*. <https://doi.org/10.1080/15583058.2017.1354094>
- Riahi, K., Rao, S., Krey, V., Cho, C., Chirkov, V., Fisher, G., Kindermann, G., Nikacenovic, N., & Rafaj, P. (2011). RCP 8.5—A scenario of comparatively high greenhouse gas emissions. *Climatic Change*, 109. <https://doi.org/https://doi.org/10.1007/s10584-011-0149-y>

Riksantikvaren. (2002). Riksantikvarens informasjon om kulturminner 3.9.4.
https://ra.brage.unit.no/ra-xmlui/bitstream/handle/11250/175403/Infoark_394_UtvendigmalingLInoljemaling.pdf?sequence=1&isAllowed=y

[Record #65 is using a reference type undefined in this output style.]

Riksantikvaren. (2013). Veileder - Råd om energisparing i gamle hus.
<https://www.riksantikvaren.no/wp-content/uploads/2020/03/Energieffektivisering-av-gamle-hus.pdf>

Riksantikvaren. (2020a). Hva kan vi lære av gamle hus og byer.
<https://www.riksantikvaren.no/klima-og-kulturminner/hvordan-reducere-klimabelastningene/hva-kan-vi-laere-av-gamle-hus-og-byer/>

Riksantikvaren. (2020b). *Miljøovervåkning og overvåkingsprogrammer*.
<https://www.riksantikvaren.no/prosjekter/miljoovervakning-og-overvakingsprogrammer/#overvakingsprogram>

Riksantikvaren. (2020c). *SEFRAK-registeret*. <https://www.riksantikvaren.no/les-om/sefrak/>

[Record #62 is using a reference type undefined in this output style.]

Sedlbauer, K. (2001, 01/01). Prediction of Mould Fungus Formation on the Surface of and Inside Building Components.

Sedlbauer, K. (2002, 2002/04/01). Prediction of Mould Growth by Hygrothermal Calculation. *Journal of Thermal Envelope and Building Science*, 25(4), 321-336.
<https://doi.org/10.1177/0075424202025004093>

Sesana, E., Bertolin, C., Loli, A., Gagnon, A. S., Hughes, J., & Leissner, J. (2019). Increasing the Resilience of Cultural Heritage to Climate Change Through the Application of a Learning Strategy. In A. Moropoulou, M. Korres, A. Georgopoulos, C. Spyarakos, & C. Mouzakis, *Transdisciplinary Multispectral Modeling and Cooperation for the Preservation of Cultural Heritage* Cham.

SINTEF Byggforsk. (1999). 471.111 Beregningsmetode for å unngå kondens eller muggvekst på innvendige overflater.

SINTEF Byggforsk. (2004). 723.511 Etterisolering av yttervegger av tre.
<https://www.byggforsk.no/dokument/679/etterisolering-av-yttervegger-av-tre>

SINTEF Byggforsk. (2013). 471.431 U-verdier. Vegger over terreng - laftet tre.

- SINTEF Byggforsk. (2014). 474.624 *Luftlekkasjemåling av bygninger. Hensikt og vurdering*. https://www.byggforsk.no/dokument/4126/luftlekkasjemaaling_av_bygninger_hensikt_og_vurdering
- SINTEF Byggforsk. (2015). 571.523 Trevirke. Treslag og materialelegenskaper.
- SINTEF Byggforsk. (2017). 723.304 Eldre laftede vegger. Metoder og materialer.
- SINTEF Byggforsk. (2019a). 472.001 Kuldebroer. Typer, konsekvenser og bruk av normalisert kuldebroverdi.
- SINTEF Byggforsk. (2019b). 523.291 Bygninger med laftede vegger.
- Solla, M., Gonçalves, L. M. S., Gonçalves, G., Francisco, C., Puente, I., Providência, P., Gaspar, F., & Rodrigues, H. (2020). A Building Information Modeling Approach to Integrate Geomatic Data for the Documentation and Preservation of Cultural Heritage. *Remote Sensing*, 12(24), 4028. <https://www.mdpi.com/2072-4292/12/24/4028>
- SSB. (2021). *Kommune - Tønsberg (Vestfold og Telemark)*. <https://www.ssb.no/kommunefakta/tonsberg>
- Stein, M., & Gustavsen, L. (2013). Digital rekonstruksjon av Holdhusmadonnaen basert på fargeundersøkelse og 3D laserskanning. *Meddelelser om konservering*.
- Svensson, A., Haugen, A., Kalbakk, T. E., & Gåsbak, J. (2012). *Energieffektivisering i eksisterende bygninger - Energisparingens konsekvenser*. https://ra.brage.unit.no/ra-xmlui/bitstream/handle/11250/176814/Energieffektivisering_SINTEFrapport.pdf?sequence=1&isAllowed=y
- Minimumskrav til energieffektivitet, (2017). <https://dibk.no/regelverk/byggteknisk-forskrift-tek17/14/14-3/>
- Thuestad, E. A., Risbøl, O., Kleppe, J. I., Barlindhaug, S., & Myrvoll, E. R. (2021). Archaeological Surveying of Subarctic and Arctic Landscapes: Comparing the Performance of Airborne Laser Scanning and Remote Sensing Image Data. *Sustainability*. <https://doi.org/https://doi.org/10.3390/su13041917>
- Vaittinada Ayar, P., Vrac, M., Bastin, S., Carreau, J., Déqué, M., & Gallardo, C. (2016, 2016/02/01). Intercomparison of statistical and dynamical downscaling models under the EURO- and MED-CORDEX initiative framework: present climate evaluations. *Climate Dynamics*, 46(3), 1301-1329. <https://doi.org/10.1007/s00382-015-2647-5>

- van Vuuren, D. P., Edmonds, J., Kainuma, M., Riahi, K., Thomson, A., Hibbard, K., Hurtt, G. C., Kram, T., Krey, V., Lamarque, J.-F., Masui, T., Meinshausen, M., Nakicenovic, N., Smith, S. J., & Rose, S. K. (2011, 2011/08/05). The representative concentration pathways: an overview. *Climatic Change*, *109*(1), 5. <https://doi.org/10.1007/s10584-011-0148-z>
- Viitanen, H., Krus, M., Ojanen, T., Eitner, V., & Zirkelbach, D. (2015a). Mold Risk Classification Based on Comparative Evaluation of Two Established Growth Models. <https://doi.org/https://doi.org/10.1016/j.egypro.2015.11.165>
- Viitanen, H., Krus, M., Ojanen, T., Eitner, V., & Zirkelbach, D. (2015b). *Mold Risk Classification Based on Comparative Evaluation of Two Established Growth Models* (Vol. 78). <https://doi.org/10.1016/j.egypro.2015.11.165>
- Volk, R., Stengel, J., & Schultmann, F. (2014, 2014/03/01/). Building Information Modeling (BIM) for existing buildings — Literature review and future needs. *Automation in Construction*, *38*, 109-127. <https://doi.org/https://doi.org/10.1016/j.autcon.2013.10.023>
- Younes, C., Abishdid, C., & Bitsuamlak, G. (2012, 01/01). Air infiltration through building envelopes: A review. *Journal of Building Physics - J BUILD PHYS*, *35*, 267-302. <https://doi.org/10.1177/1744259111423085>

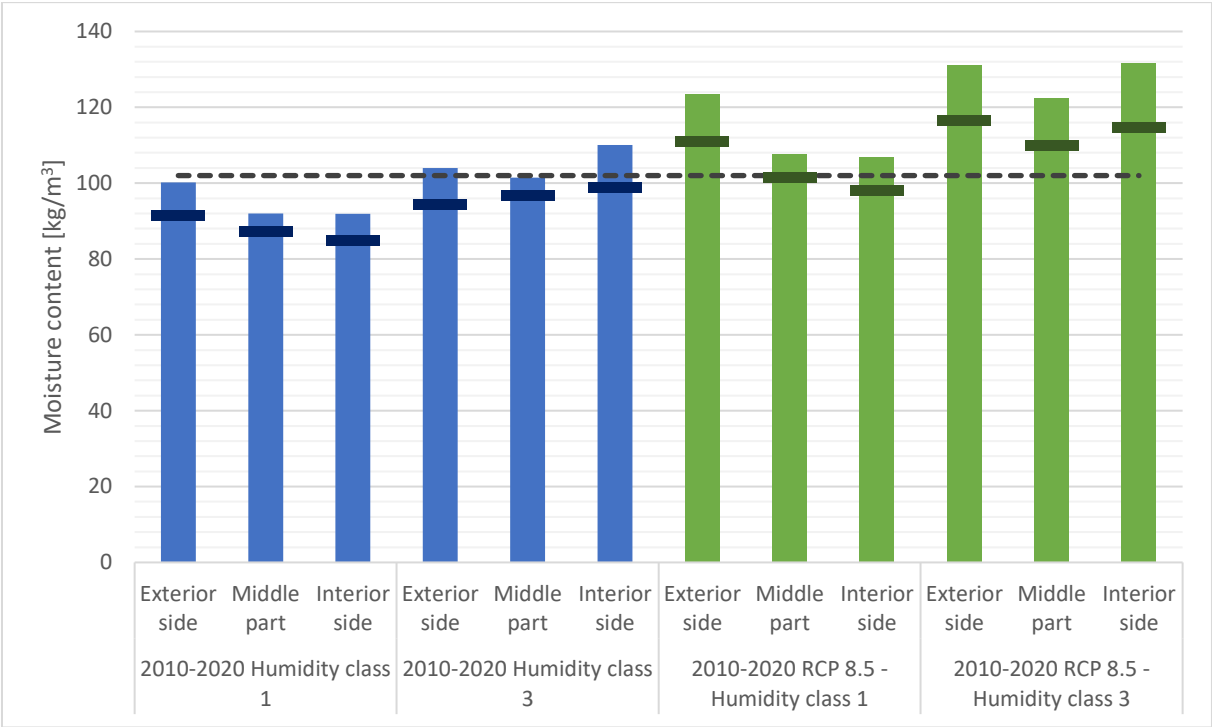
APPENDICES

APPENDIX A - Input data from WUFI

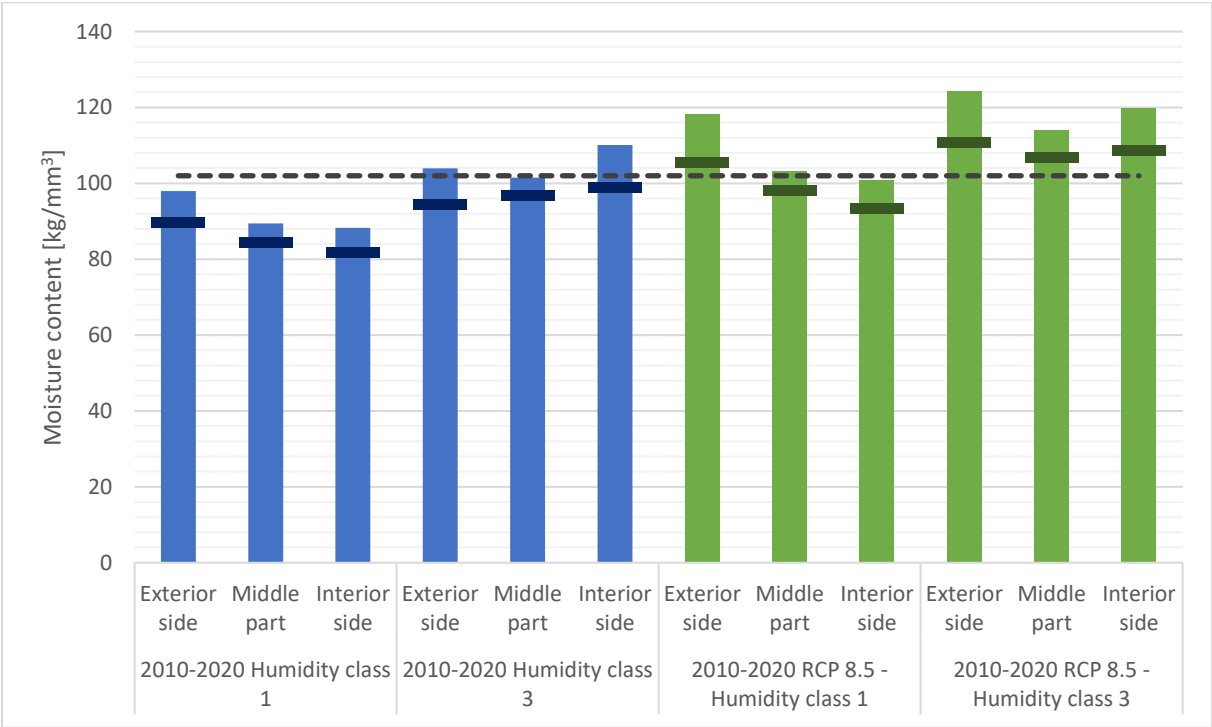
Input data in WUFI		
Construction	Structure Monitor position	Table XX Monitor position according to chapter X.X
	Orientation Height Slope	South/West/North/East Low building < 10m 90 degrees
	Surface transition coefficient: Exterior surface Heat resistance [m ² K/W] sD-value [m] Shortwave radiation absorption rate Terrain. Shortwave reflection rate Rainwater absorption rate Interior surface Heat resistance [m ² K/W] sD-value [m]	Wind dependent 0.5 0.5 0.2 – standard value 0.7 – Dependent on component slope 0.125 1.0
	Start settings: Relative humidity Temperature [°C]	 0.5 20
	Settings	Time: Start simulation End simulation
Climate	Outside	Climate file
	Inside	EN 13788 Humidity class 1 & 3

APPENDIX B - Moisture content 2010-2020, current climate vs RCP8.5

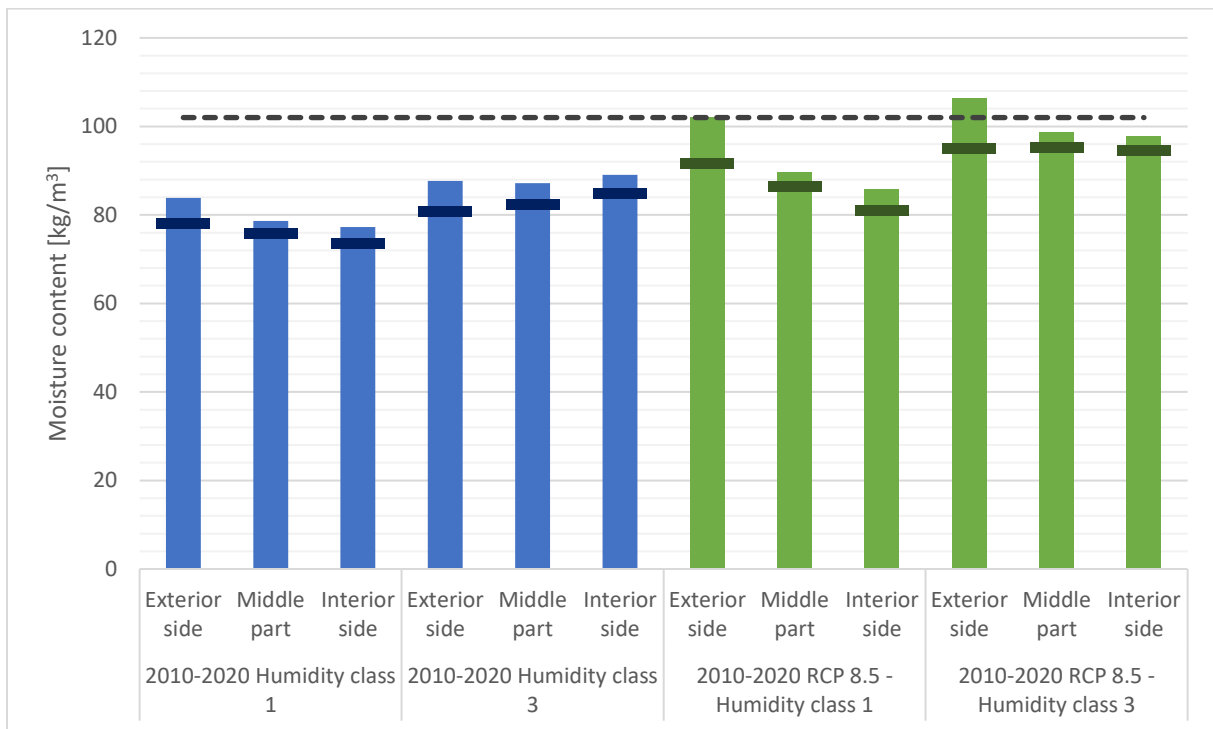
Assembly 1 – South wall, living room



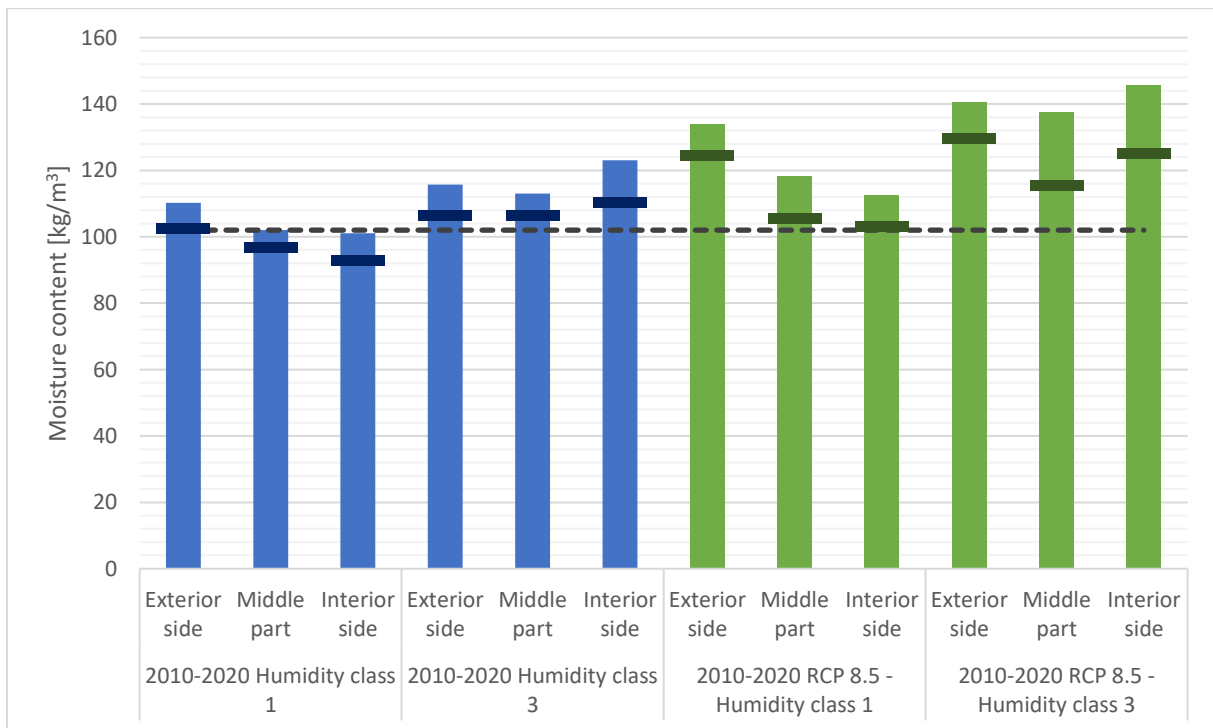
Assembly 2 – South wall, TV-room



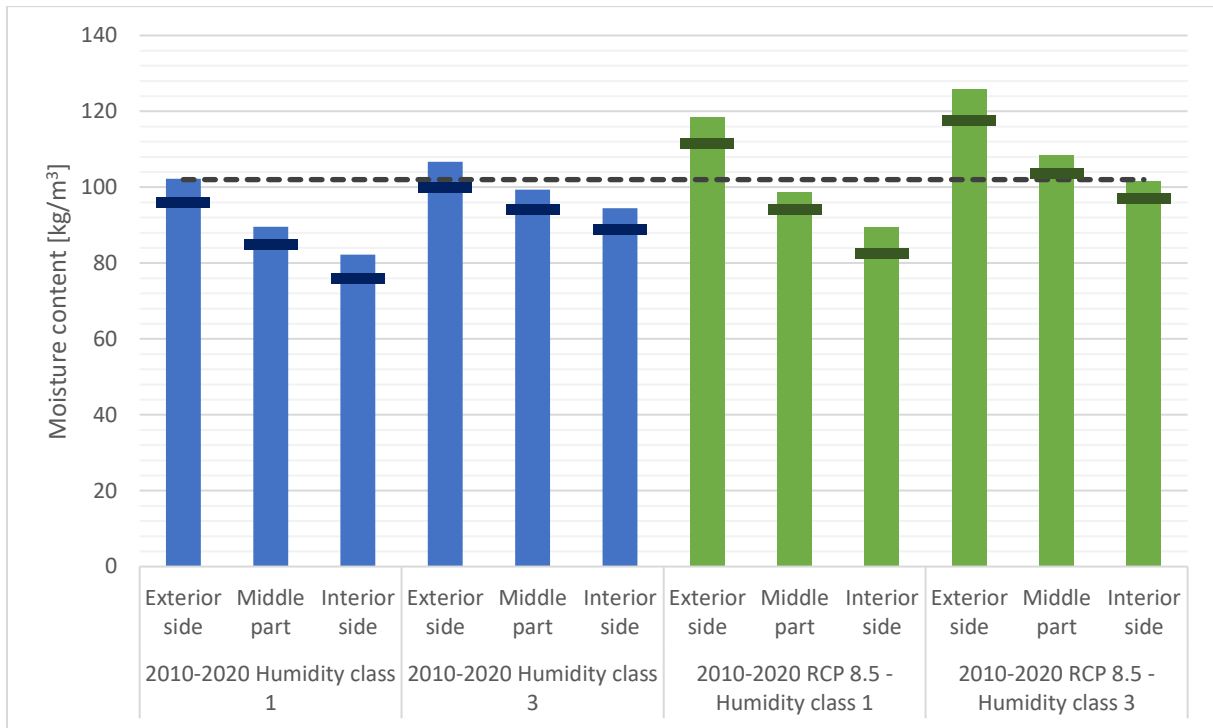
Assembly 3 – West wall, living room



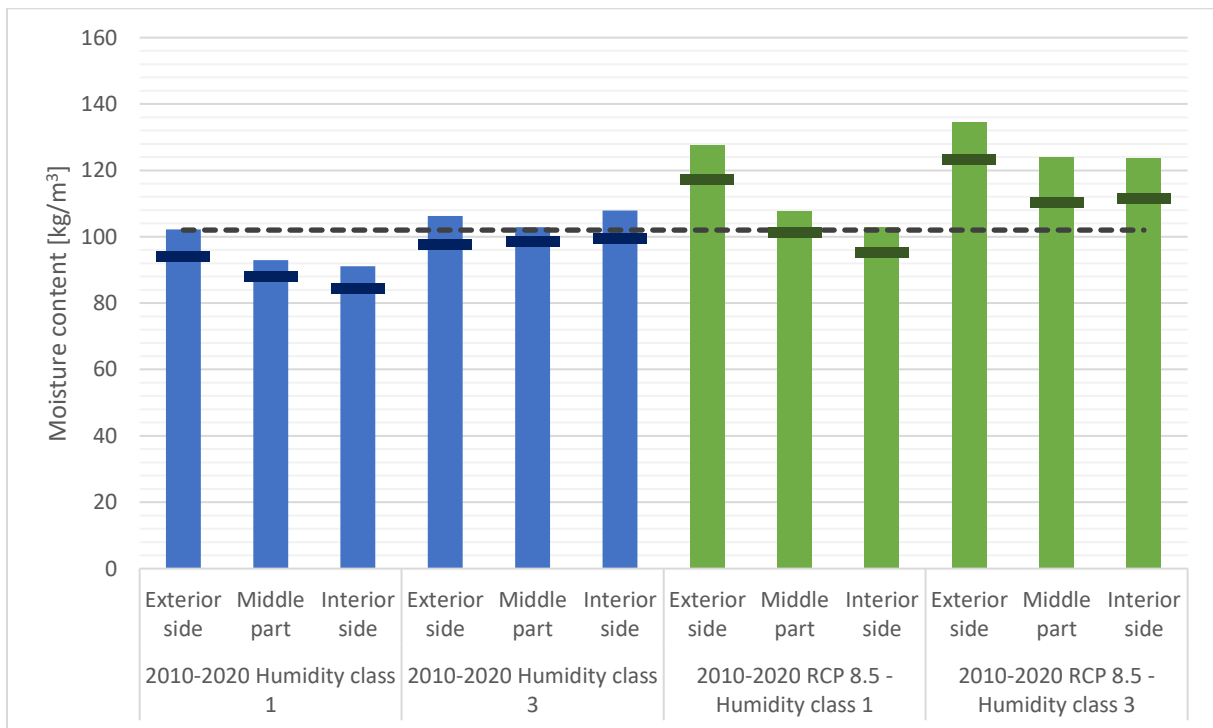
Assembly 4 – North wall, living room



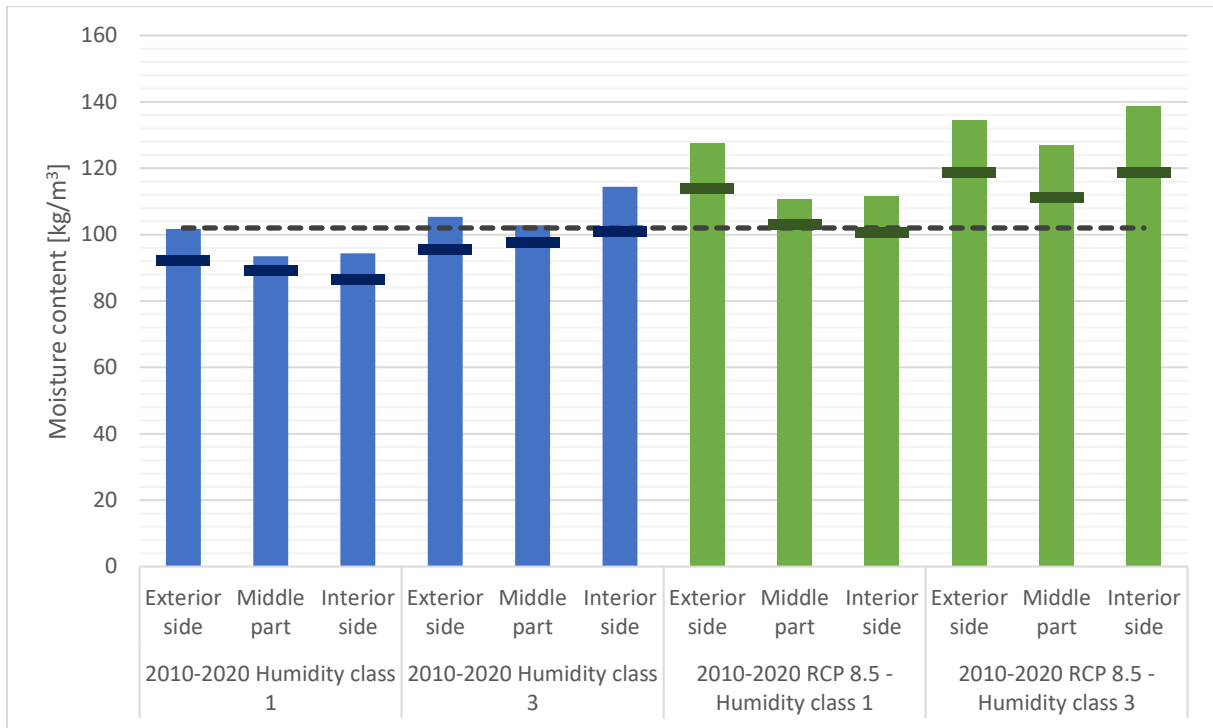
Assembly 5 – North wall, old entrance



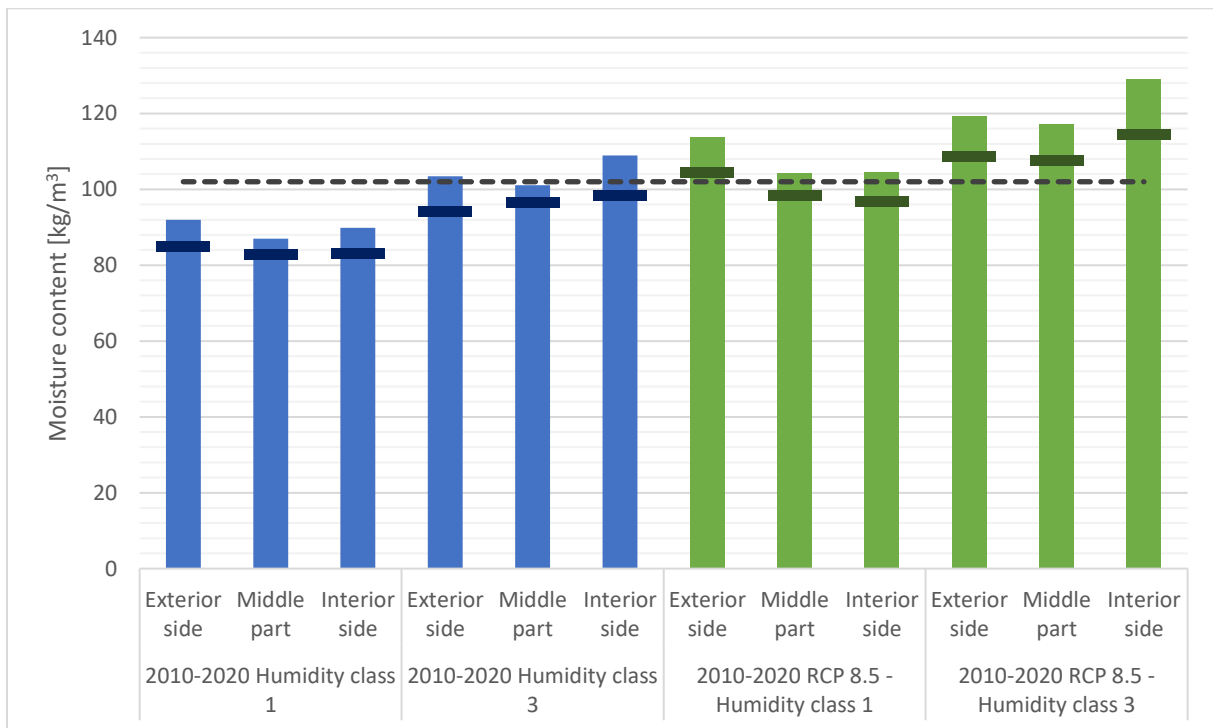
Assembly 6 – East wall, TV-room



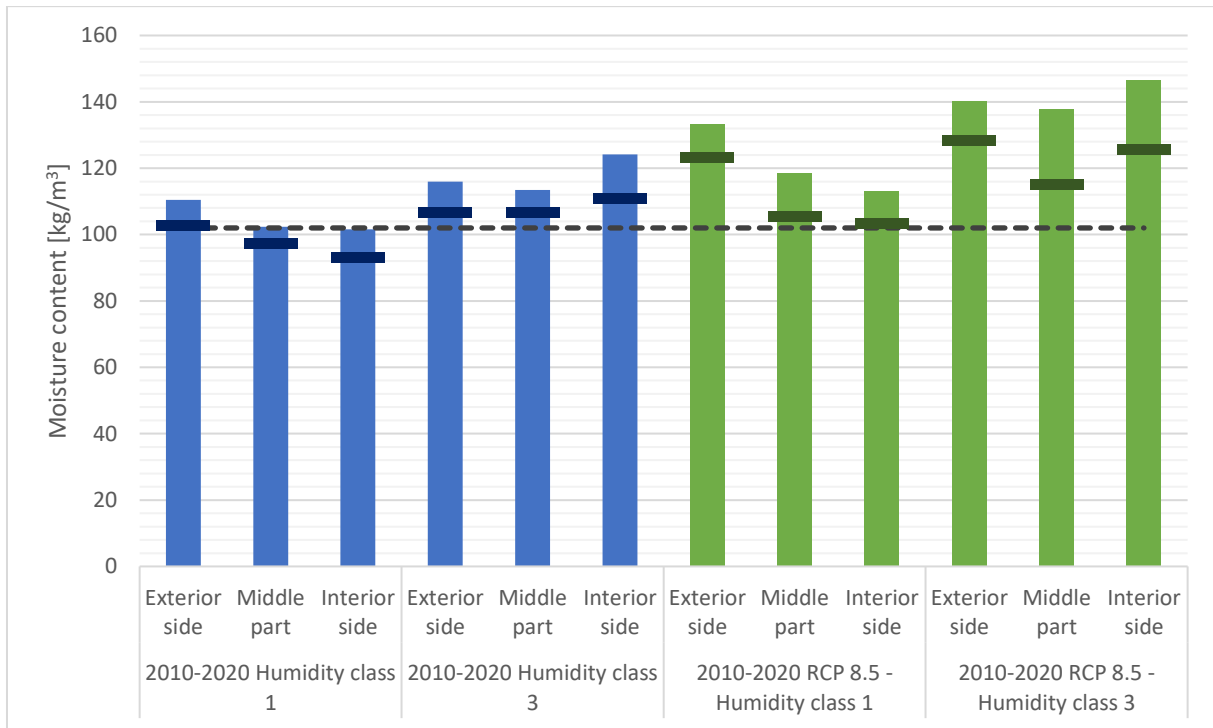
Assembly 7 – South wall, recreational room



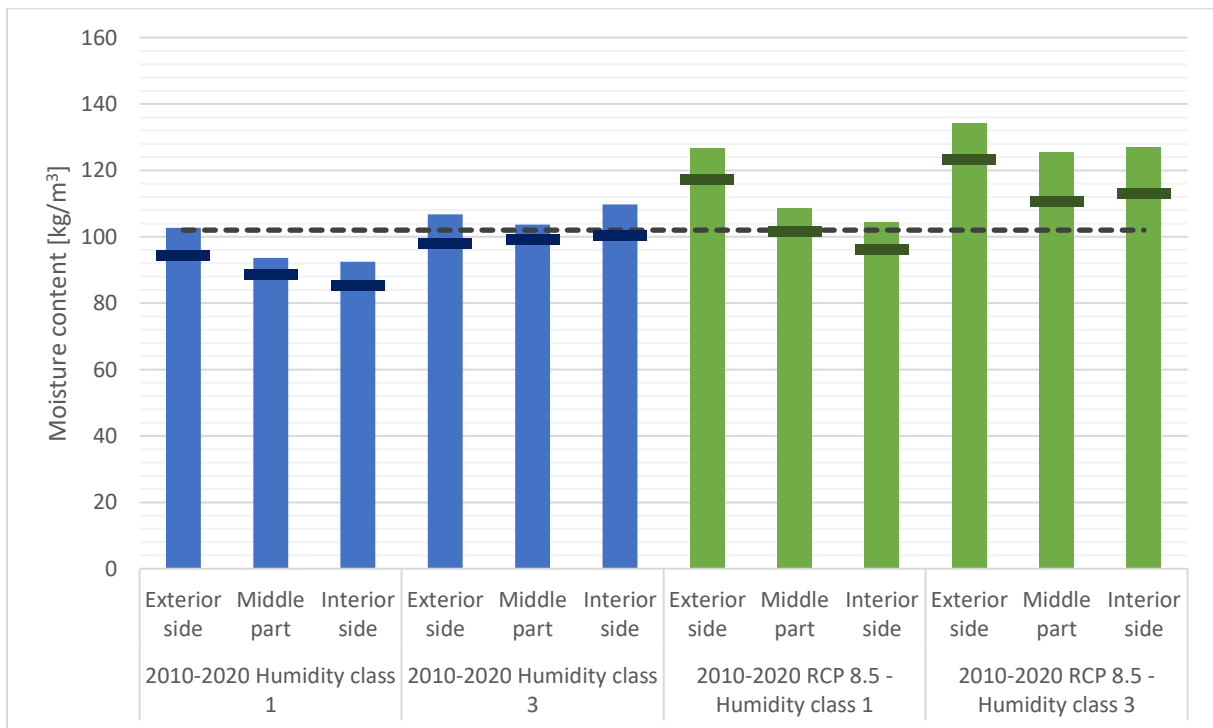
Assembly 9 – West wall, recreational room



Assembly 10 - North wall, recreational room

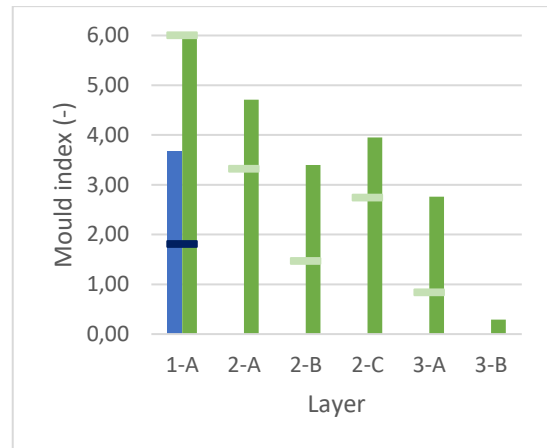
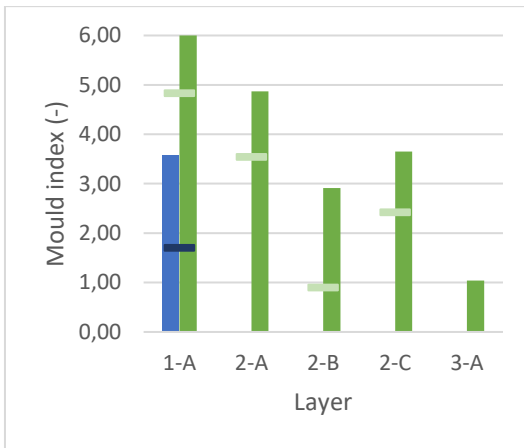


Assembly 11 – East wall, bedroom

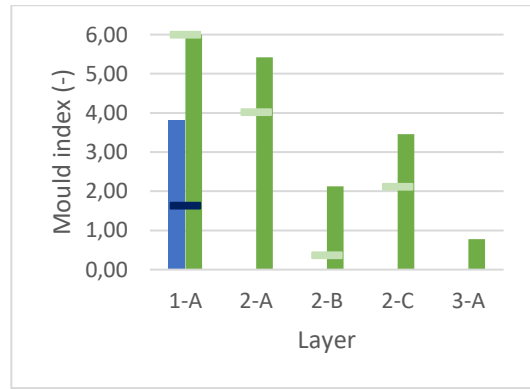
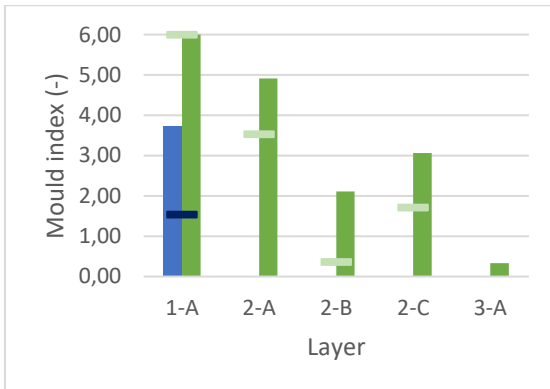


APPENDIX C - Mould index 2010-2020, current climate vs RCP8.5

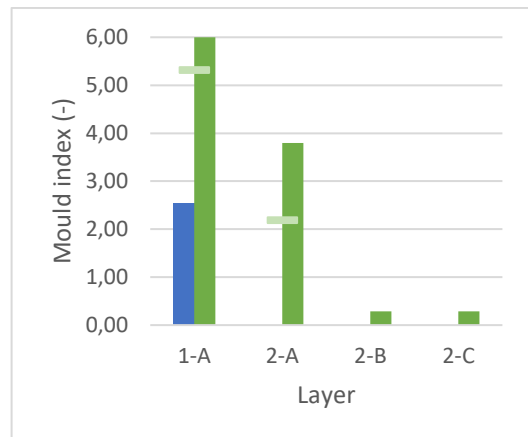
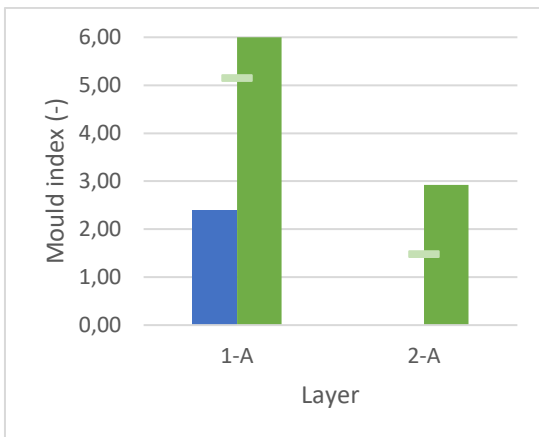
Assembly 1 – South wall, living room



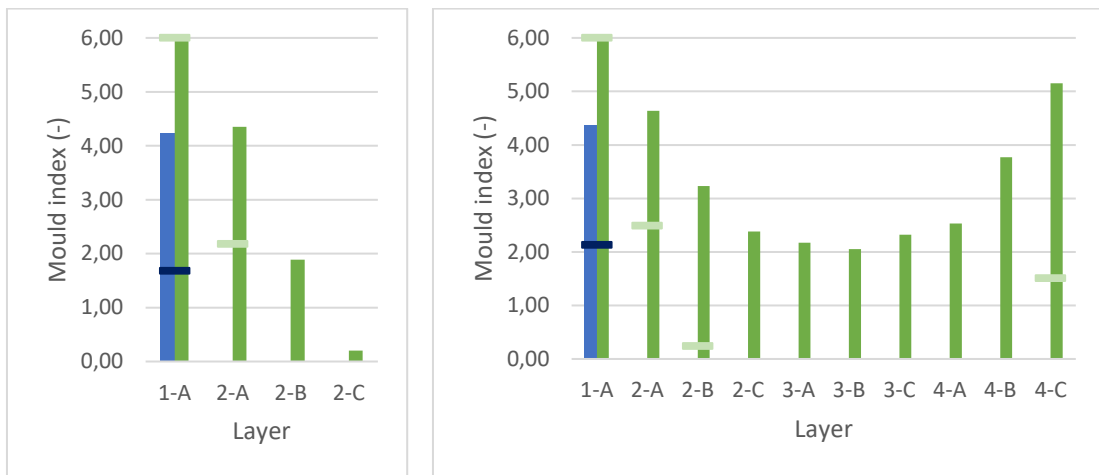
Assembly 2 – South wall, TV-room



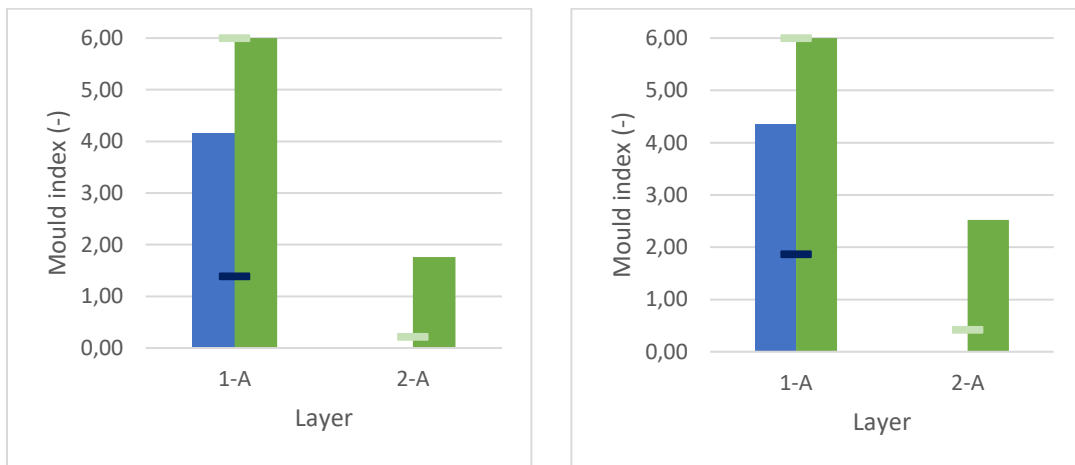
Assembly 3 – West wall, living room



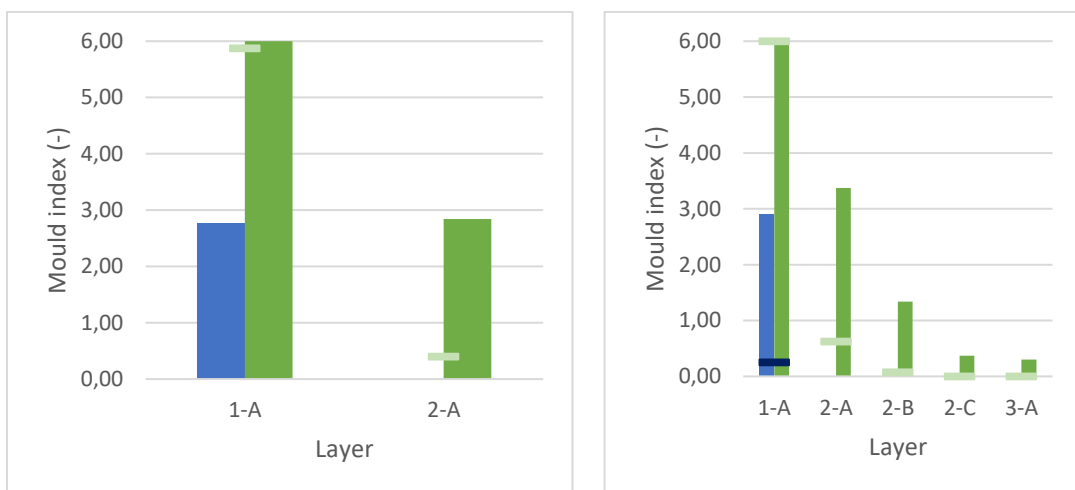
Assembly 4 – North wall, living room



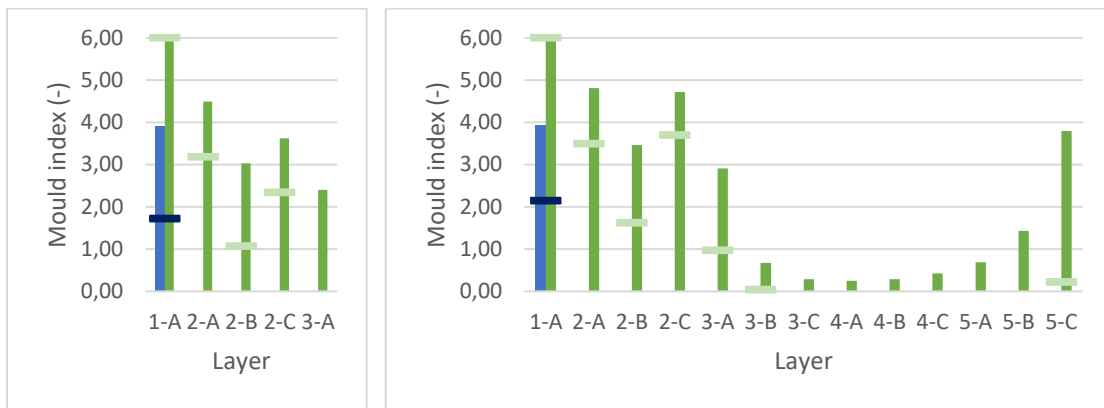
Assembly 5 – North wall, old entrance



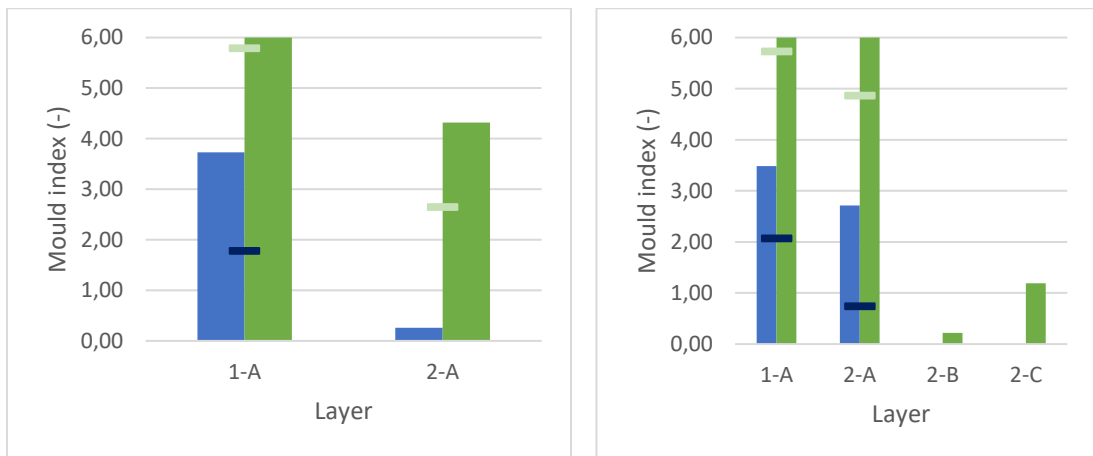
Assembly 6 – East wall, TV-room



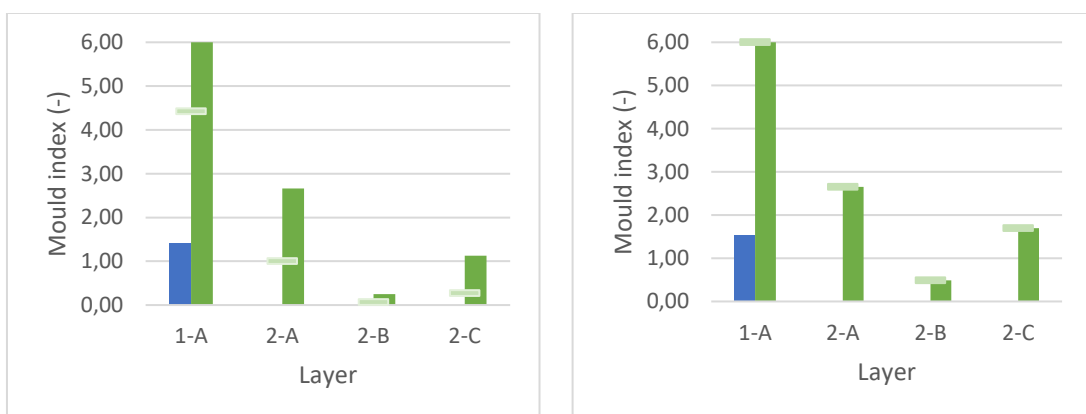
Assembly 7 – South wall, recreational room



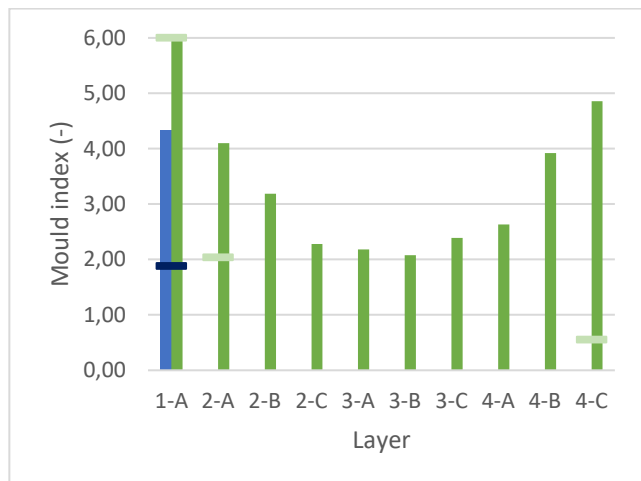
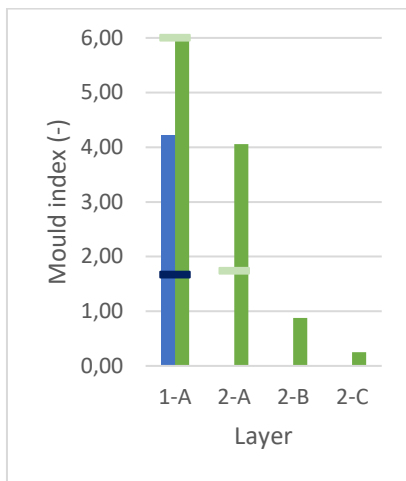
Assembly 8 – South wall, bedroom (without logs)



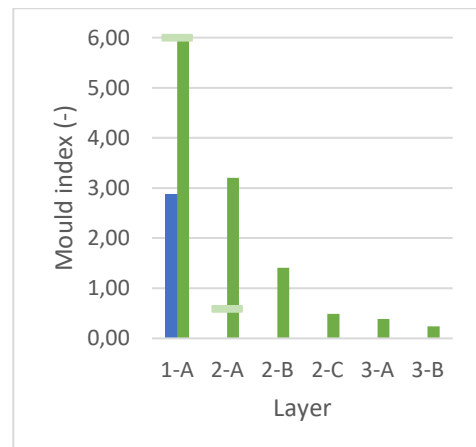
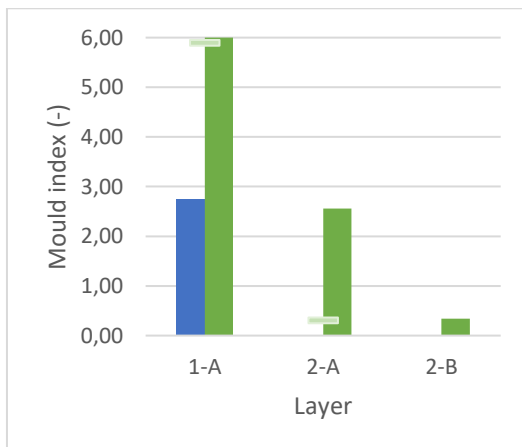
Assembly 9 – West wall, recreational room



Assembly 10 - North wall, recreational room



Assembly 11 – East wall, bedroom



APPENDIX D – Report from field study, loggers

Purpose: Monitoring of the humidity and temperature climate inside and outside Bentegården.

Conducted by: Dimitrios Kraniotis, Sindre Didrichsen and Kris A. Flaskerud

Date: 05.02.2020

Equipment: Loggers

Inside: PeakTech 5180 – Temperature & Humidity Datalogger

Outside: Extech RHT 10 - Temperature & Humidity Datalogger



Logger mounted inside (PeakTech 5180)



Logger mounted outside (Extech RHT10)

Method: The household consist of two adults and a large dog. It is a two-storey house, and the loggers was mounted in different rooms to monitor. The loggers are planned to be collected in the end of March/beginning of April, achieving at least 2 months of data.

The first indoor logger was mounted in the living room of the house. This room is the main area of the house and is where the residents spend most of the time. A fireplace is also located in this room.



Logger positioned on top of a shelf towards the west wall in the living room

The second logger was mounted in a bookshelf at the library room. Yellow circle marks the position seen from the living room.



Second logger positioned in the library



Position seen from the living room

The third logger was mounted on top of a cabinet in the tv-room which is a less heated area with less human activity.



Third logger positioned in the tv-room



Position seen towards the east façade with south façade to the right.

The fourth logger was mounted close to the corner of the large room in the second floor. This room works as a paint workshop and exercise area.



Fourth logger positioned in the recreational room



Position seen towards the corner of south-west façade

One of the loggers was mounted in the corner of the façade towards north to minimize the amount of sunlight accessing the logger.



Fifth logger positioned outside attached to the façade



Position seen towards outside in the corner between north façade and the extended part towards west

The sixth logger was mounted at the west façade and positioned behind the cladding to avoid sunlight.



Sixth logger positioned outside behind the cladding



Position seen towards the west facade

APPENDIX E - Report from field study, laser scan

Purpose: A laser scan of Bentegården to obtain exact dimensions of all building elements.

Conducted by: Sindre Didrichsen and Kris A. Flaskerud

Date: 05.02.2020

Equipment

3D-laser scanner: Leica BLK360

Software: Leica Cyclone FIELD 360



Figure 1 Leica BLK360

Method:

A laser scan was conducted for both interior and exterior of the building. All rooms inside the building were scanned and the specific location of the scanner was marked on a plan drawing of the house. *Figure 2* and *figure 3* illustrates the position of each scan conducted for each floor. Each scan was observed in Leica Cyclone FIELD 360 software on the phone to make sure the quality and connection between each scan was good.



Figure 2 Position #1



Figure 3 Position #2

The following images illustrates the position of each scan performed. First image is a overview of first floor interior side and outside, while the second image is a overview of second floor.

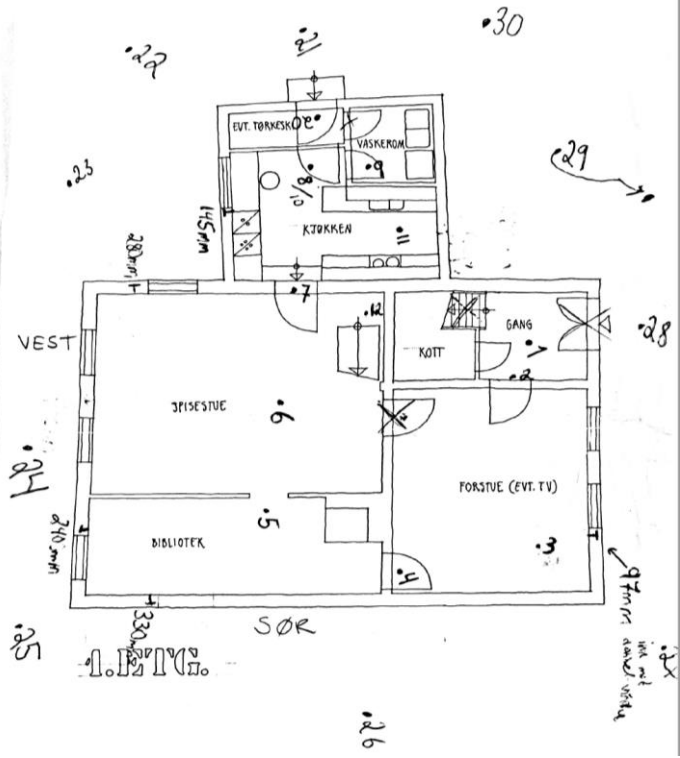


Figure 4 Position of each scan 1th floor inside and outside

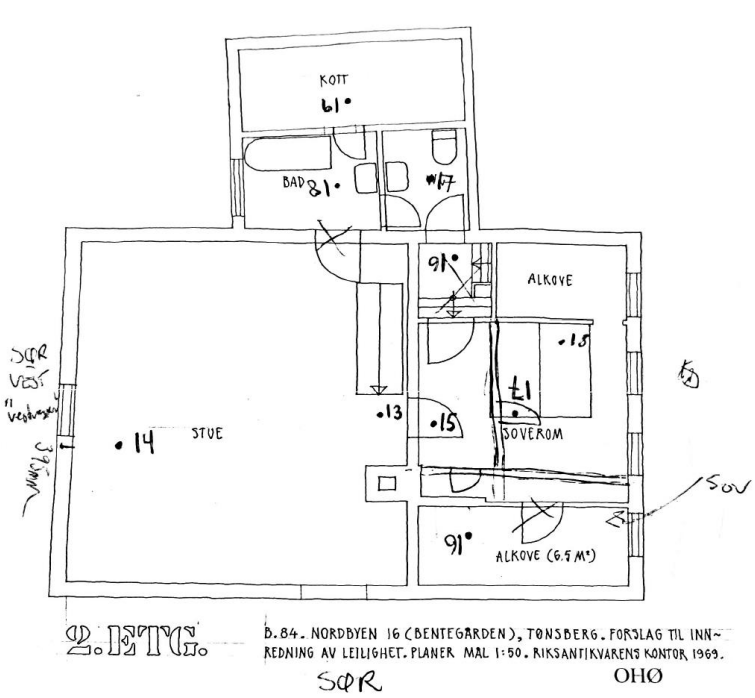


Figure 5 Position of each scan 2nd floor

APPENDIX F - Report from field study, thermography

- Purpose:** A thermography of Bentegården to detect surface temperature and thermal bridges.
- Conducted by:** Dimitrios Kraniotis, Sindre Didrichsen and Kris A. Flaskerud
- Date:** 05.02.2020
- Equipment:** Fluke thermal imager Ti 125
- Method:** All interior surfaces were observed with the thermograph camera. Observations revealed many surfaces relatively cold and thermal bridges. Figure 1 displays the thermo camera pointing at a thermal bridge in the living room.



Figure 1 Fluke thermal imager Ti 125

Location of each thermography picture:

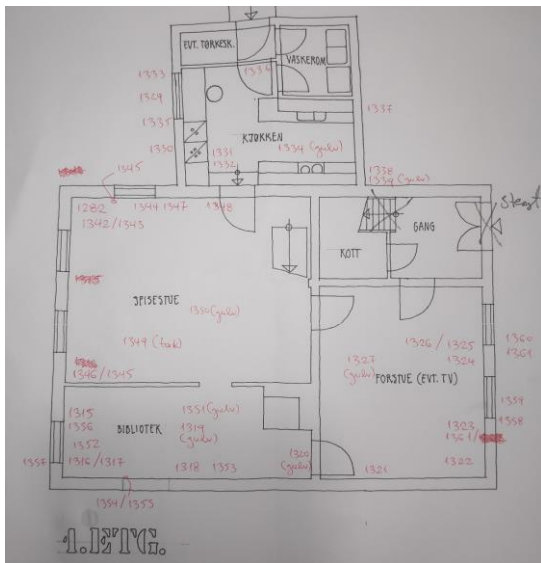


Figure 2 Thermography 1th floor

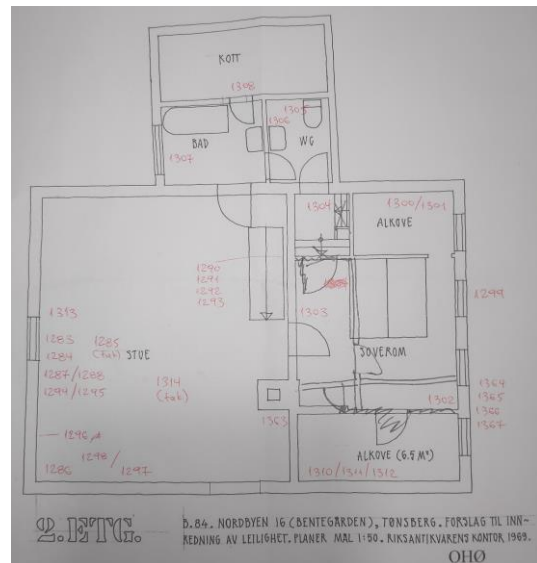


Figure 3 Thermography 2nd floor

Results:

Roof:

Figure 5 displays the surface temperature of the roof, which is close to the room temperature. No thermal bridges is observed across the roof.



Figure 4 Roof interior side

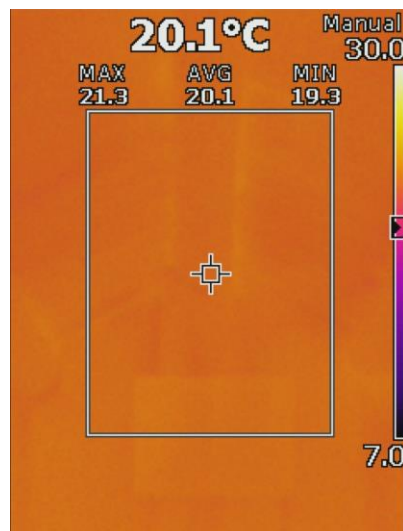


Figure 5 Thermal performance

Windows:

The windows at Bentegården are old and consist of a double wooden frame with one glass pane in each frame. The surface temperature of the windows was very low and figure 6 and 7 displays an example of a window in second floor.



Figure 6 Window 2nd floor

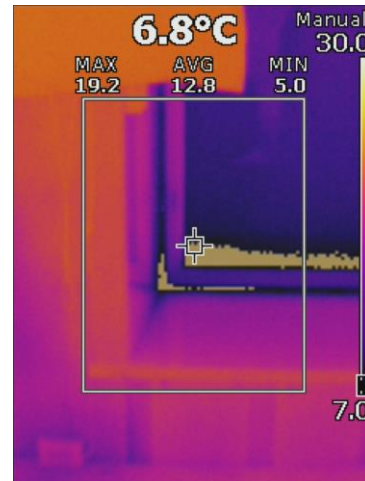


Figure 7 Thermal performance

Walls:

The exterior walls thermal performance was varying. A large difference in thickness of the exterior walls were observed and measured. Two of the exterior walls (south and west façade) was rehabilitated in 2017 and 2018.

Figure 8 and 9 displays the exterior wall at the kitchen. A thermal bridge reveals in the corner of the kitchen and the temperature of the wall was rather low.



Figure 8 Kitchen wall

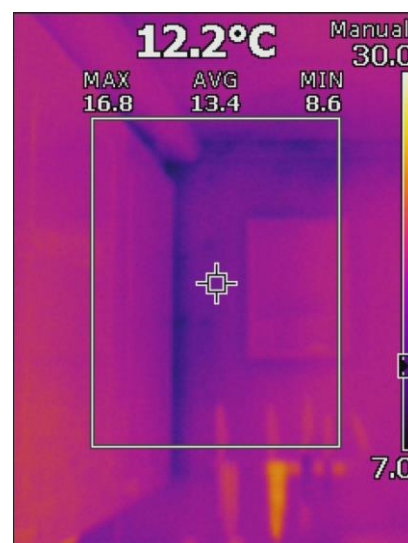


Figure 9 Thermal performance

Figure 10 and 11 displays the exterior wall of a bedroom wall in the second floor which is oriented towards east. The picture reveals a thermal bridge marked with a blue colour in the corner of the bedroom.



Figure 10 Second bedroom



Figure 11 Thermal performance

Figure 12 and 13 displays the exterior wall facing towards south.



Figure 12 Second bedroom

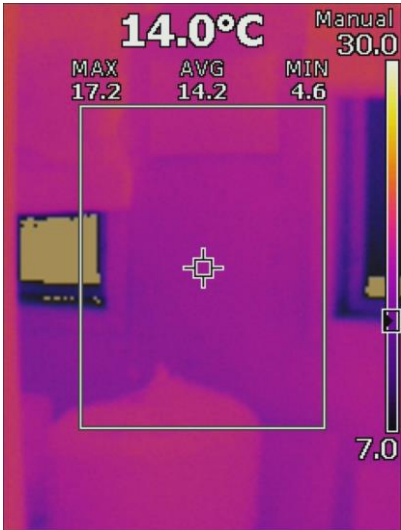


Figure 13 Thermal performance

APPENDIX G – Report from point data cloud processing

12.02.2021

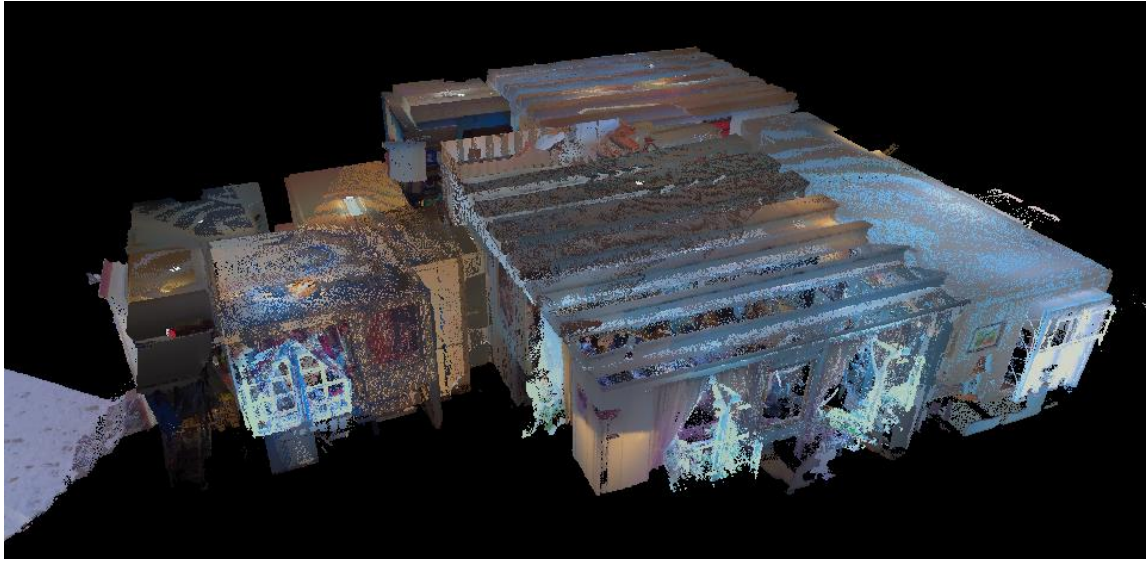
Purpose: Creating a 3D point cloud by connecting the scans

After completing the scans during the field study all the scans were imported to a computer. The software “Leica Cyclone REGISTER 360” was used to connect all the scans together and to “clean” the point cloud (remove all unnecessary data points from the cloud). This process was greatly aided by Ernst Erik Hempel from OsloMet.

The point cloud bundle of first floor is captured from the software below. The red dots illustrate the position of each scan, while the green line illustrate the connection between each scan. The blue dot illustrates a scan which is also connected to the point cloud bundle on the second floor. All the other lines which follows the interior side of the wall illustrates the data from the laser scanner, while the 3D view illustrates the data from the camera on the scanner.



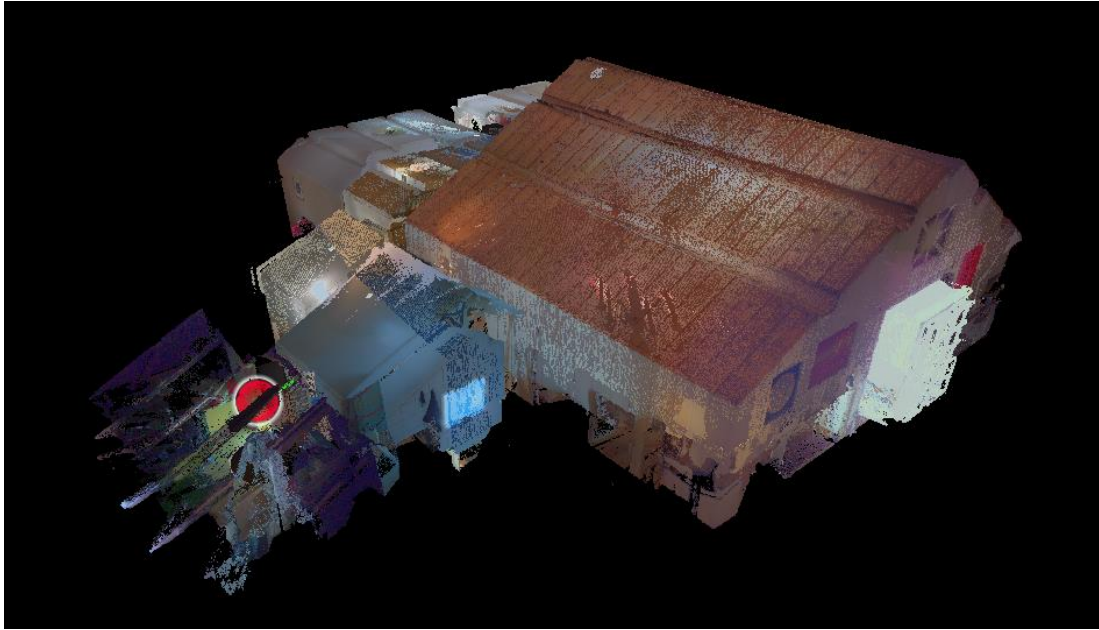
Point cloud bundle of the first floor, plan view



Point cloud bundle of the first floor, 3D view



Point cloud bundle of the second floor, plan view



Point cloud bundle of the second floor, 3D view

The first floor and second floor point cloud bundle were connected together as illustrated below.

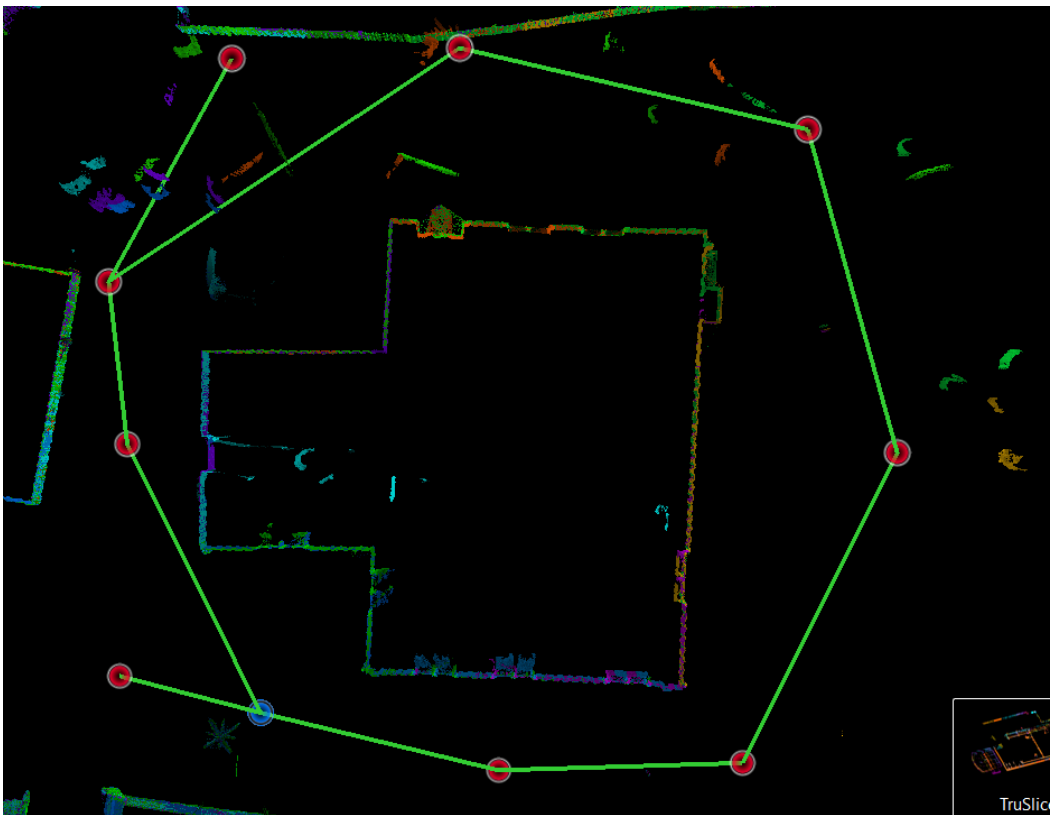


Point cloud bundle of the first floor and second floor connected. The interior wall on left side is the west wall, while the south wall to the right.

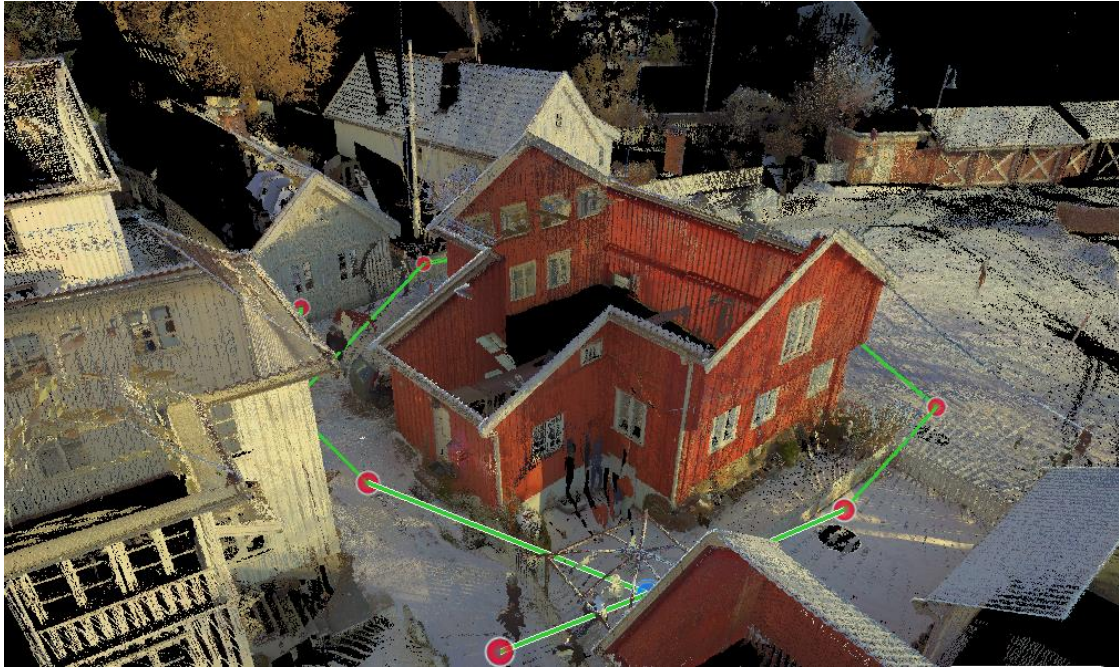


Point cloud bundle of the first floor and second floor connected. The interior wall of east wall with all the windows is on the left, while the extension is on the right side.

The images below illustrates the scans performed outside on exterior side of the walls.



Point cloud bundle of the exterior walls, plan view



Point cloud bundle of the exterior walls, 3D view

APPENDIX H – Report from the 3D modelling process

Purpose: Create a 3D-model based on the scans

Conducted by: Dimitrios Kraniotis, Sindre Didrichsen and Kris A. Flaskerud

Date: February 2021

Software: Autodesk Revit

When the point cloud bundle was complete it was imported into Autodesk Revit as a IFC-file. The point cloud bundle after import is displayed in the figure below.



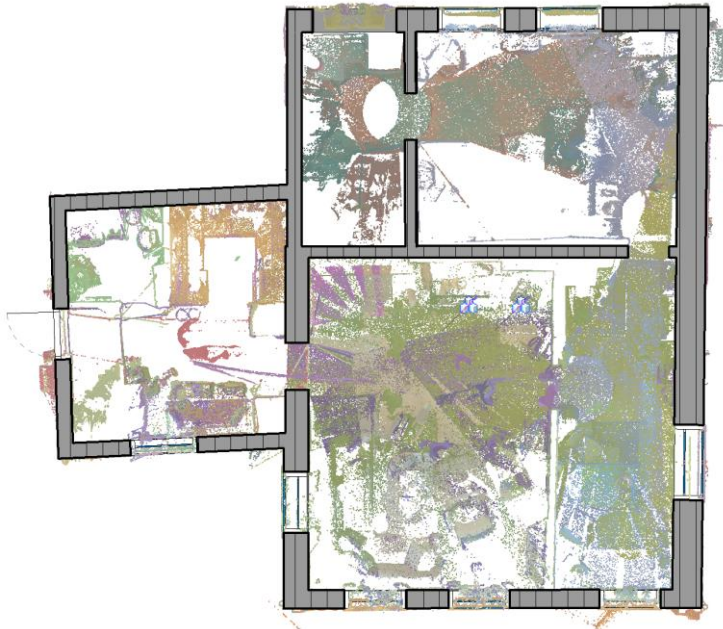
Point cloud bundle captured in Autodesk Revit

The figure below illustrates the point cloud seen from above. The next step was to create a grid and draw lines along the interior and exterior side to obtain the correct dimension of the walls.



Point cloud bundle viewed from above

The thickness of the walls was varying a lot between the different walls. Figure below illustrates the exterior and a few interior walls modelled. The structure of the walls are created similar to the actual walls.



Point cloud visible and walls constructed

The next phase involved creating the second-floor exterior walls and the log wall inside the house. Windows was also created from scratch to be accurate to the actual windows.

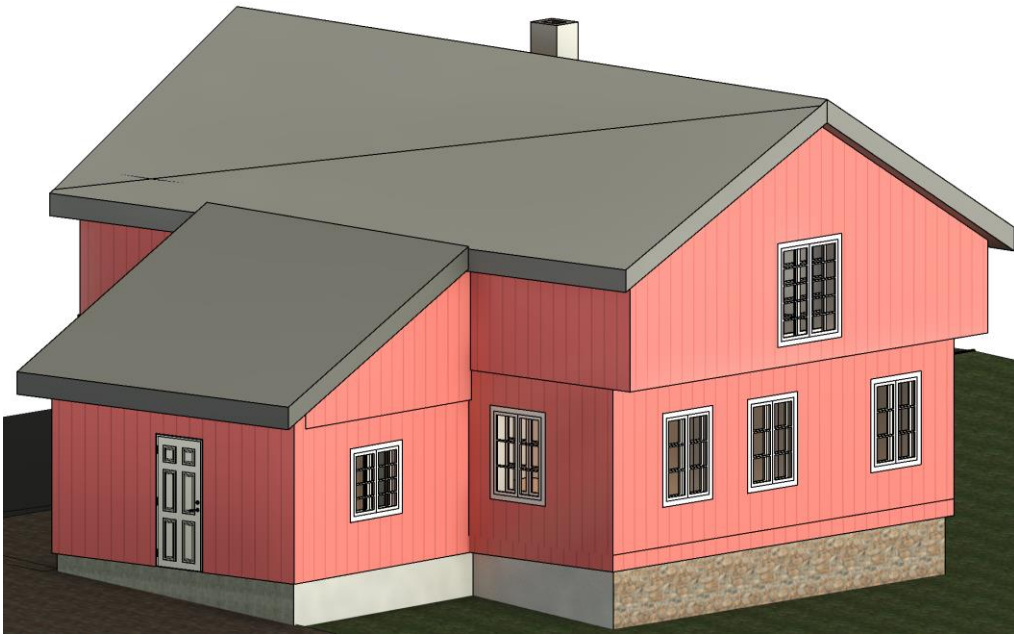


Model after modelling of 1st and 2nd floor exterior walls and the log wall inside.

Following this the floors of first and second floor was modelled, in addition to interior walls and doors.



Model after modeling 1st and 2nd floor, interior walls and doors



The digital model completed. South façade on the right side and the extended part on the left side



The digital model completed. View from the corner of south-east facade



A rendered image of the digital from seen from south-west corner



A rendered image of the digital model seen from south-east corner



A rendered image of the digital model seen from north-east corner